Chapter 1

High-Energy Astrophysical Neutrinos

Francis Halzen
Wisconsin IceCube Particle Physics Center
UW–Madison, Madison, WI USA
halzen@icecube.wisc.edu

Chargeless, weakly-interacting neutrinos are ideal astronomical messengers because they travel through space without scattering, absorption, or deflection. They provide the only unobstructed view of cosmic accelerators. But this weak interaction also makes them notoriously difficult to detect, leading to neutrino observatories requiring large-scale detectors. The IceCube experiment discovered PeV-energy neutrinos originating beyond the Sun, with energies bracketed by those of TeV-energy gamma rays and EeV-energy extragalactic cosmic rays. In this chapter, we discuss the IceCube neutrino telescope, the status of the observation of cosmic neutrinos, and what neutrinos can tell us about the nonthermal Universe. Besides the search for the sources of Galactic and extragalactic cosmic rays, the scientific missions of IceCube and similar instruments under construction in the Mediterranean Sea and Lake Baikal include the observation of Galactic supernova explosions, the search for dark matter, and the study of neutrinos themselves.

Contents

1. Neutrino Astronomy: a Brief History

Soon after the 1956 observation of the neutrino,[1] the idea emerged that it represented the ideal astronomical messenger. Neutrinos travel from the edge of the Universe without absorption and with no deflection by magnetic fields. Having essentially no mass and no electric charge, the neutrino is similar to the photon, except for one important attribute: its interactions with matter are extremely feeble. So, high-energy neutrinos may reach us unscathed from cosmic distances: from the inner neighborhood of black holes and from the nuclear furnaces where cosmic rays are born. But, their weak interactions also make cosmic neutrinos very difficult to detect. Immense particle detectors are required to collect cosmic neutrinos in statistically significant numbers.[2] By the 1970s, it was clear that a cubic-kilometer detector was needed to observe cosmic neutrinos produced in the interactions of cosmic rays with background microwave photons.[3] Subsequent estimates for observing potential cosmic accelerators such as Galactic supernova remnants and gamma-ray bursts unfortunately pointed to the same exigent requirement.[4–6] Building a neutrino telescope has been a daunting technical challenge.

Given the detector's required size, early efforts concentrated on transforming large volumes of natural water into Cherenkov detectors that collect the light produced when neutrinos interact with nuclei in or near the detector.[7] After a two-decade-long effort, building the Deep Underwater Muon and Neutrino Detector (DUMAND) in the sea off the main island of Hawaii unfortunately failed.[8] However, DUMAND paved the way for later efforts by pioneering many of the detector technologies in use today, and by inspiring the deployment of a smaller instrument in Lake Baikal[9] as well as efforts to commission neutrino telescopes in the Mediterranean.[10–12] These efforts in turn have led towards the construction of KM3NeT. But the first telescope on the scale envisaged by the DUMAND collaboration was realized instead by transforming a large volume of transparent natural Antarctic ice into a particle detector, the Antarctic Muon and Neutrino Detector Array (AMANDA). In operation beginning in 2000, it represented a proof of concept for the kilometer-scale neutrino observatory, IceCube.[13,14]

Neutrino astronomy has achieved spectacular successes in the past: neutrino detectors have "seen" the Sun and detected a supernova in the Large Magellanic Cloud in 1987. Both observations were of tremendous importance; the former showed that neutrinos have mass, opening the first crack

in the Standard Model of particle physics, and the latter confirmed the basic nuclear physics of the death of stars. Fig. 1 illustrates the neutrino energy spectrum covering an enormous range, from microwave energies (10^{-12} eV) to 10^{20} eV.[15] The figure is a mixture of observations and theoretical predictions. At low energy, the neutrino sky is dominated by neutrinos produced in the Big Bang. At MeV energy, neutrinos are produced by supernova explosions; the flux from the 1987 event is shown. At yet higher energies, the figure displays the measured atmospheric-neutrino flux, up to energies of 100 TeV by the AMANDA experiment.[16] Atmospheric neutrinos are a main player in our story, because they are the dominant background for extraterrestrial searches. The flux of atmospheric neutrinos falls dramatically with increasing energy; events above 100 TeV are rare, leaving a clear field of view for extraterrestrial sources.

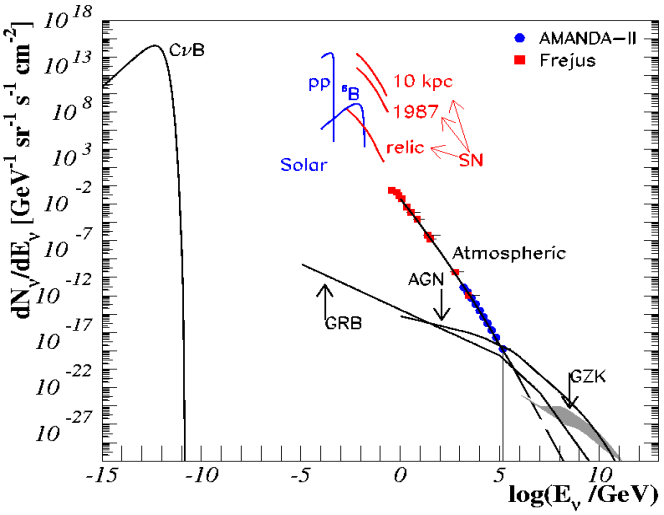

Fig. 1. The cosmic-neutrino spectrum. Sources are the Big Bang (CνB), the Sun, supernovae (SN), atmospheric neutrinos, active galactic nuclei (AGN) galaxies, and GZK neutrinos. The data points are from detectors at the Frejus underground laboratory[17] (red) and from AMANDA[16] (blue).

The highest energy neutrinos in Fig. 1 are the decay products of pions produced by the interactions of cosmic rays with microwave photons.[18] Above a threshold of $\sim 4\times10^{19}$ eV, cosmic rays interact with the microwave background introducing an absorption feature in the cosmic-ray flux, the Greisen-Zatsepin-Kuzmin (GZK) cutoff. As a consequence, the mean free path of extragalactic cosmic rays propagating in the microwave background is limited to roughly 75 megaparsecs, and, therefore, the secondary neutrinos are the only probe of the still enigmatic sources at longer distances. What they will reveal is a matter of speculation. The calculation of the neutrino flux associated with the observed flux of extragalactic cosmic rays is straightforward and yields one event per year in a kilometer-scale detector. The flux, labeled GZK in Fig. 1, shares the high-energy neutrino sky with neutrinos anticipated from gamma-ray bursts and active galactic nuclei (AGN).[4–6]

A population of cosmic neutrinos covering the 30 TeV–1 PeV energy region were revealed by the first two years of IceCube data. Association of cosmic neutrinos with these, or any other source candidates, is still a work in progress. The goal of this chapter is to discuss these topics in some detail. Subsequently, it will briefly cover other uses of neutrino telescopes.

2. IceCube

2.1. *Detecting Very High-Energy Neutrinos*

Cosmic rays have been studied for more than a century. They reach energies in excess of 10^8 TeV, populating an extreme universe that is opaque to photons because they interact with the background radiation fields. mostly microwave photons, before reaching Earth. We don't yet know where or how cosmic rays are accelerated to these extreme energies, and with the recent observation of a blazar in coincidence with the direction and time of a very high energy muon neutrino, neutrino astronomy might have taken a first step in solving this puzzle.[19,20] The rationale is however simple: near neutron stars and black holes, gravitational energy released in the accretion of matter or binary mergers can power the acceleration of protons (p) or heavier nuclei that subsequently interact with gas ("pp") or ambient radiation ("$p\gamma$"). Neutrinos are produced by cosmic-ray interactions at various epochs: in their sources during their acceleration, in the source environment after their release, and while propagating through universal radiation backgrounds from the source to Earth. In interactions of

cosmic-ray protons with background photons ($\gamma_{\rm bg}$), neutral and charged pion secondaries are produced in the processes $p + \gamma_{\rm bg} \rightarrow p + \pi^0$ and $p+\gamma_{\rm bg} \rightarrow n+\pi^+$. While neutral pions decay as $\pi^0 \rightarrow \gamma+\gamma$ and create a flux of high-energy gamma rays, the charged pions decay into three high-energy neutrinos (ν) and anti-neutrinos ($\bar{\nu}$) via the decay chain $\pi^+ \rightarrow \mu^+ + \nu_\mu$ followed by $\mu^+ \rightarrow e^+ + \bar{\nu}_\mu + \nu_e$, and the charged-conjugate process. We refer to these photons as pionic photons to distinguish them from photons radiated by electrons that may be accelerated along with the protons and nuclei. Because of their weak interactions, neutrinos will reach our detectors, unless produced within extremely dense environments. they essentially act like photons; their small mass is negligible relative to the TeV to EeV energies targeted by neutrino telescopes. They do however oscillate over cosmic distances. For instance, for an initial neutrino flavor ratio of $\nu_e : \nu_\mu : \nu_\tau \simeq 1 : 2 : 0$ from the decay of pions and muons, the oscillation-averaged composition arriving at the detector is approximately an equal mix of electron, muon, and tau neutrino flavors, $\nu_e : \nu_\mu : \nu_\tau \simeq 1 : 1 : 1$.[21]

High-energy neutrinos interact predominantly with matter via deep inelastic scattering off nucleons: the neutrino scatters off quarks in the target nucleus by the exchange of a Z or W weak boson, referred to as *neutral current* (NC) and *charged current* (CC) interactions, respectively. Whereas the NC interaction leaves the neutrino state intact, in a CC interaction a charged lepton is produced that shares the initial neutrino flavor. The average relative energy fraction transferred from the neutrino to the lepton is at the level of 80% at these energies. The inelastic CC cross section on protons is at the level of 10^{-33} cm^2 at a neutrino energy of 10^3 TeV and grows with neutrino energy as $\sigma_{\rm tot} \propto E_\nu^{0.36}$.[22,23] The struck nucleus does not remain intact and its high-energy fragments typically initiate hadronic showers in the target medium.

Immense particle detectors are required to collect cosmic neutrinos in statistically significant numbers. Already by the 1970s, it had been understood[3] that a kilometer-scale detector was needed to observe the cosmogenic neutrinos produced in the interactions of CRs with background microwave photons.[24] A variety of methods are used to detect the high-energy secondary particles created in CC and NC neutrino interactions. One particularly effective method observes the radiation of optical Cherenkov light given off by secondary charged particles produced in CC and NC interactions that travel faster than the speed of light in the medium. The detection concept is that of a Cherenkov detector, a transparent medium instrumented with photomultipliers that transform the Cherenkov light into

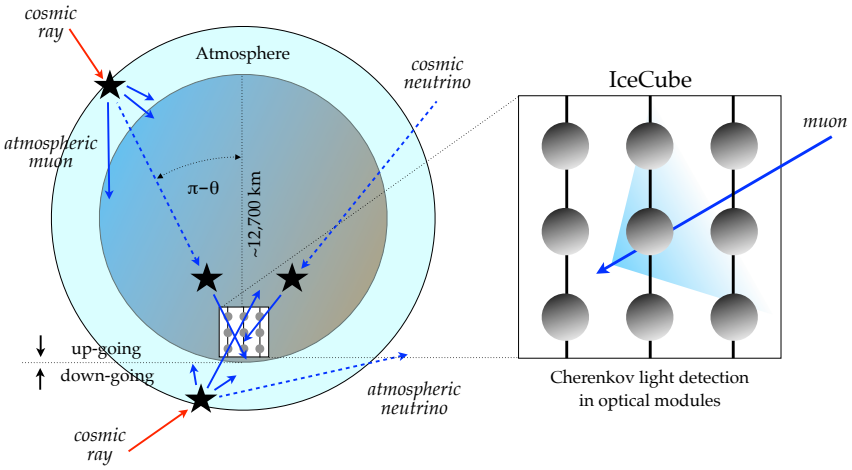

Fig. 2. The principal idea of neutrino telescopes from the point of view of IceCube located at the South Pole. Neutrinos dominantly interact with a nucleus in a transparent medium like water or ice and produce a muon that is detected by the wake of Cherenkov photons it leaves inside the detector. The background of high-energy muons (solid blue arrows) produced in the atmosphere can be reduced by placing the detector underground. The surviving fraction of muons is further reduced by looking for upgoing muon tracks that originate from muon neutrinos (dashed blue arrows) interacting close to the detector. This still leaves the contribution of muons generated by atmospheric muon neutrino interactions. This contribution can be separated from the diffuse cosmic neutrino emission by an analysis of the combined neutrino spectrum.

electrical signals using the photoelectric effect; see Figs. 2 and 3. IceCube consists of 80 strings, each instrumented with 60 10-inch photomultipliers spaced by 17 m over a total length of 1 kilometer. The deepest module is located at a depth of 2.450 km so that the instrument is shielded from the large background of cosmic rays at the surface by approximately 1.5 km of ice. Strings are arranged at apexes of equilateral triangles that are 125 m on a side. The instrumented detector volume is a cubic kilometer of dark, highly transparent and sterile Antarctic ice. Radioactive background is dominated by the instrumentation deployed into this natural ice.

Each optical sensor consists of a glass sphere containing the photomultiplier and the electronics board that digitizes the signals locally using an on-board computer. The digitized signals are given a global time stamp with residuals accurate to less than 3 ns and are subsequently transmitted to the surface. Processors at the surface continuously collect these time-stamped signals from the optical modules, each of which functions

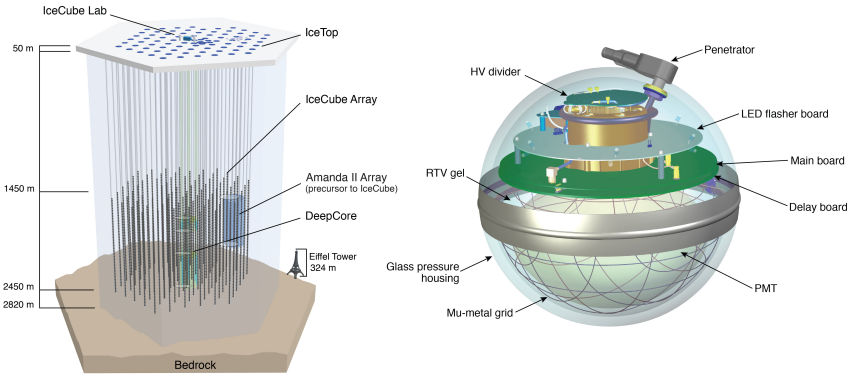

Fig. 3. Sketch of the IceCube observatory (left) and the digital optical module (right).

independently. The digital messages are sent to a string processor and a global event trigger. They are subsequently sorted into the Cherenkov patterns emitted by secondary muon tracks, or electron and tau showers, that reveal the flavor, energy and direction of the incident neutrino.[25]

There are two principle classes of Cherenkov events that can be easily identified this way, "tracks" and "cascades" as illustrated in Fig. 4. There are two basic topologies: tracks from ν_μ and cascades from ν_e, ν_τ, and the neutral current interactions from all flavors. On the scale of IceCube, PeV cascades have a length of less than 10 m and are therefore point sources of Cherenkov light in a detector of kilometer size. The term "tracks" refers to the Cherenkov emission of long-lived muons passing through the detector. These muons can be produced in CC interactions of muon neutrinos inside or in the vicinity of the detector. Energetic electrons and taus produced in CC interactions of electron and tau neutrino interactions, respectively, will in general not produce elongated tracks due to the rapid scattering of electrons and the short lifetime of the tau. Because of the large background of muons produced by CR interactions in the atmosphere, the observation of muon neutrinos is limited to upgoing muon tracks that are produced in interactions inside or close to the detector by neutrinos that have passed through the Earth[a] as illustrated in Fig. 2. The remaining background consists of atmospheric neutrinos, which are indistinguishable from cosmic neutrinos on an event-by-event basis. However, the steeply falling spectrum

[a]Note, that while at high-energy the neutrino cross section grows, resulting in a reduced mean free path (λ_ν), the range of the secondary muon (λ_μ) increases as does the probability for observing a muon, λ_μ/λ_ν; it is about 10^{-6} for a 1 TeV neutrino.

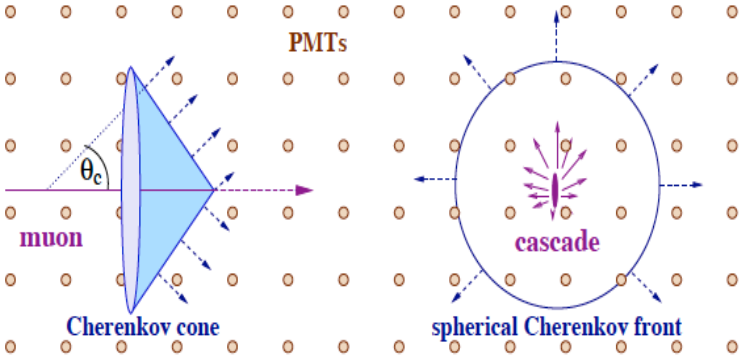

Fig. 4. Contrasting Cherenkov light patterns produced by muons (left) and by showers initiated by electron and tau neutrinos (right) and by neutral current interactions. The patterns are routinely referred to as tracks and cascades (or showers). Cascades are produced by the radiation of particle showers, whose dimensions are in the tens of meters, i.e., an approximate point source of light with respect to the dimensions of the detector.

($\propto E^{-3.7}$) of atmospheric neutrinos allows identifying diffuse astrophysical neutrino emission above a few hundred TeV by a spectral analysis, as we will highlight in the following sections. The atmospheric background is also reduced for muon neutrino observation from point-like sources, in particular transient neutrino sources.

The hadronic particle shower generated by the target struck by a neutrino in the ice also radiates Cherenkov photons. Because of the large multiplicity of secondary particles and the repeated scattering of the Cherenkov photons in the medium, the light pattern is mostly spherical; it is referred to as a "cascade." The light patterns produced by the particle showers initiated by the electron or tau produced in CC interactions of electron or tau neutrinos, respectively, will be superimposed on the cascade. The direction of the initial neutrino can only be reconstructed from the Cherenkov emission of secondary particles produced close to the neutrino interaction point, and the angular resolution is worse than for track events.

On the other hand, the energy of the initial neutrino can be constructed with a better resolution than for tracks. For both tracks and cascades, the observable energy of secondary charged leptons can be estimated from the total number of Cherenkov photons and is related to the neutrino energy of charged particles after accounting for kinematic effects and detection efficiencies. The Cherenkov light observed in cascades is proportional to the

energy transferred to the cascade and can be fully contained in the instrumented volume. In contrast, muons produced by CC muon neutrino interactions lose energy gradually by ionization, bremsstrahlung, pair production, and photo-nuclear interactions while they range our passing through the detector. This allows estimating the muon energy as it enters the detector and setting a lower limit on the neutrino energy. Using Standard Model physics, one can subsequently derive a probability distribution for the energy of the initial neutrino that determines its most probable value. The neutrino energy may only be determined within a factor of 2 or thereabout, depending on the energy, but the uncertainties drop out when measuring a neutrino spectrum involving multiple events.

Muons range out, over kilometers at TeV energy to tens of kilometers at EeV energy, generating showers along their track by bremsstrahlung, pair production, and photonuclear interactions. The charged particles produced are the sources of additional Cherenkov radiation. Because the energy of the muon degrades along its track, the energy of the secondary showers decreases, which reduces the distance from the track over which the associated Cherenkov light can trigger a PMT. The geometry of the light pool surrounding the muon track is therefore a kilometer-long cone with a gradually decreasing radius. In its first kilometer, a high-energy muon typically loses energy in a couple of showers having one-tenth of the muon's initial energy. So the initial radius of the cone is the radius of a shower with 10% of the muon energy. At lower energies of hundreds of GeV and less, the muon becomes minimum-ionizing.

Because of the stochastic nature of the muon's energy loss, the relationship between the observed energy loss inside the detector and muon energy varies from muon to muon. Additionally, only the muon energy lost in the detector can be determined; we do not know its energy loss before entering the instrumented volume nor how much energy it carries out upon exiting. An unfolding process is required to determine the neutrino energy based on the observed muon energy; fortunately, it is based on well-understood Standard Model physics. In contrast, for ν_e and ν_τ, the detector is a total energy calorimeter, and the determination of their energy is superior.

The different topologies each have advantages and disadvantages. For ν_μ interactions, the long lever arm of muon tracks, up to tens of kilometers at very high energies, allows the muon direction (and the neutrino direction) to be determined accurately with an angular resolution measured online that is better than 0.4°. Superior angular resolution can be reached for selected events. Sensitivity to point sources is therefore better as well.

The disadvantages are a large background, of atmospheric neutrinos below 100 TeV and cosmic-ray muons at all energies, and the indirect determination of the neutrino energy that must be inferred from sampling the energy loss of the muon when it transits the detector.

Observation of ν_e and ν_τ flavors represents significant advantages. They are detected from both Northern and Southern Hemispheres. (This is also true for ν_μ with energy in excess of several hundred TeV, where the background from the steeply falling atmospheric spectrum becomes negligible.) At TeV energies and above, the background of atmospheric ν_e is lower by over an order of magnitude, and there are essentially no atmospheric ν_τ produced. High energy atmospheric ν_τ are of cosmic origin (one such clear event has been observed and a complete analysis is in progress).

At higher energies, long-lived pions, the source of atmospheric ν_e, no longer decay, and relatively rare K-decays become the dominant source of background ν_e. Furthermore, because the neutrino events are totally, or at least partially, contained inside the instrumented detector volume, the neutrino energy is determined by total-absorption calorimetry. One can establish the cosmic origin of a single event by demonstrating that the energy cannot be reached by muons and neutrinos of atmospheric origin. Finally, ν_τ are not absorbed by the Earth:[26] ν_τ interacting in the Earth produce secondary ν_τ of lower energy, either directly in a neutral current interaction or via the decay of a secondary tau lepton produced in a charged-current interaction. High-energy ν_τ will thus cascade down to energies of hundred of TeV where the Earth becomes transparent. In other words, they are detected with a reduced energy but not absorbed.

Although cascades are nearly pointlike and, in practice, spatially isotropic, the pattern of arrival times of the photons at individual optical modules reveals the direction of the secondary leptons with 3°. While a fraction of cascade events can be reconstructed accurately to within a degree,[27] the precision is inferior to that reached for ν_μ events and typically not better than 10° using the present techniques.

At energies above about 100 PeV, electromagnetic showers begin to elongate because of the Landau-Pomeranchuk-Migdal effect.[28] An extended length scale is associated with the abundant radiation of soft photons that results in interactions of the shower particles on two target atoms. Negative interference in this process results in reduced energy loss.

2.2. *Detector Performance*

Cosmic neutrinos must be separated from the large backgrounds of atmospheric neutrinos and atmospheric cosmic-ray muons. This is possible for two classes of events: neutrinos that interact inside the instrumented volume ("starting events") and events where a muon enters the detector from below, created by a neutrino traversing the Earth (throughgoing events), thus pointing back to its origin. In this latter case, the Earth is used as a filter for cosmic-ray muons.

For starting events, the pathlength $l(\theta)$ traversed within the detector volume by a neutrino with zenith angle θ is determined by the detector's geometry. Neutrinos are detected if they interact within the detector volume, i.e., within the instrumented volume of one cubic kilometer. That probability is

$$P(E_\nu) = 1 - \exp[-l/\lambda_\nu(E_\nu)] \simeq l/\lambda_\nu(E_\nu)\,, \tag{1}$$

where $\lambda_\nu(E_\nu) = [\rho_{\rm ice}\ N_A\ \sigma_{\nu N}(E_\nu)]^{-1}$ is the mean free path in ice for a neutrino of energy E_ν. Here, $\rho_{\rm ice} = 0.9$ g cm^{-3} is the density of the ice, $N_A = 6.022 \times 10^{23}$ is Avogadro's number, and $\sigma_{\nu N}(E_\nu)$ is the neutrino-nucleon cross section. A neutrino flux dN/dE_ν (neutrinos per GeV per cm^2 per second) crossing a detector with energy threshold and cross sectional area A(E_ν) facing the incident beam will produce

$$N_{ev} = T \int_{E_\nu^{\rm th}} A(E_\nu)\, P(E_\nu)\, \frac{dN}{dE_\nu}\, dE_\nu \tag{2}$$

events after a time T. The "effective" detector area A(E_ν) is also a function of the zenith angle θ. It isn't strictly equal to the geometric cross section of the instrumented volume facing the incoming neutrino, because even neutrinos interacting outside the instrumented volume may produce enough light inside the detector to be detected. In practice, A(E_ν) is determined as a function of the incident neutrino direction and zenith angle by a full-detector simulation, including the trigger.

This formalism applies to contained events. For muon neutrinos, any neutrino producing a secondary muon that reaches the detector (and has sufficient energy to trigger it) will be detected. Because the muon travels kilometers at TeV energy and tens of kilometers at PeV energy, neutrinos can be detected outside the instrumented volume; the probability is obtained by substitution in Eq. 1,

$$l \to \lambda_\mu\,, \tag{3}$$

thereby giving,

$$P = \lambda_\mu / \lambda_\nu \,. \tag{4}$$

Here, λ_μ is the range of the muon determined by its energy losses. Values for the neutrino nucleon cross section and the range of the muon can be found in Ref.[29]

The complete expression for the flux of ν_μ-induced muons at the detector is given by a convolution of the neutrino spectrum ϕ ($= dN/dE_\nu$) with the probability P to produce a muon reaching the detector:[4–6]

$$\phi_\mu(E_\mu^{\rm min}, \theta) = \int_{E_\mu^{\rm min}} P(E_\nu, E_\mu^{\rm min}) \, \exp[-\sigma_{\rm tot}(E_\nu) \, N_A \, X(\theta)] \, \phi(E_\nu, \theta) dE_\nu . \tag{5}$$

The additional exponential factor accounts for the absorption of neutrinos along a chord of the Earth of length $X(\theta)$ at zenith angle θ. Absorption becomes important for $\sigma_\nu(E_\nu) \gtrsim 10^{-33}\,{\rm cm}^2$ or $E_\nu \gtrsim 100$ TeV. For back-of-the-envelope calculations, the P-function can be approximated by

$$P \simeq 1.3 \times 10^{-6} E^{2.2} \quad \text{for } E = 10^{-3}\text{–}1 \text{ TeV} \,, \tag{6}$$

$$\simeq 1.3 \times 10^{-6} E^{0.8} \quad \text{for } E = 1\text{–}10^3 \text{ TeV} \,. \tag{7}$$

At EeV energy, the increase is reduced to only $E^{0.4}$. Clearly, high-energy neutrinos are more likely to be detected because of the increase with energy of both the cross section and muon range.

Tau neutrinos interacting outside the detector can be observed provided the tau lepton they produce reaches the instrumented volume within its lifetime. In Eq. 1, l is replaced by

$$l \to \gamma c\tau = E/mc\tau \,, \tag{8}$$

where m, τ, and E are the mass, lifetime, and energy of the tau, respectively. The tau's decay length $\lambda_\tau = \gamma c\tau \approx 50 \text{ m} \times (E_\tau/10^6)$ GeV grows linearly with energy and actually exceeds the range of the muon near 1 EeV. At yet higher energies, the tau eventually ranges out by catastrophic interactions, just like the muon, despite the reduction of the energy-loss cross sections by a factor of $(m_\mu/m_\tau)^2$.

Tracks and showers produced by tau neutrinos are difficult to distinguish from those initiated by muon and electron neutrinos, respectively. To be clearly identified, both the initial neutrino interaction and the subsequent tau decay must be contained within the detector; for a cubic- kilometer detector, this happens for neutrinos with energies from a few PeV to a few tens of PeV.[30]

For an in-depth discussion of neutrino detection, energy measurement, and flavor separation, and for detailed references, see the IceCube Preliminary Design Document[13] and Ref.[2]

2.3. *Atmospheric Neutrinos*

Muons and neutrinos from decay of mesons produced by cosmic-ray interactions in the atmosphere are the background in the search for neutrinos of extraterrestrial origin. The 3 kHz trigger rate of IceCube is dominated by atmospheric muons from decay of pions and kaons produced in the atmosphere above the detector. The distribution peaks near the zenith and decreases with increasing angle as the muon energy required to reach the deep detector increases. Most atmospheric muons are easily identified as entering tracks from above and rejected. Because of the large ratio of muons to neutrinos, however, misreconstructed atmospheric muons remain an important source of background for all searches.

Measurement of the spectrum of atmospheric neutrinos is an important benchmark for a neutrino telescope. IceCube detects an atmospheric neutrino every six minutes. The spectrum of atmospheric ν_μ has been measured by unfolding the measured rate and energy deposition of neutrino-induced muons entering the detector from below the horizon,[31] as shown in Fig. 9. More challenging is the measurement of the flux of atmospheric electron neutrinos. This has been done by making use of DeepCore, the more densely instrumented subarray in the deep center of IceCube, to identify contained shower events. The known spectrum of ν_μ is used to calculate the contribution of neutral current interactions to the observed rate of showers. Subtracting the neutral current contribution leads to the measurement of the spectrum of atmospheric electron neutrinos from 100 GeV to 10 TeV,[32] as shown in Fig. 9.

In general, atmospheric neutrinos are indistinguishable from astrophysical neutrinos. An important exception occurs in the case of muon neutrinos from above when the neutrino energy is sufficiently high and the zenith angle sufficiently small that the muon produced in the same decay as the neutrino is guaranteed to reach the detector.[33] This is used to reject atmospheric neutrinos in analyses where they are a background. Monte Carlo simulation can be used to evaluate the atmospheric neutrino passing rate more generally by also including other high-energy muons produced in the same cosmic-ray shower as the neutrino. In this way, the method can be extended to electron neutrinos. In practice, the passing rate is significantly reduced for zenith angles $\theta < 70^\circ$ and $E_\nu > 100$ TeV.

The spectrum of atmospheric neutrinos becomes one power steeper than the spectrum of primary nucleons at high energy as the competition between interaction and decay of pions and kaons increasingly suppresses their decay.

For the dominant kaon channel, the characteristic energy for the steepening is $E_\nu \sim 1$ TeV$/\cos\theta$. A further steepening occurs above 100 TeV as a consequence of the knee in the primary spectrum. Astrophysical neutrinos should reflect the cosmic-ray spectrum in the source and are therefore expected to have a significantly harder spectrum than atmospheric neutrinos. Establishing an astrophysical signal above the steep atmospheric background requires an understanding of the atmospheric neutrino spectrum around 100 TeV and above.

Although there is some uncertainty associated with the composition through the knee region,[34] the major uncertainty in the spectrum of atmospheric neutrinos at high energy is the level of charm production. The short lived charmed hadrons preferentially decay up to a characteristic energy of 10^7 GeV, producing prompt muons and neutrinos with the same spectrum as their parent cosmic rays. This prompt flux of leptons has not yet been measured. Existing limits[35,36] allow a factor of two or three around the level predicted by a standard calculation[37] (after correction for steepening at the knee). For reasonable assumptions, the charm contribution is expected to dominate the conventional spectrum above ~ 10 TeV for ν_e, above ~ 100 TeV for ν_μ, and above ~ 1 PeV for muons.[38]

The expected hardening in the spectrum of atmospheric neutrinos due to prompt neutrinos is partially degenerate with a hard astrophysical component. However, the spectrum of astrophysical neutrinos should reflect the spectrum of cosmic rays at their sources, which is expected to be harder than the spectrum of cosmic rays at Earth. It should eventually be possible with IceCube to measure the charm contribution by requiring a consistent interpretation of neutrino flavors and cosmic-ray muons for which there is no astrophysical component. An additional signature of atmospheric charm is the absence of seasonal variations for this component.[39]

3. Rationale for the Construction of Kilometer-Scale Neutrino Detectors

The construction of kilometer-scale neutrino detectors was primarily motivated by the prospect of detecting neutrinos associated with the sources of high-energy cosmic rays. Cosmic accelerators produce particles with energies in excess of 100 EeV; we still do not know where or how;[40] see Fig. 5[b].

[b]We will use energy units TeV, PeV and EeV, increasing by factors of 1000 from GeV energy.

The bulk of the cosmic rays are Galactic in origin. Any association with our Galaxy presumably disappears at EeV energy when the gyroradius of a proton in the Galactic magnetic field exceeds its size. The cosmic-ray spectrum exhibits a rich structure above an energy of $\sim 0.1\,\mathrm{EeV}$, but where exactly the transition to extragalactic cosmic rays occurs is a matter of debate.

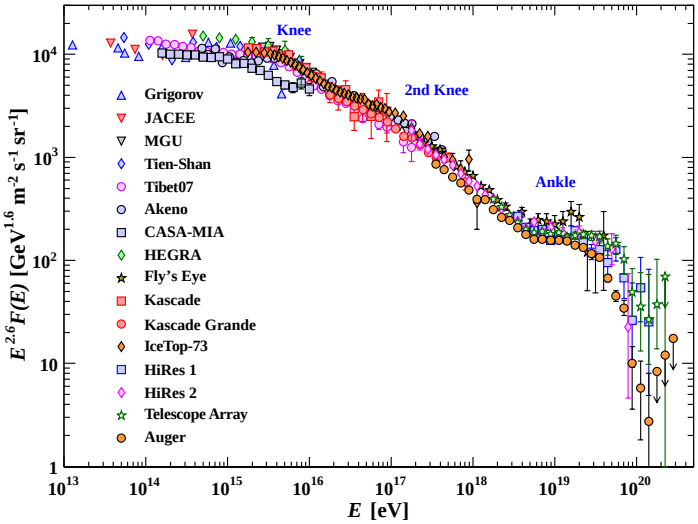

Fig. 5. At the energies of interest here, the cosmic-ray spectrum follows a sequence of three power laws. The first two are separated by the "knee," the second and third by the "ankle." Cosmic rays beyond the ankle are a new population of particles produced in extragalactic sources. Note that the spectrum $F(E)(= dN/dE)$ has been multiplied by a power $E^{2.7}$ in order to visually enhance the structure in the spectrum (data compiled by Particle Data Group[29]).

3.1. *Cosmic-Ray Accelerators*

The detailed blueprint for a cosmic-ray accelerator must meet two challenges: the highest-energy particles in the beam must reach energies beyond $10^3\,\mathrm{TeV}$ ($10^8\,\mathrm{TeV}$) for Galactic (extragalactic) sources and their luminosities must accommodate the observed flux. Both requirements represent severe constraints that have guided theoretical speculations. Acceleration of protons (or nuclei) to TeV energy and above requires massive bulk flows of relativistic charged particles. The blueprint of the accelerator can be copied from solar flares where particles are accelerated to GeV energy by

shocks and, possibly, reconnection; see Fig. 6. Requiring that the gyroradius of the accelerated particle be contained within the accelerating B-field region, $E/ZecB \leq R$, leads to an upper limit on the energy of the particle,

$$E \leq Ze\,c\,B\,R\,. \tag{9}$$

Reaching energies much above 10 GeV in solar flares is dimensionally impossible. In a solar flare, the extent R of the accelerating region and the magnitude of the magnetic fields B are not large enough to accelerate particles of charge Ze to energies beyond GeV; their velocity is taken to be the speed of light, c. The central idea for accommodating the higher energies of the Galactic and extragalactic cosmic rays observed is that a fraction of the gravitational energy released in a stellar collapse is converted into particle acceleration, presumably by shocks.

Baade and Zwicky[41] suggested as early as 1934 that supernova remnants could be sources of the Galactic cosmic rays. It is assumed that, after the collapse, $\sim 10^{51}$ erg of energy is transformed into particle acceleration by diffusive shocks associated with young ($\sim$1000 year old) supernova remnants expanding into the interstellar medium. Like a snowplow, the shock sweeps up the $\sim 1\,\mathrm{proton/cm^3}$ density of hydrogen in the Galactic plane. The accumulation of dense filaments of particles in the outer reaches of the shock, clearly visible as sources of intense X-ray emission, are the sites of high magnetic fields; see Fig. 7. It is theorized that particles crossing these structures multiple times can be accelerated to high energies following an approximate power-law spectrum $dN/dE \sim E^{-2}$. The mechanism copies solar flares where filaments of high magnetic fields, visible in Fig. 6, are the sites for accelerating nuclear particles to tens of GeV. The higher energies reached in supernova remnants are the consequence of particle flows of much larger intensity powered by the gravitational energy released in the stellar collapse.

This idea has been widely accepted despite the fact that to date no source has been conclusively identified, neither by cosmic rays nor by accompanying gamma rays and neutrinos produced when the cosmic rays interact with Galactic hydrogen. Galactic cosmic rays reach energies of at least several PeV, the "knee" in the spectrum; therefore, their interactions should generate gamma rays and neutrinos from the decay of secondary pions reaching hundreds of TeV. Such sources, referred to as PeVatrons, have not been found; see, however, Ref.[42] Nevertheless, Zwicky's suggestion has become the stuff of textbooks, and the reason is energetics: three Galactic

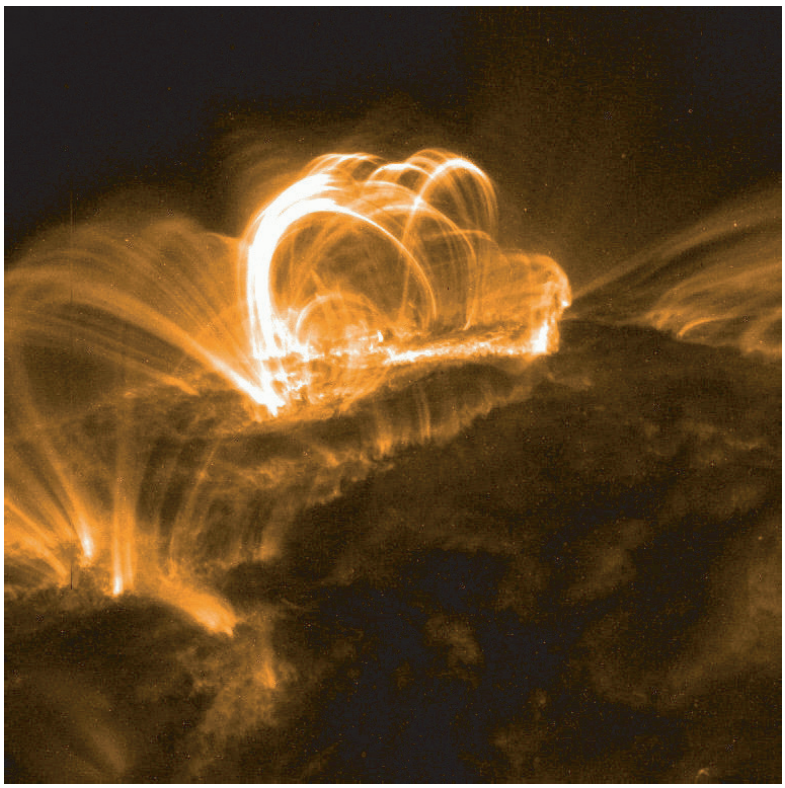

Fig. 6. Opportunities exist near intense charged particle flows, seen as filaments in this X-ray picture of a solar flare, for solar particles to accelerate to GeV energy.

supernova explosions per century converting a reasonable fraction of a solar mass into particle acceleration can accommodate the steady flux of cosmic rays in the Galaxy. It is interesting to note that Zwicky originally assumed that the sources were extragalactic since the most recent supernova in the Milky Way was in 1572. After diffusion in the interstellar medium was understood, supernova explosions in the Milky Way became the source of choice for the origin of Galactic cosmic rays,[43] although after more than 50 years the issue is still debated.[44]

Energetics also guides speculations on the origin of extragalactic cosmic rays. By integrating the cosmic-ray spectrum above the ankle at $\sim 4\,\mathrm{EeV}$, it is possible to estimate[45] the energy density in extragalactic cosmic rays as $\sim 3 \times 10^{-19}\,\mathrm{erg\ cm^{-3}}$. This value is rather uncertain because of our ignorance of the energy where the transition from Galactic to extragalactic

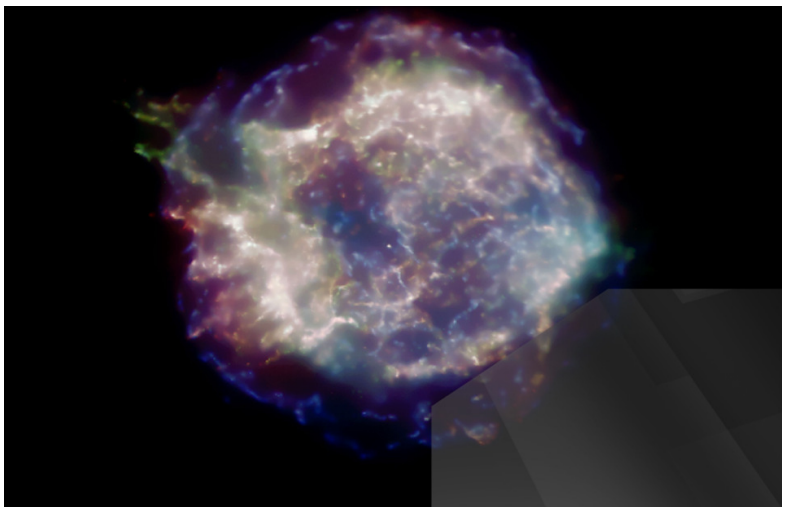

Fig. 7. This X-ray picture of the supernova remnant CasA reveals strong particle flows near its periphery. We believe they are the site for accelerating Galactic cosmic rays to energies reaching the "knee" in the spectrum.

sources occurs. The power required for a population of sources to generate this energy density over the Hubble time of 10^{10} years is 2×10^{37} erg s^{-1} per Mpc^3. Long-duration gamma-ray bursts have been associated with the collapse of massive stars to black holes, and not to neutron stars, as is the case in a collapse powering a supernova remnant. A gamma-ray-burst fireball converts a fraction of a solar mass into the acceleration of electrons, seen as synchrotron photons. The observed energy in extragalactic cosmic rays can be accommodated with the reasonable assumption that shocks in the expanding gamma-ray burst (GRB) fireball convert roughly equal energy into the acceleration of electrons and cosmic rays.[46] It so happens that 2×10^{51} erg per GRB will yield the observed energy density in cosmic rays after 10^{10} years, given that their rate is on the order of 300 per Gpc^3 per year. Hundreds of bursts per year over a Hubble time produce the observed cosmic-ray density, just as three supernovae per century accommodate the steady flux in the Galaxy.

Problem solved? Not really: it turns out that the same result can be achieved assuming that active galactic nuclei convert, on average, 2×10^{44} erg s^{-1} each into particle acceleration.[15] This is an amount that matches their output in electromagnetic radiation. An active galactic nucleus (AGN) is the center of a galaxy that hosts a supermassive black hole.

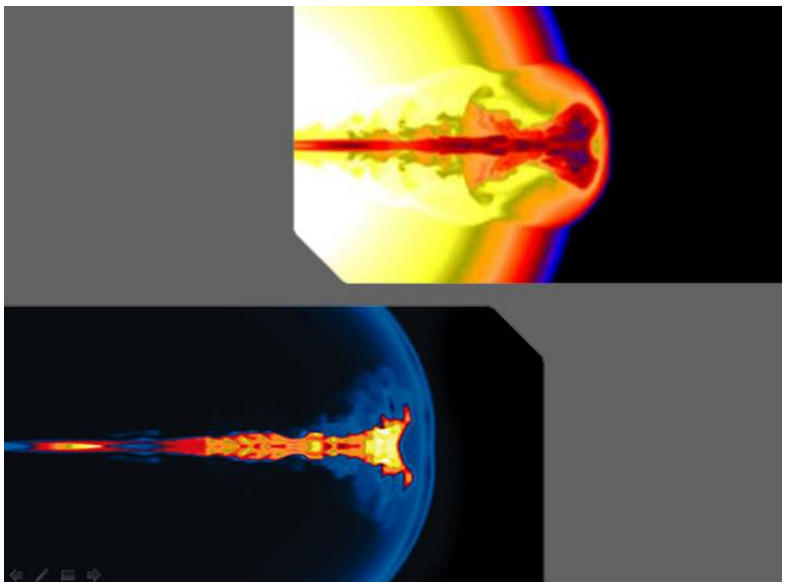

Fig. 8. Colliding shocks in the simulation of a gamma-ray burst (GRB) fireball may accelerate cosmic rays to the highest energies observed. The filaments in the particle flow are directed along the rotation axis of the black hole. Animated view at http://www.nasa.gov/centers/goddard/news/topstory/2003/0618rosettaburst.html.

We will return to this point further on.

3.2. *Neutrinos and Gamma Rays Associated with Cosmic Rays*

Neutrinos will be produced at some level in association with the cosmic-ray beam. Cosmic rays accelerated in regions of high magnetic fields near black holes or neutron stars inevitably interact with radiation surrounding them. Thus, cosmic-ray accelerators are also "beam dumps" producing neutrino beams. The method is what is used for the production of neutrino beams at accelerator laboratories: the beam is dumped in a dense target where it produces pions and kaons that decay into neutrinos. All particles are absorbed in the extended target except for the neutrinos. Cosmic rays accelerated in supernova shocks interact with gas in the Galactic disk, producing equal numbers of pions of all three charges that decay into pionic photons and neutrinos. A larger source of secondaries is likely to be gas near the sources, for example cosmic rays interacting with high-density molecular clouds that

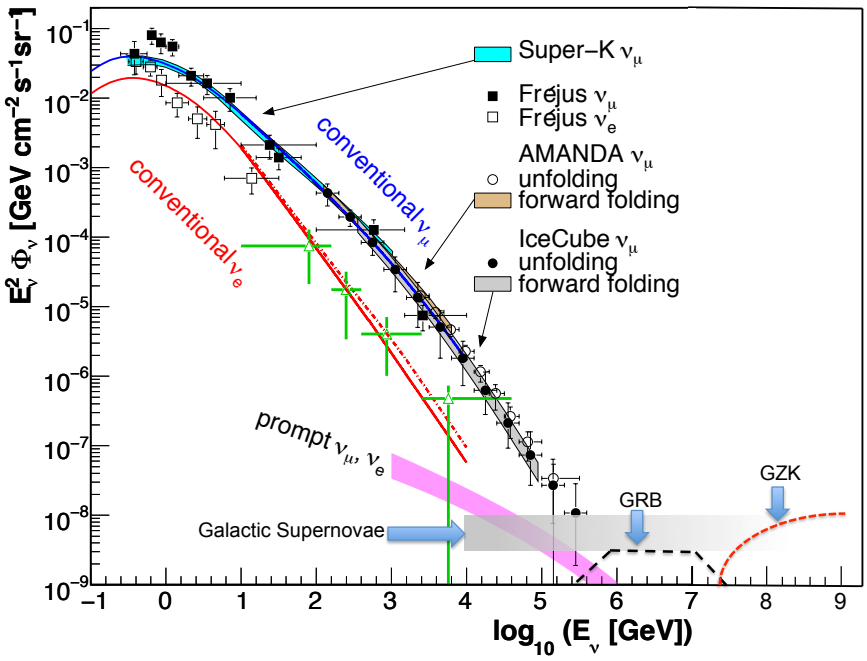

Fig. 9. Anticipated astrophysical neutrino fluxes compared with measured and calculated fluxes of atmospheric neutrinos. Measurements of ν_μ from Super-K,[47] Frejus,[48] AMANDA,[49,50] and IceCube[31,51] are shown along with the electron-neutrino spectrum at high energy from Ref.[32] (green open triangles). Calculations of conventional ν_e (red line) and ν_μ (blue line) from Honda et al.,[52] ν_e (red dotted line) from Bartol,[53] and charm-induced neutrinos (magenta band)[37] are also shown.

are ubiquitous in the star-forming regions where supernovae are more likely to explode. For extragalactic sources, the neutrino-producing target may be electromagnetic, for instance photons radiated by the accretion disk of an AGN, or synchrotron photons that coexist with protons in the expanding fireball producing a GRB. In Fig. 9, estimates of astrophysical neutrino fluxes are compared with measurements of atmospheric neutrinos. The shaded band indicates the level of model-dependent expectations for high-energy neutrinos of astrophysical origin. The estimates that we will discuss in more detail further on optimistically predicted a neutrino flux at a level of

$$E_\nu^2 \, \mathrm{d}N_\nu/\mathrm{d}E_\nu \simeq 10^{-8} \, \mathrm{GeV \, cm^{-2} s^{-1} sr^{-1}} \tag{10}$$

per flavor and formed the rationale for building a kilometer-scale detector; this is indeed the magnitude of the cosmic component of the neutrino spectrum above 100 TeV revealed by IceCube's data.

How many neutrinos and, inevitably, gamma rays are produced in association with the cosmic-ray beam? Generically, a cosmic-ray source should also be a beam dump. Cosmic rays accelerated in regions of high magnetic fields near black holes may interact with radiation surrounding them, e.g., UV photons in some active galaxies or MeV photons in GRB fireballs. In these interactions, neutral and charged pion secondaries are produced by the processes

$$p + \gamma \to \Delta^+ \to \pi^0 + p \;\text{ and }\; p + \gamma \to \Delta^+ \to \pi^+ + n. \tag{11}$$

While secondary protons may remain trapped and lose energy in the high magnetic fields, neutrons and the decay products of neutral and charged pions escape with high energy. The energy escaping the source is therefore distributed among cosmic rays, gamma rays and neutrinos, particles produced by the decay of neutrons, neutral pions and charged pions, respectively.

Galactic supernova shocks are in contrast an example of a hadronic beam dump. Cosmic rays mostly interact with the hydrogen in the Galactic disk, producing equal numbers of pions of all three charges in hadronic collisions $p + p \to n_\pi\,[\,\pi^0 + \pi^+ + \pi^-] + X$; n_π is the pion multiplicity.

In a generic cosmic beam dump, accelerated cosmic rays, assumed to be protons for illustration, interact with a photon target. These may be photons radiated by the accretion disk in AGNs and synchrotron photons that co-exist with protons in the exploding fireball producing a GRB. Their interactions produce charged and neutral pions according to Eq. 11, with probabilities of 2/3 and 1/3, respectively. Subsequently, the pions decay into gamma rays and neutrinos that carry, on average, 1/2 and 1/4 of the energy of the parent pion. We further assume that, on average, the four leptons in the decay $\pi^+ \to \nu_\mu + \mu^+ \to \nu_\mu + (e^+ + \nu_e + \bar{\nu}_\mu)$ equally share the charged pion's energy. The energy of the pionic leptons relative to the proton is:

$$x_\nu = \frac{E_\nu}{E_p} = \frac{1}{4}\langle x_{p\to\pi}\rangle \;\simeq\; \frac{1}{20} \tag{12}$$

and

$$x_\gamma = \frac{E_\gamma}{E_p} = \frac{1}{2}\langle x_{p\to\pi}\rangle \;\simeq\; \frac{1}{10}. \tag{13}$$

Here,

$$\langle x_{p\to\pi}\rangle \;=\; \langle\frac{E_\pi}{E_p}\rangle \;\simeq\; 0.2 \tag{14}$$

is the average energy transferred from the proton to the pion.

While both gamma-ray and neutrino fluxes can be calculated knowing the density of the accelerated protons and the density of the target material, their relative flux is independent of the details of the production mechanism. The spectral production rates $\mathrm{d}N/\mathrm{d}E\mathrm{d}t$ of neutrinos and gamma rays are related by

$$\frac{1}{3}\sum_{\nu_\alpha} E_\nu \frac{\mathrm{d}N_\nu}{\mathrm{d}E_\nu \mathrm{d}t}(E_\nu) \simeq \frac{K_\pi}{2} E_\gamma \frac{\mathrm{d}N_\gamma}{\mathrm{d}E_\gamma \mathrm{d}t}(E_\gamma)\,. \tag{15}$$

Here, N and E denote the number and energy of neutrinos and gamma rays and ν stands for the neutrino flavor. Note that this relation is solid and depends only on the charged-to-neutral secondary pion ratio, with $K_\pi = 1(2)$ for $\gamma(pp)$ neutrino-producing interactions. In deriving the relative number of neutrinos and gamma rays, one must be aware of the fact that the neutrino flux represents the sum of the neutrinos and antineutrinos, which cannot be separated by current experiments: in short, a π^0 produces two γ rays for every charged pion producing a $\nu_\mu + \bar{\nu}_\mu$ pair. A more formal derivation of this relation will be given in Section 7.

The production rate of gamma rays described by Eq. 15 is not necessarily the emission rate observed. For instance, in cosmic accelerators that efficiently produce neutrinos via $p\gamma$ interactions, the target photon field can also efficiently reduce the pionic gamma rays via pair production. This is a calorimetric process that will, however, conserve the total energy of hadronic gamma rays. The production of photons in association with cosmic neutrinos is inevitable. The relation is however calorimetric; unlike neutrinos, photons reach Earth after propagation in the universal microwave and infrared photon backgrounds to reach our telescopes with TeV energy, or below. Also, one must be aware of the fact that inverse-Compton scattering and synchrotron emission by accelerated electrons in magnetic fields in the source have the potential to produce gamma rays; not every high-energy gamma ray is pionic.

The estimates in Fig. 9 of the neutrino flux associated with cosmic rays accelerated in supernova remnants and GRBs are relatively straightforward as both the beam, identified with the observed cosmic-ray flux, and the targets, observed by astronomers, are known. In the case of supernova remnants, the main uncertainty is the availability of nearby target material.

In the case of GRBs, the main uncertainty is the fraction of the extragalactic cosmic ray population that comes from this source. The ongoing search by IceCube for neutrinos in coincidence with and in the direction of GRB alerts issued by astronomical telescopes has limited the GRB neutrino flux to less that 1% of the diffuse cosmic neutrino flux actually observed by the experiment.[54,55] However, this may not conclusively rule out GRBs as a source of cosmic rays; the events that produce the spectacular photon displays catalogued by astronomers as GRBs may not be the stellar collapses that are sources of high-energy neutrinos. We will return to this point further on when we discuss acceleration of cosmic rays in GRB fireballs. Nevertheless, the failure of IceCube to observe neutrinos from GRBs has lately promoted AGNs as the best-bet source of the cosmic neutrinos observed.

Active galaxies are complex systems with many possible sites for accelerating cosmic rays and for targets to produce neutrinos. First, if acceleration occurs mainly at the spectacular termination shocks of the jets in intergalactic space,[56] there would be little target material available and few neutrinos produced. In contrast, production of neutrinos near the black hole,[57] or in collisions with interstellar matter of the accelerated particles diffusing in the magnetic field of the galaxy hosting the black hole,[58] could yield fluxes at the level observed. We will work through these examples further on.

One generic picture in which the neutrino luminosity is directly related to the contribution of the sources to extragalactic cosmic rays arises if acceleration occurs in the jets of AGNs (or GRBs).[59,60] High-energy protons interact in the intense radiation fields inside the jets. In the $p\gamma \to p\pi^0$ channel, the protons remain in the accelerator. In the $p\gamma \to n\pi^+$ channel, however, the neutrons escape and eventually decay to produce cosmic-ray protons, while the pions decay to neutrinos. The luminosity of neutrinos from photo-pion production is then directly related by kinematics to the cosmic-ray protons that come from decay of the escaping neutrons.

TeV gamma rays are measured from many AGN blazars.[62] Although the observed gamma rays are likely to be from accelerated electrons, which radiate more efficiently than protons, the gamma-ray luminosity may give an indication of the overall cosmic-ray luminosity and hence of the possible level of neutrino production.[63,64] In this context, we introduce Fig. 10[65] showing IceCube upper limits[61] on the neutrino flux from nearby AGNs as a function of their distance. The sources at red shifts between 0.03 and 0.2 are Northern Hemisphere blazars for which distances and intensities are listed

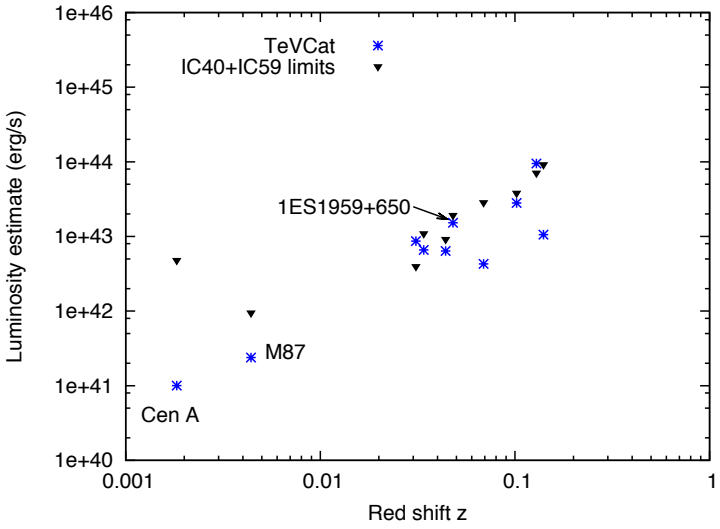

Fig. 10. Limits on the neutrino flux from selected active galaxies derived from IceCube data taken during construction, when the instrument was operating with 40 and 59 strings of the total 86 instrumented strings of DOMs.[61] These are compared with the TeV photon flux for nearby AGNs. Note that energy units are in ergs, not TeV.

in TeVCat[62] and for which IceCube also has upper limits. In several cases, the muon-neutrino limits have reached the level of the TeV photon flux. One can sum the sources shown in the figure into a diffuse flux. The result, after accounting for the distances and luminosities, is $3\times10^{-9}\,\mathrm{GeV\,cm^{-2}\,s^{-1}\,sr^{-1}}$, or approximately $10^{-8}\,\mathrm{GeV\,cm^{-2}\,s^{-1}\,sr^{-1}}$ for all neutrino flavors. This is at the level of the generic astrophysical neutrino flux of Eq. 10. At this intensity, neutrinos from theorized cosmic-ray accelerators will cross the steeply falling atmospheric neutrino flux above an energy of $\sim 300\,\mathrm{TeV}$; see Fig. 9. The level of events observed in a cubic-kilometer neutrino detector is $10 \sim 100$ ν_μ-induced events per year. Such estimates reinforce the logic for building a cubic kilometer neutrino detector.[66]

4. Neutrinos Associated with Cosmic Ray Accelerators

In this section we will introduce the generic framework used to calculate the neutrino flux associated with a astronomical source that accelerate a proton beam to energies exceeding the threshold for producing pions that decay into neutrinos. Next, we will apply the formalism to three examples: the production of neutrinos in active galaxies when protons accelerated near the black hole interact with nearby gas or radiation fields, the production of neutrinos in the interactions of Galactic cosmic rays with nearby gas or molecular clouds, and, finally, the production of neutrinos when protons interact with photons in the relativistically expanding fireball following stellar collapse, such as in a gamma ray burst.

4.1. *Neutrino-Producing Cosmic Beam Dumps*

Neutrinos are produced when pions, and, at higher energies, kaons and charm particles decay. We start by calculating the number of pions produced when an accelerated proton beam interacts with a target of density n in its vicinity. We introducing the source function $q_\pi(E_\pi)$ defined such that $q_\pi(E_\pi)\,dE_\pi$ represents the rate at which pions are produced within the energy range E_π and $E_\pi + dE_\pi$ per time:

$$q_\pi = \frac{dN_\pi}{dE_\pi dt} = \int dE_p \int_0^\tau d\tau' \frac{dN_p}{dE_p}\, e^{-\tau'}\, \frac{dN_\pi}{dE_\pi}(E_\pi)\ . \tag{16}$$

Here a proton beam, with a flux dN/dE_p, in units $GeV^{-1}cm^{-2}s^{-1}$, is absorbed in a target with optical depth τ producing secondary pions with an energy distribution dN_π/dE_π, normalized to unity. In the case that all pions are produced with the same energy

$$\frac{dN_\pi(E_p)}{dE_\pi} = n_{\pi^\pm}\,\delta\left(E_\pi - \langle E_\pi\rangle\right)\ , \tag{17}$$

where we assume that a multiplicity of n_π secondary pions are produced with average energy $< E_\pi >$. The optical depth of the target is

$$\tau = \exp(-\int_0^l dr'\alpha(r'))\,, \tag{18}$$

where l is the path length of the beam in a target and α is the attenuation coefficient (the inverse of the mean-free path λ) which is determined by the cross section and the density n

$$\alpha = n\sigma\,, \tag{19}$$

and, assuming isotropy,

$$\tau = nl\sigma \ = N\sigma \,, \tag{20}$$

where N is the optical depth.

Typically, one also makes the approximation that the proton cross section is independent of energy, $\sigma \approx 3 \cdot 10^{-26}$ cm^2 and therefore the integrals over τ and E_p separate:

$$q_{\pi^\pm} = (1 - \exp(-\tau)) \int dE_{\rm p} \, \frac{dN_p}{dE_p} \, n_\pi \, \delta \left(E_\pi - \langle E_\pi \rangle \right) \,, \tag{21}$$

In most astrophysical situations, where the optical depth is small, the pion production efficiency $(1 - \exp(-\tau)) \to \tau$, with $\tau = l \, n \, \sigma$.

The integral can be performed by rewriting the delta function as a function of E_p. Each time a proton interacts, it deposits $K_p E_p$ energy into $\langle n_\pi \rangle$ pions of average energy $\langle E_\pi \rangle$; here, K_p is the total proton inelasticity. Energy conservation implies that

$$K_p E_p = E_\pi^{tot} = n_{\pi^\pm} \, \langle E_\pi \rangle \ . \tag{22}$$

It is common to introduce at the is point the energy fraction f_π of the pions relative to the proton beam

$$f_\pi = \frac{\langle E_\pi \rangle}{E_p} = \frac{K_p}{n_\pi}. \tag{23}$$

We obtain the result that

$$q_{\pi^\pm} = \tau \, n_\pi \int dE_{\rm p} \frac{dN_p}{dE_p} \, \delta \left(E_\pi - f_\pi E_p \right) \,, \tag{24}$$

or

$$q_{\pi^\pm} = N \, \sigma \, n_\pi \, \frac{1}{f_\pi} \, \frac{dN_p}{dE_p} \left(\frac{E_\pi}{f_\pi} \right) \,. \tag{25}$$

The result is transparent: the pion source function is proportional to the intensity of the intensity of the proton beam, the optical depth of the target and the cross section, and the multiplicity of the pions produced.

We are now able to compute the rate at which sources are produced, with the total rate *at the source* given by the sum of the emissivities of the first muon neutrino, directly from the pion, and those of the second muon neutrino and the electron neutrino from the muon decay:

$$q_{\nu,\rm tot} = q^{(1)}_{\nu_\mu} + q^{(2)}_{\nu_\mu} + q_{\nu_e} \,. \tag{26}$$

As previously discussed, we will make the approximation that the total energy of the pions is distributed equally among the four decay leptons (see e.g., Ref.[67]),

$$q_{\nu_i}(E_{\nu_i}) = q_\pi(4E_{\nu_\imath}) dE_\pi / dE_{\nu_i} = 4 q_\pi(4E_{\nu_i}) \tag{27}$$

for each neutrino, $\nu_i = \overline{\nu}_e \,\text{or}\, \nu_\text{e}, \nu_\mu, \overline{\nu}_\mu$. As IceCube does not distinguish between neutrinos and antineutrinos, we will not separate them. In this approximation the number of neutrinos produced per flavor in the energy bin dE_ν originate from the original pion in the energy bin $dE_\pi = 4dE_\nu$; therefore, $q_\nu(E_\nu)\, dE_\nu = q_\pi(4\, E_\nu) dE_\pi$.

The point source flux observed at Earth is $q_\nu(E_\nu)/4\pi r^2$, where r is the distance to the source. So far IceCube has not pinpointed such a flux, instead it discovered a diffuse flux from a, yet unidentified, source population with uniform density $\rho(r)$ in the Universe. We introduce the diffuse flux

$$\Phi = \frac{1}{4\pi} \int d^3r\, \rho\,(r)\, \frac{q_\nu\,(E_\nu)}{4\pi r^2}\,, \tag{28}$$

where the first factor $1/4\pi$ is introduced in order to define the diffuse flux with the conventional units $GeV^{-1}cm^{-2}s^{-1}sr^{-1}$. We obtain the result

$$\Phi = \frac{1}{4\pi} \int dr\, 4\pi r^2 \rho\,(r)\, \frac{q_\nu\,(E_\nu)}{4\pi r^2}\,, \tag{29}$$

or

$$\Phi = \frac{1}{4\pi} \int dr \rho\,(r)\, q_\nu\,(E_\nu)\ . \tag{30}$$

This is the Euclidian result which can at best be an approximation for nearby sources. Integrating over the cosmology of the Universe is done by changing the integration from $dr \Rightarrow cdt \Rightarrow cdz(dt/dz)$, with $dz/dt = H(z)$, the Hubble scaling factor. We thus can rewrite the integral in covariant form

$$\Phi = \frac{c}{4\pi} \int \frac{dz}{H\,(z)}\, \rho\,(z)\, q_\nu\,((1+z)\, E_\nu)\ . \tag{31}$$

For the standard ΛCDM cosmological model, the Hubble parameter scales as $H^2(z) = H_0^2[(1+z)^3\Omega_\text{m} + \Omega_\Lambda]$, with $\Omega_\text{m} \simeq 0.3$, $\Omega_\Lambda \simeq 0.7$, and $c/H_0 \simeq 4.4$ Gpc.[68] A more formal derivation on how to introduce the cosmological evolution of the sources can be found in section 6.2.

In the following, we will assume that the neutrino emission rate q_{ν_α} follows a power law $E^{-\gamma}$. The flavor-averaged neutrino flux can then be written as

$$\frac{1}{3}\sum_\alpha E_\nu^2 \phi_{\nu_\alpha}(E_\nu) = \frac{c}{4\pi}\frac{\xi_z}{H_0}\rho_0 \frac{1}{3}\sum_\alpha E_\nu^2 q_{\nu_\alpha}(E_\nu)\,, \tag{32}$$

where we introduce the redshift factor

$$\xi_z = \int_0^\infty \text{d}z \frac{(1+z)^{-\gamma}}{\sqrt{\Omega_\Lambda + (1+z)^3\Omega_\text{m}}} \frac{\rho(z)}{\rho(0)}\,. \tag{33}$$

A spectral index of $\gamma \simeq 2.0$ and no source evolution, $\rho(z) = \rho_0$, yields $\xi_z \simeq 0.6$, whereas the same spectral index and source evolution following the star formation rate yields $\rho \simeq 2.4$.

The identical procedure can be followed for the production of neutral pions that subsequently decay into two gamma rays. This will lead to Eq. 15, previously introduced.

4.2. *Cosmic Neutrinos and Ultra-High-Energy Cosmic Rays*

The charged pion production rate $q_{\pi^\pm}$ is proportional to the density of the protons in the cosmic accelerator beam that produces the pions, q_p, by the "bolometric" proportionality factor $f_\pi \leq 1$ introduced above. For, both, *pp* and $p\gamma$ interactions $f_\pi = K_p/n_\pi \simeq 0.2$. The average energy per pion is then $\langle E_\pi \rangle = f\pi E_p$, and the average energy of the pionic leptons relative to the nucleon is $\langle E_\nu \rangle \simeq \langle E_\pi \rangle/4 = (f_\pi/4)E_N \simeq 0.05 E_p$. In summary f_π denotes the average inelasticity *per pion* and therefore normalizes the conversion of proton energy into pion energy on the target. Therefore:

$$E_\pi^2 q_{\pi^\pm}(E_\pi) \simeq f_\pi \, \frac{K_\pi}{1+K_\pi} \, \left[E_p^2 q_p(E_p)\right]_{E_p = E_\pi/f_\pi} \, , \tag{34}$$

with, as before, $K_\pi \simeq 2$ for *pp* and $K_\pi \simeq 1$ for $p\gamma$ interactions.

In many application the accelerated "proton" beam is associated with the observed flux of cosmic rays. The association is often introduced to investigate a possible common origin of the extragalactic cosmic rays and the IceCube cosmic neutrinos. Do they have common sources?

In general, the "proton" emission rate, q_p, has to be generalized to the composition of the cosmic rays; using superposition one can relate the spectra of nuclei with mass number A as $q_N(E_N) = \sum_A A^2 q_A(AE_N)$. One can derive an upper limit on the diffuse cosmic neutrino flux by assuming that the flux of the extragalactic neutrinos is dominated by protons and that the sources are transparent, i.e. $f_\pi << 1$.[69,70] The local emission rate *density* of cosmic rays is given by $Q_p = \rho_0 \times q_p$, where ρ is the local density of the sources. It is insensitive to the luminosity evolution of sources at high redshift and can be estimated from the measured spectra to be at the level of $\left[E_p^2 \, Q_p(E_p)\right]_{10^{19.5}\mathrm{eV}} \sim (0.5-2.0) \times 10^{44} \mathrm{erg/Mpc^3/yr}$.[71–73] Note, that measurements indicate that the mass composition above the ankle also requires a contribution of heavier nuclei. However, the estimated local UHE CR power density based on proton models is a good proxy for that of UHE CR models including heavy nuclei, as long as the spectral index is close to $\gamma \simeq 2$. For instance, a recent analysis of Auger[74] provides a

solution with spectral index $\gamma \simeq 2.04$ and a combined nucleon density of $[E_N^2 Q_N(E_N)]_{10^{19.5}\mathrm{eV}} \sim 2.2 \times 10^{43}\,\mathrm{erg/Mpc^3/yr}$.

4.2.1. *Example I: Neutrino Production in Active Galaxies*

An active galaxy presents multiple opportunities for the acceleration of particles in the inflows and outflows associated with a supermassive black hole. The high-energy particles may subsequently produce neutrinos in interactions with a variety of possible targets such as the dense matter near the black hole, the hydrogen in the galactic disk of the galaxy associated with the black hole and photons produced in the jet or radiated from the accretion disk on the black hole. It is therefore useful to start by considering a generic beam dump where a beam of protons with an initial flux dN_p/dE_p interacts with a target of density n over a distance l using the formalism introduced above. For analytic calculations one can use the a parameterization that allows for the increase of the pion multiplicity with proton energy starting from a pair of pions produced at threshold E_{th} in the reaction $pp \to pp + \pi^+\pi^-$:[75]

$$\langle n_{\pi^\pm} \rangle = 2 \left(\frac{E_p - E_{th}}{\mathrm{GeV}} \right)^{1/4}, \tag{35}$$

and

$$\langle E_\pi \rangle = \frac{1}{6}(E_p - m_p c^2)^{3/4}\,\mathrm{GeV}. \tag{36}$$

The approximations reproduce the results of simulations. Given the number of protons produced by the accelerator per energy and time interval

$$\frac{dN_p}{dE_p} = A_p \left(\frac{E_p - m_p c^2}{\mathrm{GeV}} \right)^{-\gamma}, \tag{37}$$

we obtain a pion rate *at the source* using Eq. 21:

$$q_{\pi^\pm}(E_\pi) \approx 26\, n\, l\, A_p\, \sigma \left(\frac{6E_\pi}{\mathrm{GeV}} \right)^{-\frac{4}{3}(\gamma - \frac{1}{2})}. \tag{38}$$

The final result for the total neutrino emission rate at the source is given by

$$q_{\nu,\mathrm{tot}} \approx 3 \times 10^2\, n\, l\, A_p\, \sigma \left(\frac{24E_\nu}{\mathrm{GeV}} \right)^{-\frac{4}{3}\gamma + \frac{2}{3}}, \tag{39}$$

which provides us with an estimate of the total neutrino flux at the source in terms of three key quantities: A_p and γ, the normalization and spectral

slope of the flux of the accelerator, and the column density of the target $N \sim ln$. The spectral index is routinely taken to be $\gamma = 2$, a value suggested by diffusive shock acceleration and, in any case, typical for the spectra of gamma rays observed for nonthermal sources.

The column density $N = ln$ is taken from astronomical information, with l being the distance that the cosmic rays travel through a photon target of density n. For instance l could be the diffusion length of the cosmic rays in the magnetic field of the galaxy. This allows the protons to interact with the typical density of hydrogen of $n \simeq 1\,\mathrm{cm}^{-3}$ over an extended pathlength determined by the diffusion time. The diffusion distance before escaping galaxy is given by

$$d_{diff} = 2\sqrt{D(E_\mathrm{p})\,t_{esc}}\,, \tag{40}$$

where D is the diffusion coefficient and t_{esc} is the escape time. In this case, the size of the target is identified with $l = ct_{esc}$. For instance $l = 10$ kpc for our own Galaxy.

The normalization of the proton flux A_p can be obtained from the requirement that the aggregate diffuse proton flux from all AGN reproduces the cosmic ray flux observed at Earth.[58] He finds that this calculation also accommodates the diffuse high energy photon flux observed by Fermi. Alternatively, in Ref.[57] A_p is obtained from the radio luminosity of AGNs, L, resulting from the synchrotron radiation of accelerated electrons with $L_e = \chi L$ with $\chi \geq 1$. A_p is obtained from the assumptions that protons and electrons are connected by a constant fraction f_e: $L_\mathrm{e} = f_e L_\mathrm{p}$, which is on the order of 0.1:[57]

$$L_p = \int \frac{dN_\mathrm{p}}{dE_p}\,dE_p \approx \frac{\chi L}{f_e}\,, \tag{41}$$

and

$$A_p = A_p(L,z) = \frac{\chi L}{f_e}\left[\ln\left(E_\mathrm{max}/E_\mathrm{min}\right)\right]^{-1}\ \mathrm{GeV}^{-2} \tag{42}$$

for $\gamma = 2$; the generalization for $\gamma \neq 2$ is straightforward.

Having related the proton flux to the radio luminosity, we obtain the neutrino for a single AGN from Eq. 39. The diffuse flux that can be confronted with the IceCube data is obtained using the formalism for summing over the sources previously introduced:

$$\Phi_\nu = \int_L \int_z \frac{q_{\nu,tot}}{4\,\pi\,d_L(z)^2}\,\frac{dn_\mathrm{AGN}}{dV\,dL}\,\frac{dV}{dz}\,dz\,dL\,. \tag{43}$$

Here, d_L is the luminosity distance, $dn_\mathrm{AGN}/(dV\,dL)$ is the radio luminosity function of the AGN, and dV/dz is the comoving volume at a

fixed redshift z. The radio luminosity function is usually separated into the product of a luminosity-dependent and a redshift-dependent function, $dn_{\rm AGN}/(dV\,dL) = g(L)f(z)$. The result matches the IceCube observations; more details can be found in Ref.[57] for column densities typical for the relatively dense matter near the black hole.

The two calculations illustrate how two different mechanisms manage to accommodate the IceCube result. Hooper normalizes the proton flux to the cosmic ray flux and generates the neutrino flux by diffusing the protons through the Galaxy, while Tjus *et al.* relate the proton flux to the radio emission of the galaxies and produce the neutrinos in the dense matter near the supermassive black hole.

AGNs are episodic sources producing gamma rays in bursts, with episodes where the flux increases by over one order of magnitude for periods of seconds to days, sometimes even years. A correlation of the arrival of IceCube neutrinos in coincidence with such bursts can provide a smoking gun for their origin; for a recent discussion, see Ref.[76]

4.2.2. *Example II: Neutrino Production in the Jets of Active Galaxies*

Blazars are the brightest sources of high energy gamma rays in the Universe making up most, if not all, of the diffuse extragalactic gamma ray flux. We will show later that the diffuse cosmic neutrino flux observed by IceCube is likely to generate a significant fraction, possibly all, of these photons. Their engines must not only be powerful, but also extremely compact because their luminosities are observed to flare by over an order of magnitude over time periods that are occasionally as short as minutes. Blazars are AGN with the jet directly pointing at our telescopes thus further boosting the energy of the gamma rays and contracting the duration of the episodes of emission. The drawing of a blazar, shown in Fig. 11, displays its most prominent features: an accretion disk of stars and gas falling onto the spinning supermassive black hole as well as a pair of jets aligned with the rotation axis. Large magnetic fields originating from the inflow of particles on the black hole are wound up along the rotation axis and launch a pair of jets that are the site of the acceleration of electron and proton beams.

The energy spectrum E^2dN/dE of gamma rays radiated by a blazar jet shows the classic double-hump structure with lower energy gamma rays resulting from synchrotron radiation by a beam of accelerated electrons and a higher energy component resulting from inverse Compton scattering of

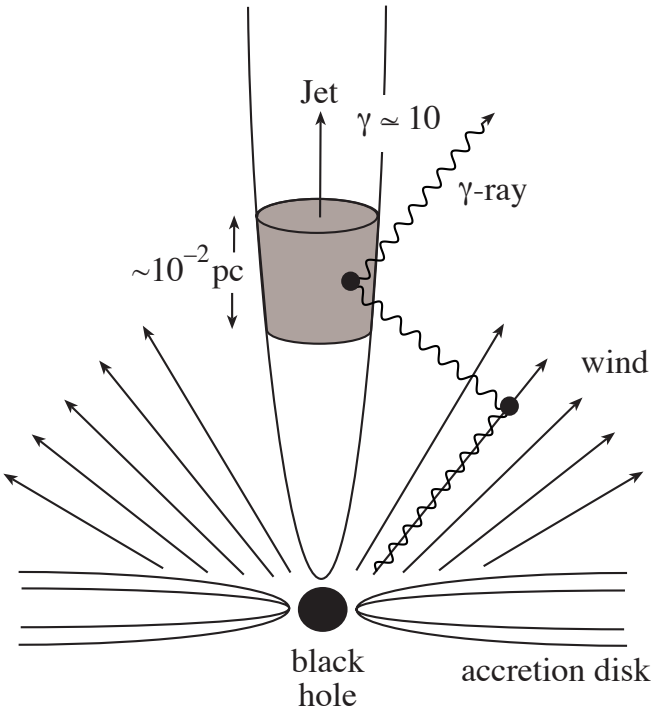

Fig. 11. Blueprint for the production of high energy photons and neutrinos near the super-massive black hole powering an AGN. Particles, electrons and protons, accelerated in sheets or blobs moving along the jet, interact with photons radiated by the accretion disk or produced by the interaction of the accelerated particles with magnetic fields. The jet is pointing at the Earth in the subclass of AGN dubbed blazars.

the same photons. Because of their reduced synchrotron radiation, protons, unlike electrons, efficiently transfer energy in the presence of the magnetic field in the jet. They provide a mechanism for the energy transfer from the central engine over distances as large as 1 parsec as well as for the observed heating of the dusty disk over distances of several hundred parsecs. If protons are accelerated along with the electrons multiple opportunities exist

for the production of neutrinos by pion photoproduction, e.g. in interactions with the synchrotron photons, or photons radiated off the accretion disk and the dusty torus in the AGN. The protons may also interact with the broadline emission clouds.

While the relative merits of the electron and proton blazar are hotly debated, the issue has been settled by the first multiwavelength detection of a flaring blazar TXS0506+056 in coincidence with an IceCube cosmic neutrino IC170922. The opportunities for studying the first identified cosmic ray accelerator are wonderfully obvious.

Confronted with the challenge of explainig a $\sim E^{-2}$ high-energy photon emission spectrum reaching TeV energies, which is occassionally radiated in bursts of a duration of less than one day, models have converged on the blazar blueprint shown in Fig. 11. Particles are accelerated by shocks in blobs of matter traveling along the jet with a bulk Doppler (Lorenz) factor of $\Gamma \sim 10$ and higher. This factor combines the effects of special relativity and the geometry of the moving source. The jet consists of relatively small structures with short lifetime often referred to as blobs. In the following, primes will refer to a reference frame attached to the blob, which is moving with a Doppler factor Γ relative to the observer. In general, the transformation between blob and observer frame is $R' = \Gamma R$ and $E' = \frac{1}{\Gamma} E$ for distances and energies, respectively. Blazar bursts appear more spectacular to the observer than they actually are because, in the frame of the blob, distances are larger and times longer. High energy emission is associated with the periodic formation of these blobs. The blobs are clearly identified in X-ray images of AGN jets, e.g. in M87. In order to accommodate bursts lasting a day, or less, in the observer's frame, the size of the blob must be of order $\Gamma c \Delta t \sim 10^{-2}$ parsecs or less. The blobs are actually more like sheets, thinner than the jet's size of roughly 1 parsec. The observed radiation at all wavelengths is produced by the interaction of the accelerated electrons and protons in the blob with the multiple radiation fields in the complex AGN structure, for instance synchrotron photons produced by electrons or the ambient radiation in the AGN which has a significant prominent component concentrated in the so-called "UV-bump"of $\sim 10\,\mathrm{eV}$ photons.

In order for a proton accelerated in the jet to produce pions on target photons of energy E_γ, a process dominated by the photoproduction of the Δ resonance, it must exceed the threshold energy:

$$E'_p > \frac{m_\Delta^2 - m_p^2}{4} \, \frac{1}{E'_\gamma} \,, \tag{44}$$

or,

$$E_p > \Gamma^2 \, \frac{m_\Delta^2 - m_p^2}{4E_\gamma} \, . \tag{45}$$

Furthermore, the blob must be transparent to gamma rays that are actually detected at Earth from the burst. Therefore the center-of-mass energy s must be below the threshold for $\gamma + \gamma$ interactions in the blob, or

$$s < (2m_e)^2 \, , \tag{46}$$

or,

$$E_\gamma E_{\gamma,obs} < \Gamma^2 m_e^2 \, . \tag{47}$$

The kinematic constraints imply that Γ must exceed a few (~ 40) for target photon energies 10 eV (1 KeV) typical for UV (synchrotron) photons. These values of Γ render the jet transparent to 50 GeV (500 GeV) photons, for example.

From the observed luminosity L_γ we deduce the energy density of photons in the shocked region of size R':

$$u'_\gamma = \frac{L'_\gamma \Delta t}{\frac{4}{3}\pi R'^3} = \frac{L_\gamma \Delta t}{\Gamma} \, \frac{1}{\frac{4}{3}\pi (\Gamma c \Delta t)^3} = \frac{3}{4\pi c^3} \, \frac{L_\gamma}{\Gamma^4 \Delta t^2} \, , \tag{48}$$

where Δt is the duration of the flare. The fraction of energy f_π lost by protons to pion production when traveling a distance R' through a photon field of density $n'_\gamma = u'_\gamma / E'_\gamma$ is given by the number of interactions lengths of the proton fitting inside the photon target of size R':

$$f_\pi = \frac{R'}{\lambda_{p\gamma}} = R' n'_\gamma \sigma_{p\gamma \to \Delta} \, \langle x_{p\to\pi} \rangle \tag{49}$$

where $\lambda_{p\gamma}$ is the proton interaction length, with $\sigma_{p\gamma\to\Delta\to n\pi^+} \simeq 10^{-28}\,\mathrm{cm}^2$ and $\langle x_{p\to\pi}\rangle \simeq 0.2$ the energy transferred from the proton to the pion. The final result is given by

$$f_\pi \simeq \frac{R'}{\lambda_{p\gamma}} \simeq \frac{L_\gamma}{E_{\rm ph}} \frac{1}{\Gamma^2 \Delta t} \frac{3\sigma_\Delta \langle x_{p\to\pi}\rangle}{4\pi c^2} \, . \tag{50}$$

If f_π approaches unity, pions will be absorbed before decaying into neutrinos, requiring the substitution of f_π by $1 - e^{-f_\pi}$.

For a total injection rate in high-energy protons $E_N^2 Q_N$, the total energy in neutrinos is $1/2 f_\pi t_H E_N^2 Q_N$, where $t_H \sim 10^{10}$ Gyr is the Hubble time. The secondary ν_μ have energy $E_\nu = x_\nu E_p$, with $x_\nu \simeq 0.05$, the fraction of energy transferred, on average, from the proton to the neutrino via the

Δ-resonance. The factor 1/2 accounts for the fact that 1/2 of the energy in charged pions is transferred to $\nu_\mu + \bar{\nu}_\mu$, see above. The neutrino flux is

$$\Phi_\nu = E_\nu \frac{dN}{dE_\nu} = \frac{c}{4\pi}\frac{1}{E_\nu}\,[\frac{1}{2} f_\pi\, t_H\, E_N^2 Q_N]\,, \tag{51}$$

There is another more direct way to approach the problem that, additionally, allows for the fact that these sources are variable on all scales, e.g. the neutrino flare observed from TXS 0506+056 by IceCube covered a period $\Delta t \simeq 110$ days. When discussing the IceCube observations later on we will show that such flaring blazars are capable of reproducing the observed cosmic neutrinos flux provided that their efficiency for producing pions, f_π, is close to unity. The desired result can be achieved when protons in neutrino-producing blazar jets interact with the 10 eV photons in the galaxy (the blue bump) via the Δ-resonance; $p\gamma \to \Delta \to \pi N$. The pion efficiency of the jet depends on the Lorentz factor of the jet (Γ), the target photon energy (E_γ), luminosity of the target photons (L_γ), and the duration of the flare (Δt), for instance,

$$f_\pi \simeq \frac{L_\gamma}{E_\gamma}\frac{1}{\Gamma^2 \Delta t}\frac{3\sigma_\Delta \langle x_{p\to\pi}\rangle}{4\pi c^2}\,, \tag{52}$$

and

$$f_\pi = 0.8 - 10 \simeq \left(\frac{L_\gamma}{(4-6)\times 10^{46}\,\mathrm{erg/s}}\right)\left(\frac{10\,\mathrm{eV}}{E_\gamma}\right)\left(\frac{1}{\Gamma^2}\right)\left(\frac{110\,\mathrm{d}}{\Delta t}\right) \times\left(\frac{3\sigma_\Delta \langle x_{p\to\pi}\rangle}{4\pi c^2}\right) \tag{53}$$

This suggests that sources with small Lorentz factor of the jet and a UV luminosity exceeding $\mathcal{O}(10^{46})$ is required for production of high-energy cosmic neutrinos. This level of UV luminosity has been reported in reference.[77]

We will revisit blazars when we discuss the discovery of the first blazar TXS 0506+056 in both neutrinos and gamma rays.

4.3. *Generic Fireballs*

Whereas we have confidence that the electromagnetic radiation in some Galactic sources is produced by the decay of neutral pions, there is no straightforward gamma-ray path to the neutrino flux expected from extragalactic cosmic-ray accelerators. We presented model calculations to show that AGNs can plausibly accommodate the cosmic neutrino flux observed,

assuming that they accelerate protons at the level of the sources of the extragalactic cosmic rays. In fact, we showed how very different blueprints for the beam dump can fit the diffuse neutrino flux observed. As already discussed, there is an yet another possibility. Massive stars collapsing to black holes and observed by astronomers as GRBs have the potential to accelerate protons to 100 EeV energy. Neutrinos of 100 TeV − PeV energy should be produced by pion photoproduction when protons and photons coexist in the GRB fireball.[78] As previously discussed, the model is promising because the observed cosmic-ray flux can be accommodated with the assumption that roughly equal energy is shared by electrons, observed as synchrotron photons, and protons. Indeed, the IceCube observations indicate equal extragalactic energy densities of photons and neutrinos, as we will see further on.

The phenomenology that successfully accommodates the astronomical observations is the creation of a hot fireball of electrons, photons, and protons that is initially opaque to radiation. The hot plasma therefore expands by radiation pressure, and particles are accelerated to a Lorentz factor Γ that grows until the plasma becomes optically thin and produces the GRB display. From this point on, the fireball coasts with a Lorentz factor that is constant and depends on its baryonic load. The baryonic component carries the bulk of the fireball's kinetic energy. The energetics and rapid time structure of the burst can be successfully associated with successive shocks (shells), of width ΔR, that develop in the expanding fireball. The rapid temporal variation of the gamma-ray burst, t_v, is on the order of milliseconds and can be interpreted as the collision of internal shocks with a varying baryonic load leading to differences in the bulk Lorentz factor. Electrons, accelerated by first-order Fermi acceleration, radiate synchrotron gamma rays in the strong internal magnetic field and thus produce the spikes observed in the burst spectra.

The usual approach followed in the interpretation of routine IceCube GRB searches[79] has the proton content of the fireball derived from the observed electromagnetic emission. The basic assumption is that a comparable amount of energy is dissipated in fireball protons and electrons, where the latter are observed as synchrotron radiation,

$$E^2 \frac{dN_\nu}{dE} = \left(\frac{\epsilon_p}{\epsilon_e}\right) \frac{1}{2}\, x_\nu \left[E_\gamma^2 \frac{dN_\gamma}{dE_\gamma}(E_\gamma)\right]_{\rm syn}, \tag{54}$$

where ϵ_p and ϵ_e are the energy fractions in the fireball in protons and electrons,[79] respectively. One can then use the data to determine the baryon

loading in the GRB fireball, $\epsilon_p \,/\, \epsilon_e$. Within this framework one can estimate the baryon loading or relative abundance of protons and electrons in the fireball from the neutrino observations; no prediction is made. The abundance of protons in the fireball is determined, or, at present, limited by the observations.[54]

Although simulations of GRB fireballs have reached a level of sophistication,[80] a simple energy estimate is sufficient to predict the neutrino flux associated with GRB fireballs assuming that they are the sources of the cosmic rays.

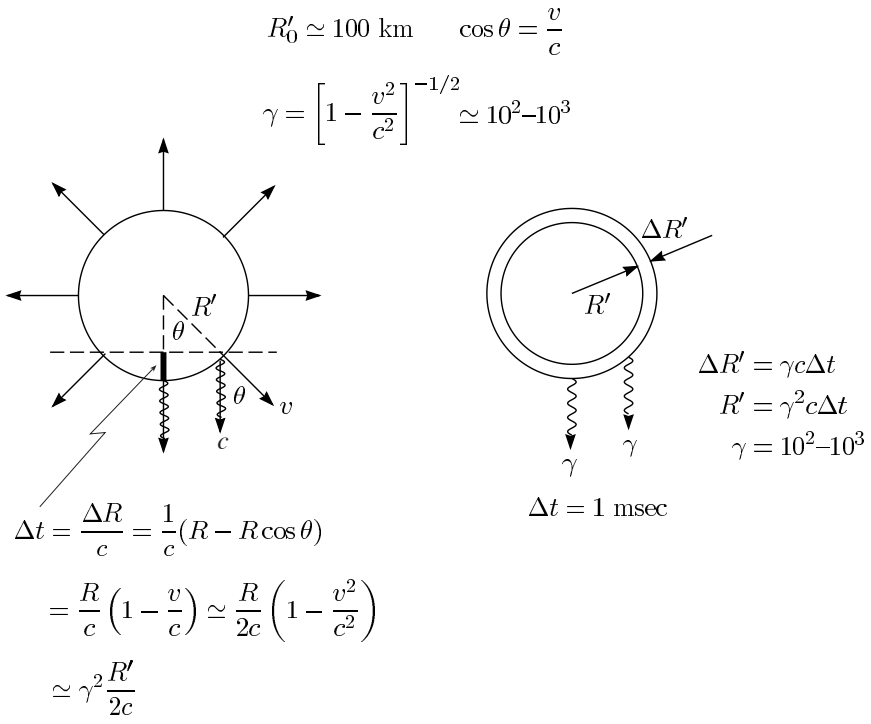

Fig. 12. Kinematics of a relativistically expanding fireball on the left, and the resulting shell(s) expanding under radiation pressure on the right.

Simple relativistic kinematics (see Fig. 12) relates the radius and width

R' and $\Delta R'$ to the observed duration of the photon burst $c\Delta t$:

$$R' = \gamma^2 (c\Delta t) \tag{55}$$

$$\Delta R' = \gamma c \Delta t \tag{56}$$

From the observed GRB luminosity L_γ, we compute the photon energy density in the shell:

$$U'_\gamma = \frac{(L_\gamma \Delta t)/\gamma}{4\pi R'^2 \Delta R'} = \frac{L_\gamma}{4\pi \Delta t^2 c^3 \gamma^6} \tag{57}$$

The pion production by shocked protons in this photon field is, as before, calculated from the interaction length:

$$\frac{1}{\lambda_{p\gamma}} = N_\gamma \sigma_\Delta \langle x_{p\to\pi}\rangle = \frac{U'_\gamma}{E'_\gamma}\sigma_\Delta \langle x_{p\to\pi}\rangle \qquad \left(E'_\gamma = \frac{1}{\gamma}E_\gamma\right). \tag{58}$$

Also as before, σ_Δ is the cross section for $p\gamma \to \Delta \to n\pi^+$ and $\langle x_{p\to\pi}\rangle \simeq 0.2$. The fraction of energy going into π-production is

$$f_\pi \cong \frac{\Delta R'}{\lambda_{p\gamma}} \tag{59}$$

$$f_\pi \simeq \frac{1}{4\pi c^2}\frac{L_\gamma}{E_\gamma}\frac{1}{\gamma^4 \Delta t}\sigma_\Delta \langle x_{p\to\pi}\rangle \tag{60}$$

$$f_\pi \simeq 0.14 \left[\frac{L_\gamma}{10^{51}\,\mathrm{ergs}^{-1}}\right]\left[\frac{1\ \mathrm{MeV}}{E_\gamma}\right]\left[\frac{300}{\gamma}\right]^4\left[\frac{1\ \mathrm{msec}}{\Delta t}\right] \times \left[\frac{\sigma_\Delta}{10^{-28}\,\mathrm{cm}^2}\right]\left[\frac{\langle x_{p\to\pi}\rangle}{0.2}\right]. \tag{61}$$

The relevant photon energy in the problem is 1 MeV, the energy where the typical GRB spectrum exhibits a break. The contribution of higher energy photons is suppressed by the falling spectrum, and lower energy photons are less efficient at producing pions. Given the large uncertainties associated with the astrophysics, it is an adequate approximation to neglect the explicit integration over the GRB photon spectrum. The proton energy for production of pions via the Δ-resonance is

$$E'_p = \frac{m_\Delta^2 - m_p^2}{4E'_\gamma}. \tag{62}$$

Therefore,

$$E_p = 1.4 \times 10^{16}\,\mathrm{eV}\left(\frac{\gamma}{300}\right)^2\left(\frac{1\ \mathrm{MeV}}{\mathrm{E}_\gamma}\right) \tag{63}$$

$$E_\nu = \frac{1}{4}\langle x_{p\to\pi}\rangle E_p \simeq 7 \times 10^{14}\,\mathrm{eV}. \tag{64}$$

We are now ready to calculate the neutrino flux:

$$\frac{dN_\nu}{dE_\nu} = \frac{c}{4\pi}\frac{U'_\nu}{E'_\nu} = \frac{c}{4\pi}\frac{U_\nu}{E_\nu} = \frac{c}{4\pi}\frac{1}{E_\nu}\left[\frac{1}{2}f_\pi t_H \dot{E}\right], \tag{65}$$

where the factor 1/2 accounts for the fact that only 1/2 of the energy in charged pions is transferred to $\nu_\mu + \bar{\nu}_\mu$. As before, $\dot{E}$ is the injection rate in cosmic rays beyond the ankle ($\sim 4 \times 10^{44}\,\mathrm{erg\,Mpc^{-3}\,yr^{-1}}$) and t_H is the Hubble time of $\sim 10^{10}$ Gyr. Numerically,

$$\frac{dN_\nu}{dE_\nu} = 2 \times 10^{-14}\,\mathrm{cm^{-2}\,s^{-1}\,sr^{-1}}\left[\frac{7\times 10^{14}\,\mathrm{eV}}{\mathrm{E}_\nu}\right]\left[\frac{f_\pi}{0.14}\right]\left[\frac{t_H}{10\ \mathrm{Gyr}}\right] \times \left[\frac{\dot{E}}{10^{44}\,\mathrm{erg\,Mpc^{-3}\,yr^{-1}}}\right] \tag{66}$$

The only subtlety here is the γ^2 dependence of the shell radius R'; for a simple derivation, see Ref.[6] The result is insensitive to beaming. Beaming yields more energy per burst, but fewer bursts are actually observed. The predicted rate is also insensitive to the neutrino energy E_ν because higher average energy yields fewer νs, but more are detected. Both effects are approximately linear. Neutrino telescopes are essentially background free for such high-energy events and should be able to identify neutrinos at all zenith angles.

For typical choices of the parameters, $\gamma \sim 300$ and $t_v \sim 10^{-2}s$, about 100 events per year are predicted in IceCube, a flux that was already challenged[81] by the limit on a diffuse flux of cosmic neutrinos obtained with one-half of IceCube in one year.[82] As before, the energy density of extragalactic cosmic rays of $\sim 10^{44}$ TeV Mpc^{-3} yr^{-1} depends on the unknown transition energy between the Galactic and extragalactic components of the spectrum. In the end, the predictions can be stretched, but having failed by now to observe high-energy neutrinos in spatial and temporal coincidence with over 1000 GRB observations, IceCube has set a limit that is less than 1% of the PeV cosmic neutrino flux that is actually observed.

We have nevertheless discussed fireballs in some detail to illustrate their generic potential as cosmic accelerators and to point out that they may produce cosmic neutrinos without being the sources of cosmic rays. For instance, they may produce neutrinos of lower energy in events where the boost factor is limited, $\gamma \leq 10$. Candidate events have been observed and are referred to as "low luminosity GRBs."[83] There is also the possibility that high-energy gamma rays and neutrinos are produced when the shock expands further into the interstellar medium. This mechanism has been

invoked as the origin of the delayed high-energy gamma rays. Adapting the previous calculation to the external shock is straightforward.[84] The timescale is seconds rather than milliseconds, and the break in the spectrum shifts from 1 to 0.1 MeV. Although f_π is reduced by two orders of magnitude, in the external shocks higher energies can be reached, and this increases the neutrino detection efficiency. In the end, the observed rates are an order of magnitude smaller than in internal shocks, but the inherent ambiguities of the estimates are such that it is difficult to establish with confidence their relative neutrino yields.

4.4. *Galactic Neutrino-Producing Beam Dumps*

The rationale for kilometer-scale neutrino detectors is that their sensitivity is sufficient to reveal generic cosmic-ray sources with an energy density in neutrinos comparable to their energy density in cosmic rays[59] and pionic TeV gamma rays.[63] Interestingly, this condition may be satisfied by the sources of Galactic cosmic rays.

The energy density of the cosmic rays in our Galaxy is $\rho_E \sim 10^{-12}\,\mathrm{erg\,cm^{-3}}$. Galactic cosmic rays do not exist forever; they diffuse within microgauss fields and remain trapped for an average containment time of 3×10^6 years. The power needed to maintain a steady energy density requires accelerators delivering 10^{41} erg/s. This happens to be 10% of the power produced by supernovae releasing 10^{51} erg every 30 years (10^{51} erg correspond to 1% of the binding energy of a neutron star after 99% is initially lost to neutrinos). This coincidence is the basis for the idea that shocks produced by supernovae exploding into the interstellar medium are the accelerators of Galactic cosmic rays.

A generic supernova remnant releasing an energy of $W \sim 10^{50}$ erg into the acceleration of cosmic rays will inevitably generate TeV gamma rays by interacting with the hydrogen in the Galactic disk. The emissivity in pionic gamma rays is calculated using the formalism previously introduced for the calculation of the neutrino flux with $q_{\pi^0} = \frac{1}{2} q_{\pi^\pm}$; the latter is given by Eq. 21.

Before proceeding, a short discussion of the production of pionic photons follows. For this calculation, we define the production rate Q_{π^0}, per unit volume and time, by converting dl to cdt in the τ' integration in Eq. 21. Additionally one assumes that a single pion is produced carrying a fraction

$f_\pi \simeq 0.2$ of the proton momentum. This yields

$$Q_{\pi^0} = c\, n\, \sigma_{pp} \int dE_p\, n_p\,(E_p)\; \delta\,(E_{\pi^0} - f_\pi E_p)\;, \tag{67}$$

which in turn yields the final result

$$Q_{\pi^0}\,(E_{\pi^0}) = c\, \sigma_{pp}\, n\, \frac{1}{f_\pi}\, n_p \left(\frac{E_{\pi^0}}{f_\pi}\right). \tag{68}$$

The emissivity Q_{π^0} is simply proportional to the number density of hydrogen targets and the number of cosmic rays $n_p \simeq 4 \times 10^{-14}\ (E_p/TeV)^{-1.7}\ \mathrm{cm}^{-3}$ obtained from the spectrum:

$$n_p = \frac{4\pi}{c} \int dE \frac{dN_p}{dE}. \tag{69}$$

The emissivity of photons is obtained from the fact that every pion produces two photons with half its energy, therefore

$$Q_\gamma\,(E_\gamma) = 2 \times 2\, Q_{\pi^0}\,(2E_\gamma) \simeq Q_{\pi^0}\,, \tag{70}$$

where the latter equality holds for an E^{-2} spectrum.

Our final result is

$$Q_\gamma\,(E_\gamma) \simeq c\, \frac{1}{f_\pi}\, \sigma_{pp}\, n\, n_{cr}(E_p > \frac{E_\gamma}{f_\pi})\,, \tag{71}$$

or, assuming an E^{-2} spectrum,

$$Q_\gamma(>1\,\mathrm{TeV}) \simeq 10^{-29} \left(\frac{n}{\mathrm{cm}^{-3}}\right) \mathrm{cm}^{-3}\,\mathrm{s}^{-1}\,. \tag{72}$$

Notice the transparency of this result. The proportionality factor in Eq. 71 is determined by particle physics, where $\lambda_{pp} = (n\sigma_{pp})^{-1}$ is the proton interaction length ($\sigma_{pp} \simeq 40\,\mathrm{mb}$) in a density n of hydrogen atoms. The corresponding luminosity is

$$L_\gamma(>1\,\mathrm{TeV}) \simeq Q_\gamma\, \frac{W}{\rho_E} \tag{73}$$

where W/ρ_E is the volume occupied by the supernova remnant; given the ambient density $\rho_E \sim 10^{-12}\,\mathrm{erg\,cm}^{-3}$ of Galactic cosmic rays,[4] a supernova with energy $W \sim 10^{50}\,\mathrm{erg}$ in cosmic rays occupies the volume W/ρ_E. We here made the approximation that the density of particles in the remnant is not very different from the ambient energy density.

We thus predict[85,86] a rate of TeV photons from a supernova remnant at a nominal distance d on the order of 1 kpc of

$$\int_{E>1\mathrm{TeV}} \frac{dN_\gamma}{dE_\gamma} dE_\gamma = \frac{L_\gamma(>1\mathrm{TeV})}{4\pi d^2}$$
$$\simeq 10^{-12} - 10^{-11} \left(\frac{\mathrm{TeV}}{\mathrm{cm}^2\,\mathrm{s}}\right) \left(\frac{W}{10^{50}\,\mathrm{erg}}\right) \left(\frac{n}{1\,\mathrm{cm}^{-3}}\right) \left(\frac{d}{1\,\mathrm{kpc}}\right)^{-2}. \tag{74}$$

As discussed in the introduction, the position of the knee in the cosmic ray spectrum indicates that some sources accelerate cosmic rays to energies of several PeV. These PeVatrons therefore produce pionic gamma rays whose spectrum can extend to several hundred TeV without cutting off. For such sources the gamma-ray flux in the TeV energy range can be parametrized in terms of a spectral slope α_γ, an energy $E_{cut,\gamma}$ where the accelerator cuts off, and a normalization k_γ:

$$\frac{dN_\gamma(E_\gamma)}{dE_\gamma} = k_\gamma \left(\frac{E_\gamma}{\mathrm{TeV}}\right)^{-\alpha_\gamma} \exp\left(-\sqrt{\frac{E_\gamma}{E_{cut,\gamma}}}\right). \tag{75}$$

The estimate in Eq. 74 indicates that fluxes as large as $dN_\gamma/dE_\gamma \sim 10^{-12}$–$10^{-14}$ (TeV^{-1} cm^{-2} s^{-1}) can be expected at energies of $\mathcal{O}$ (10 TeV). We will therefore concentrate on the search for PeVatrons, supernova remnants with the required energetics to produce cosmic rays, at least up to the knee in the spectrum.

These sources are well within the sensitivity of existing high-energy gamma ray detectors such air Cherenkov telescopes and large acceptance ground-based detectors like Milagro. They may have been revealed by the highest energy all-sky survey in $\sim 20\,\mathrm{TeV}$ gamma rays using the Milagro detector.[87] A subset of sources, located within nearby star-forming regions in Cygnus and in the vicinity of Galactic latitude $l = 40\,\mathrm{degrees}$, are identified; some cannot be readily associated with known supernova remnants or with nonthermal sources observed at other wavelengths. Subsequently, directional air Cherenkov telescopes were pointed at three of the sources, revealing them as PeVatron candidates with an approximate E^{-2} energy spectrum that extends to tens of TeV without evidence for a cutoff,[88] in contrast with the best studied supernova remnants RX J1713-3946 and RX J0852.0-4622 (Vela Junior).

Some Milagro sources may actually be molecular clouds illuminated by the cosmic-ray beam accelerated in young remnants located within $\sim 100\,\mathrm{pc}$. Indeed, one expects that multi-PeV cosmic rays are accelerated only over a short time period when the shock velocity is high, i.e., towards the end of the free expansion of the remnant. The high-energy particles can produce photons and neutrinos over much longer periods when they diffuse through the interstellar medium to interact with nearby molecular clouds.[89] An association of molecular clouds and supernova remnants is expected, of course, in star-forming regions. In this case, any confusion with synchrotron photons is unlikely.

Ground-based and satellite-borne instruments with improved sensitivity are able to conclusively pinpoint supernova remnants as the sources of cosmic-ray acceleration by identifying accompanying gamma rays of pion origin. The Fermi Large Area Telescope has detected pion-decay feature in the gamma-ray spectra of two supernova remnants, IC 443 and W44.[90] In contrast, GeV gamma-ray data from Fermi LAT have challenged the hadronic interpretation of the GeV-TeV radiation from one of the best-studied candidates, RX J1713-3946.[91] The most promising PeVatron candidate to date is, instead, the center of the Galaxy, as reported by the HESS Collaboration, see Ref.[42] Detecting the accompanying neutrinos from supernova remnants or the Galactic Center would provide incontrovertible evidence for cosmic-ray acceleration.

Particle physics dictates the relation between pionic gamma rays and neutrinos and basically predicts the production of a $\nu_\mu + \bar{\nu}_\mu$ pair for every two gamma rays seen by Milagro. This calculation can be performed using the formalism discussed with approximately the same outcome. Operating the complete IceCube detector for several years should yield confirmation that some of the Milagro sources produce pionic gamma rays; see Fig. 13.

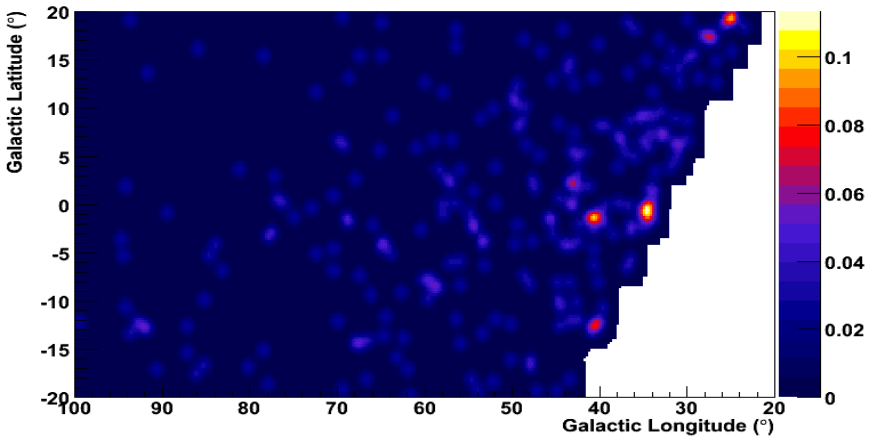

Fig. 13. Simulated sky map of IceCube in Galactic coordinates after five years of operation of the completed detector. Two Milagro sources are visible with four events for MGRO J1852+01 and three events for MGRO J1908+06 with energy in excess of 40 TeV. These, as well as the background events, have been randomly distributed according to the resolution of the detector and the size of the sources.

The quantitative statistics can be summarized in the following. For average values of the parameters describing the flux, we find that the IceCube detector could confirm sources in the Milagro sky map as sites of cosmic-ray acceleration at the 3σ level in less than one year and at the 5σ level in three years.[85] We here assume that the source extends to 300 TeV, or 10% of the energy of the cosmic rays near the knee in the spectrum. These results agree with previous estimates.[92,93] There are intrinsic ambiguities in this estimate of an astrophysical nature that may reduce or extend the time required for a 5σ observation.[85] In particular, the poorly known extended nature of some of the Milagro sources and the value of the cutoff represent a challenge for IceCube analyses that are optimized for point sources. The absence of any observation of an accumulation of high-energy neutrinos in the direction of these sources will seriously challenge the concept that gamma-ray telescopes are seeing actual sources of cosmic rays.

These predictions have been stable over the years and have recently been updated in the context of new gamma-ray information, in particular from the HAWC experiment; see reference.[88] The predicted fluxes for Galactic sources in the Northern hemisphere are close to IceCube's current upper limits on a point source flux of $10^{-12}\,\mathrm{TeVcm^{-2}s^{-1}}$;[94] see also Ref.[95]

4.5. *Cosmogenic Neutrinos*

The production of neutrinos in the sources that accelerate the high-energy cosmic rays depends on the source environment. In order to efficiently accelerate cosmic rays, any loss mechanism, including pion production in $p\gamma$ and pp interactions, must be suppressed as it reduces the acceleration time. Efficient accelerators are likely to be inefficient beam dumps for producing neutrinos. High-efficiency neutrino production can be achieved by separating the sites of acceleration and neutrino production. For instance, after acceleration, extragalactic cosmic rays propagate over cosmological distances of more than 10 Mpc and can efficiently produce neutrinos on the dilute extragalactic medium.

In this section, we will discuss the production of neutrinos in the interactions of extragalactic cosmic rays with cosmic radiation backgrounds. Soon after the discovery of the cosmic microwave background (CMB), Greisen, Zatsepin and Kuzmin[96,97] (GZK) realized that extragalactic cosmic rays are attenuated by interactions with background photons. Actually, protons interact resonantly via $p\gamma \to \Delta^+ \to \pi^+ n$ with background photons with mean energy $\epsilon \simeq 0.33$ meV at energies $E_p \simeq (m_\Delta^2 - m_p^2)/4/\epsilon \simeq 500$ EeV.

The width of the Planck spectrum leads to a significant attenuation of proton fluxes after propagation over distances on the order of 200 Mpc at an energy above $E_{\rm GZK} \simeq 50$ EeV, which is known as the GZK suppression. Also heavier nuclei are attenuated at a similar energy by photodisintegration of the nucleus by CMB photons via the giant dipole resonance.

The pions produced in GZK interactions decay, resulting in a detectable flux of *cosmogenic* neutrinos first estimated by Berezinsky and Zatsepin[24] in 1969. This *guaranteed* flux of neutrinos became one of the benchmarks for high–energy neutrino astronomy leading early on to the concept of kilometer-scale detectors. The flux of cosmogenic neutrinos peaks at EeV neutrino energy depending on the chemical composition and the evolution with redshift of the unknown sources. The largest neutrino flux results from proton–dominated models.[18,98,99] A particularly strong emission can be expected in such models if the proton spectrum extends below the ankle. Referred to as "dip models," the ankle results from the absorption of protons by Bethe–Heitler pair production on CMB photons. A fit to the observed cosmic-ray spectrum requires relative strong source evolution with redshift[100–103] that enhances pion production. However, the corresponding electromagnetic emission via neutral pions as well as $e^{\pm}$ pairs is constrained by the isotropic gamma-ray background (IGRB) observed by the Fermi LAT satellite [104,105] and limits the neutrino intensity of these proton–dominated scenarios.[106–111] Recent upper limits on cosmogenic neutrinos resulting from the failure by IceCube to observe EeV neutrinos constrains proton–dominated models.[112]

In contrast, the IceCube constraint can be accommodated by introducing a heavy nuclear composition. Resonant neutrino production still proceeds via the interaction of individual nucleons with background photons, but the threshold of the production is increased to $E_{\rm CR} \gtrsim AE_{\rm GZK}$ for nuclei with mass number A. Therefore, efficient cosmogenic neutrino production would require an injected cosmic-ray flux that extends well above $E_{\rm GZK}$. Especially for heavier nuclear composition of the primary flux, the production of neutrinos on photons of the extragalactic background light (EBL) becomes relatively important.[71,109,113–120] The interaction with optical photons produces neutrino fluxes in the PeV energy range. However, the overall level is much lower because of the low intensity of the EBL photons. It is unlikely that the PeV neutrino flux observed with IceCube could be related to the neutrino production in the EBL[121] (see also Ref.[122]). The observed PeV neutrino flux level is too high to be consistent with associated electromagnetic contributions to the IGRB or upper limits on the EeV

neutrino flux.

5. Status Of the Observations of Cosmic Neutrinos

For neutrino astronomy, the first challenge is to select a pure sample of neutrinos, roughly 100,000 per year above a threshold of 0.1 TeV for IceCube, in a background of ten billion cosmic-ray muons (see Fig. 9), while the second is to identify the small fraction of these neutrinos that is astrophysical in origin, roughly at the level of tens of events per year. Atmospheric neutrinos are a background for cosmic neutrinos, at least at neutrino energies below ~ 300 TeV. Above this energy, the atmospheric neutrino flux reduces to less than one event per year, even in a kilometer-scale detector, and thus events in that energy range are cosmic in origin.

There are two primary methods used to identify neutrinos of cosmic origin. As previously discussed, neutrino searches have historically focused on the observation of muon neutrinos that interact primarily outside the detector, producing kilometer-long muon tracks that pass through the detection volume. Although this allows observation of neutrinos that interact outside the detector, it is then necessary to use the Earth as a filter in order to remove the huge background of cosmic-ray muons. Even at a depth of 1,450 meters, IceCube detects atmospheric cosmic-ray muons originating in the Southern Hemisphere at a rate of 3,000 per second. This method limits the neutrino view to a single flavor and half the sky. An alternative method exclusively identifies neutrinos interacting inside the detector. It divides the instrumented volume of ice into an outer veto shield and a roughly 500 megaton inner fiducial volume. The advantage of focusing on neutrinos interacting inside the instrumented volume of ice is that the detector then functions as a total absorption calorimeter, measuring energy with a 10-15 % resolution. Also, neutrinos from all directions in the sky can be identified, including both muon tracks, produced in muon-neutrino charged-current interactions, and secondary showers, produced by electron and tau neutrinos as well as in neutral-current interactions of neutrinos of all flavors. The Cherenkov patterns initiated by an electron (or tau) neutrino of 1 PeV, or petaelectronvolt (10^{15} eV), energy and by a muon neutrino depositing 2.6 PeV energy while traversing the detector are contrasted in Fig. 14.

In general, the particle's trajectory is determined from the arrival times of photons at the optical sensors,[123] while the number of photons is a proxy for the amount of energy deposited. The two methods for separating neutri-

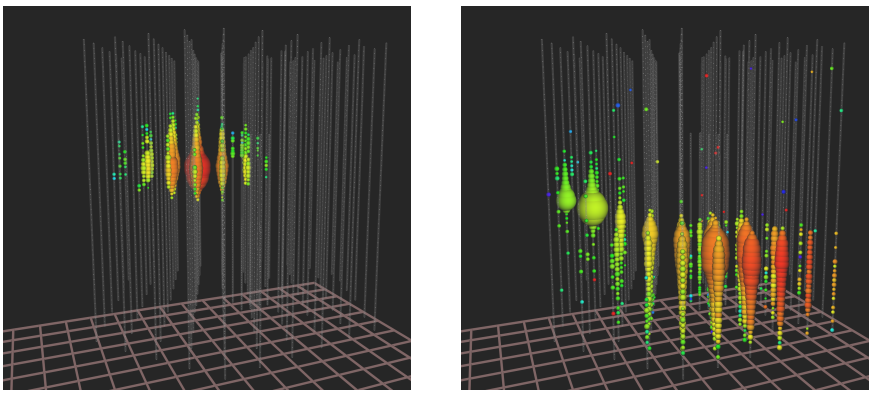

Fig. 14. Light pools produced in IceCube by neutrino interactions. White dots represent sensors with no signal. For the colored dots, the color indicates arrival time, from red (early) to purple (late) following the rainbow, and size reflects the number of photons detected. Left: A shower initiated by an electron or a tau neutrino or by the neutral current interaction of a neutrino of any of the three flavors. The measured energy of the shower is 1.14 PeV, which represents a lower limit on the energy of the neutrino that initiated the shower. Right: An upgoing muon track traverses the detector at an angle of 11° below the horizon. The deposited energy inside the detector is 2.6 PeV.

nos from the cosmic-ray muon background have complementary advantages. The long tracks produced by muon neutrinos can point back to their sources with a 0.4° angular resolution. In contrast, the reconstruction of the direction of secondary showers, still in the development stage in IceCube,[124] can be determined to within $10^\circ \sim 15^\circ$ of the direction of the incident neutrino. Determining the deposited energy from the observed light pool is, however, relatively straightforward, and a resolution of better than 15% is possible.

By now, IceCube has observed cosmic neutrinos using both methods for rejecting background, and each analysis has reached a statistical significance of more than 5σ.[125,126] Based on different methods for reconstruction and energy measurement, the results agree, pointing at extragalactic sources whose flux has equilibrated in the three flavors after propagation over cosmic distances. Its total energy matches that of extragalactic photons and cosmic rays.

Using the Earth as a filter, a flux of neutrinos has been identified that is predominantly of atmospheric origin. IceCube has measured this flux over three orders of magnitude in energy with a result that is consistent with theoretical calculations. However, with eight years of data, an excess of events is observed at energies beyond 100 TeV,[127–129] which cannot be

accommodated by the atmospheric flux; see Fig. 16. Allowing for large uncertainties on the extrapolation of the atmospheric component to higher energy, the statistical significance of the excess astrophysical flux is 6.7σ. While IceCube measures only the energy of the secondary muon inside the detector, from Standard Model physics we can infer the energy spectrum of the parent neutrinos. The best-fit neutrino spectrum then allows deriving the probability distribution of neutrino energy for individual events. For instance, for the highest energy event, shown in Fig. 14 on the right, the median energy of the parent neutrino is about 7 PeV as indicated in Fig. 15. Note that this calculation[128] takes into account the additional tracks from charged current interactions of $\nu_\tau + \bar{\nu}_\tau$ as well as resonant interactions of $\bar{\nu}_e$ with electrons (Glashow resonance) assuming a democratic composition of neutrino and antineutrino flavors. Independent of any calculation, the energy lost by the muon inside the instrumented detector volume is 2.6 ± 0.3 PeV. The cosmic neutrino flux is well described by a power law with a spectral index $\Gamma = 2.19 \pm 0.10$ and a normalization at 100 TeV neutrino energy of $(1.01^{+0.26}_{-0.23}) \times 10^{-18}\,\mathrm{GeV}^{-1}\mathrm{cm}^{-2}\mathrm{sr}^{-1}$.[129] The error range is estimated from a profile likelihood using Wilks' theorem and includes both statistical and systematic uncertainties. The neutrino energies contributing to this power-law fit cover the range from 119 TeV to 4.8 PeV.

However, using only two years of data, it was the alternative HESE method, which selects neutrinos interacting inside the detector, that revealed the first evidence for cosmic neutrinos.[132,133] The segmentation of the detector into a surrounding veto and active signal region has been optimized to reduce the background of atmospheric muons and neutrinos to a handful of events per year, while keeping most of the cosmic signal. Neutrinos of atmospheric and cosmic origin can be separated not only by using their well-measured energy but also on the basis that background atmospheric neutrinos reaching us from the Southern Hemisphere can be removed because they are accompanied by particles generated in the same air shower where they originate. A sample event with a light pool of roughly one hundred thousand photoelectrons extending over more than 500 meters is shown in the left panel of Fig. 14. With PeV energy, and no trace of accompanying muons from an atmospheric shower, these events are highly unlikely to be of atmospheric origin. It is indeed important to realize that the muon produced in the same pion or kaon decay as an atmospheric neutrino will reach the detector provided that the neutrino energy is sufficiently high and the zenith angle sufficiently small.[33,134] As a consequence, PeV atmospheric neutrinos originating from above the detector have a built-in

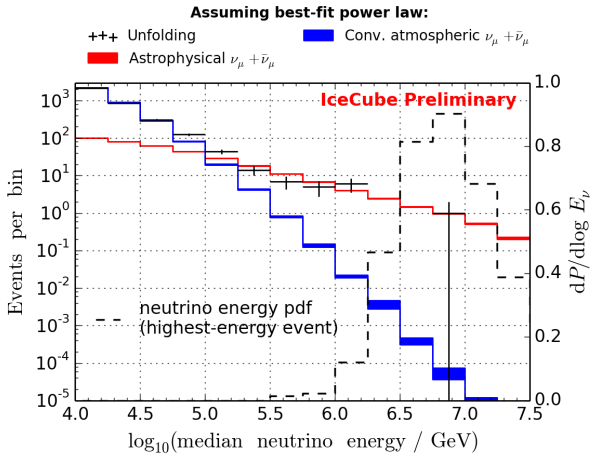

Fig. 15. Distribution of tracks initiated by muon neutrinos that have traversed the Earth, i.e., with zenith angle less than 5° above the horizon, as a function of the neutrino energy. Due to the event-by-event variation of the energy transferred to and lost by the muon before it reaches the detector, the initial neutrino energy is shown by its median. The black crosses represent the data. The blue colored band shows the expectation for the atmospheric neutrino flux, while the red line represents a power-law fit to the cosmic component with spectral index $\Gamma = 2.13$. Additionally, the probability density function for the neutrino energy of the highest energy event is shown assuming the best-fit spectrum (dashed line).

self-veto in the HESE analysis by their accompanying atmospheric muons.

The deposited energy and zenith dependence of the high-energy starting events collected in six years of data[129] is compared to the atmospheric background in Fig. 17. The expected number of events for the best-fit astrophysical neutrino spectrum following a two-component power-law fit is shown as dashed lines in the two panels. The corresponding neutrino spectrum is also shown in Fig. 18. It is, above an energy of 200 TeV, consistent with a power-law flux of muon neutrinos penetrating the Earth inferred by the data shown in Fig. 15. A purely atmospheric explanation of the observation is excluded at 8σ. In summary, IceCube has observed cosmic neutrinos using both methods for rejecting background. Based on different methods for reconstruction and energy measurement, their results agree, pointing at extragalactic sources whose flux has equilibrated in the three flavors after propagation over cosmic distances[135] with $\nu_e : \nu_\mu : \nu_\tau \sim 1 : 1 : 1$.

The six-year data set contains a total of 82 neutrino events with de-

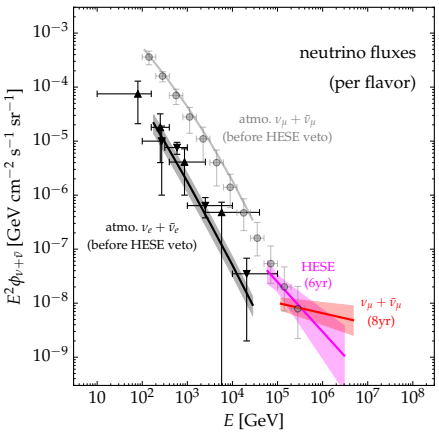

Fig. 16. Summary of diffuse neutrino observations (per flavor) by IceCube. The black and grey data show IceCube's measurement of the atmospheric $\nu_e + \bar{\nu}_e$[32,130] and $\nu_\mu + \bar{\nu}_\mu$[31] spectra. The magenta line and magenta-shaded area indicate the best-fit and 1σ uncertainty range of a power-law fit to the six-year HESE data. Note that the HESE analysis vetoes atmospheric neutrinos and can probe astrophysical neutrinos below the atmospheric neutrino flux, as indicated in the plot (cf. Fig. 17). The corresponding fit to the eight-year $\nu_\mu + \bar{\nu}_\mu$ analysis is shown in red.

posited energies ranging from 60 TeV to 10 PeV. The data in both and Fig. 17 are consistent with an astrophysical component with a spectrum close to E^{-2} above an energy of ~ 200 TeV. An extrapolation of this high-energy flux to lower energy suggests an excess of events in the $30 - 100$ TeV energy range over and above a single power-law fit; see Fig. 18. This conclusion is supported by a subsequent analysis that has lowered the threshold of the starting-event analysis[136] and by a variety of other analyses. The astrophysical flux measured by IceCube is not featureless; either the spectrum of cosmic accelerators cannot be described by a single power law or a second component of cosmic neutrino sources emerges in the spectrum. Because of the self-veto of atmospheric neutrinos in the HESE analysis, i.e., the veto triggered by accompanying atmospheric muons, it is very difficult to accommodate the component below 100 TeV as a feature in the atmospheric background.

In Figure 19 we show the arrival directions of the most energetic events in the eight-year upgoing $\nu_\mu + \bar{\nu}_\mu$ analysis ($\odot$) and the six-year HESE data sets. The HESE data are separated into tracks ($\otimes$) and cascades ($\oplus$). The median angular resolution of the cascade events is indicated by thin circles around the best-fit position. The most energetic muons with energy

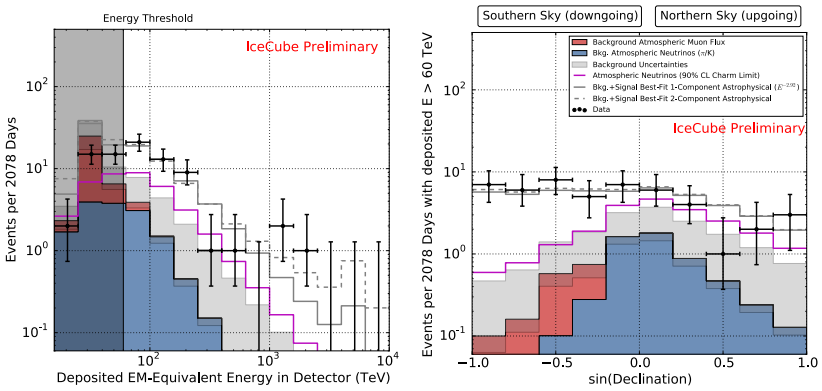

Fig. 17. **Left Panel:** Deposited energies, by neutrinos interacting inside IceCube, observed in six years of data.[129] The grey region shows uncertainties on the sum of all backgrounds. The atmospheric muon flux (blue) and its uncertainty is computed from simulation to overcome statistical limitations in our background measurement and scaled to match the total measured background rate. The atmospheric neutrino flux is derived from previous measurements of both the π, K, and charm components of the atmospheric spectrum.[131] Also shown are two fits to the spectrum, assuming a simple power-law (solid gray) and a broken power-law (dashed gray). **Right Panel:** The same data and models, but now showing the distribution of events with deposited energy above 60 TeV in declination. At the South Pole, the declination angle δ is equivalent to the distribution in zenith angle θ related by the identity, $\delta = \theta - \pi/2$. It is clearly visible that the data is flat in the Southern Hemisphere, as expected from the contribution of an isotropic astrophysical flux.

$E_\mu > 200$ TeV in the upgoing $\nu_\mu + \bar{\nu}_\mu$ data set accumulate near the horizon in the Northern Hemisphere. Elsewhere, muon neutrinos are increasingly absorbed in the Earth before reaching the vicinity of the detector because of their relatively large high-energy cross sections. This causes the apparent anisotropy of the events in the Northern Hemisphere. Also HESE events with deposited energy of $E_{\rm dep} > 100$ TeV suffer from absorption in the Earth and are therefore mostly detected when originating in the Southern Hemisphere. After correcting for absorption, the arrival directions of cosmic neutrinos are isotropic, suggesting extragalactic sources. In fact, no correlation of the arrival directions of the highest energy events, shown in Fig. 19, with potential sources or source classes has reached the level of 3σ.[136]

The absence of strong anisotropies in the arrival direction of IceCube data disfavors scenarios with strong Galactic emission. However, the limited number of events and the low angular resolution of cascade-dominated

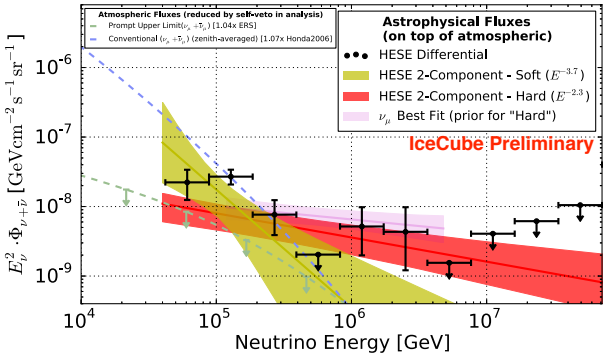

Fig. 18. Unfolded spectrum for six years of HESE neutrino events starting inside the detector. The yellow and red bands show the 1σ uncertainties on the result of a two-power-law fit. Superimposed is the best fit to eight years of the upgoing muon neutrino data (pink). Note the consistency of the red and pink bands. Figure from Ref.[129]

samples can hide this type of emission. At a minimum, it is possible that some of the data originates in Galactic sources. Various Galactic scenarios have been considered for the diffuse neutrino flux in the TeV-PeV energy range, including the diffuse emission from Galactic CRs,[137–142] the joint emission of Galactic CR sources,[143–145] or very extended emission from the *Fermi bubbles*[137,146,147] or the Galactic halo.[148,149] More exotic scenarios consider dark matter decay[150–156] in the Galactic dark matter halo. Most of these scenarios also predict the production of pionic PeV gamma rays. These gamma rays are absorbed via pair production in the scattering off CMB photons with an absorption length of about 10 kpc. Therefore, the observation of PeV gamma rays would be a "smoking gun" of Galactic PeV neutrino emission.[137,157]

However, the isotropic arrival direction of neutrinos would be a natural consequence of extragalactic source populations. A plethora of models have been considered, including galaxies with intense star formation,[158–165] cores of active galactic nuclei (AGNs),[166–168] low-luminosity AGNs,[169,170] quasar-driven outflows,[171] blazars,[172–179] low-power gamma-ray bursts (GRBs),[78,180–182] choked GRBs,[83,183,184] cannonball GRBs,[185] intergalactic shocks,[186] galaxy clusters,[159,187–189] tidal disruption events,[190–194] or cosmogenic neutrinos.[121,122] We will discuss in the following how we can use multimessenger information to pinpoint the true origin of the neutrino emission.

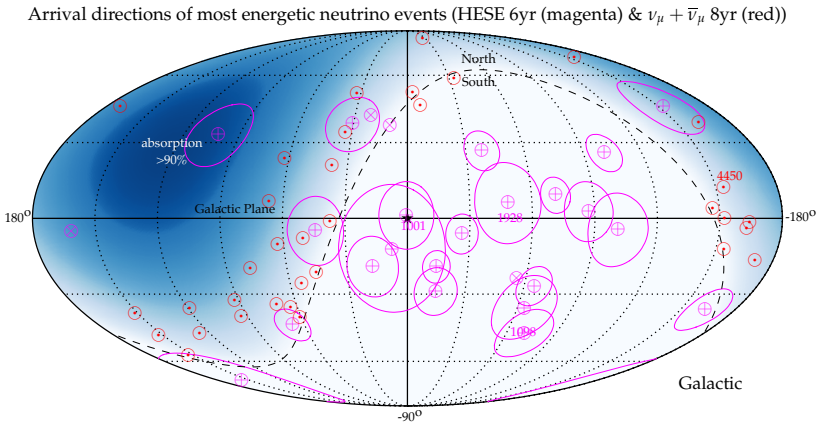

Fig. 19. Mollweide projection in Galactic coordinates of the arrival direction of neutrino events. We show the results of the eight-year upgoing track analysis[129] with reconstructed muon energy $E_\mu \gtrsim 200$ TeV ($\odot$). The events of the six-year high-energy starting event (HESE) analysis with deposited energy larger than 100 TeV (tracks $\otimes$ and cascades $\oplus$) are also shown.[129,195,196] The thin circles indicate the median angular resolution of the cascade events ($\oplus$). The blue-shaded region indicates the zenith-dependent range where Earth absorption of 100 TeV neutrinos becomes important, reaching more than 90% close to the nadir. The dashed line indicates the horizon and the star ($\star$) the Galactic Center. We highlight the four most energetic events in both analyses by their deposited energy (magenta numbers) and reconstructed muon energy (red number).

6. Multimessenger Interfaces

The most important message emerging from the IceCube measurements is not apparent yet: the prominent and surprisingly important role of protons relative to electrons in the nonthermal universe. To illustrate this point, we show in Fig. 20 the observed neutrino flux ϕ in terms of the product $E^2\phi$, which is a measure of its energy density. One can see that the cosmic energy density of high-energy neutrinos is comparable to that of γ-rays observed with the Fermi satellite[105] (blue data) and to that of ultra-high-energy (UHE) cosmic rays (above 10^9 GeV) observed, e.g., by the Auger observatory[197] (green data). This might indicate a common origin of the signal and provides excellent conditions for multi-messenger studies.

A challenge to most galactic and extragalactic scenarios is the large neutrino flux in the range of $10 - 100$ TeV, which implies an equally high intensity of gamma rays from the decay of neutral pions produced along with the charged pions that are the source of the observed neutrino flux.[20] For extragalactic scenarios, this gamma-ray emission is not directly ob-

served because of strong absorption of photons by e^+e^- pair production in the extragalactic background light (EBL) and CMB. The high-energy leptons initiate electromagnetic showers of repeated inverse-Compton scattering and pair production in the CMB that eventually yield photons that contribute to the Fermi γ-ray observations in the GeV-TeV range.

The extragalactic γ-ray background observed by Fermi[105] has contributions from identified point-like sources on top of an isotropic γ-ray background (IGRB) shown in Fig. 20. This IGRB is expected to consist mostly of emission from the same class of γ-ray sources that are individually below Fermi's point-source detection threshold (see, e.g., Ref.[198]). A significant contribution of γ-rays associated with IceCube's neutrino observation would have the somewhat surprising implication that indeed many extragalactic γ-ray sources are also neutrino emitters, while none has been detected so far.

Another intriguing observation is that the high-energy neutrinos observed at IceCube could be related to the sources of UHE CRs. The simple argument is as follows: UHE CR sources can be embedded in environments that act as "storage rooms" for cosmic rays with energies far below the "ankle" ($E_{\rm CR} \ll 1$EeV). This energy-dependent trapping can be achieved via cosmic ray diffusion in magnetic fields. While these cosmic rays are trapped, they can produce γ-rays and neutrinos via collisions with gas. If the conditions are right, this mechanism can be so efficient that the total energy stored in low-energy cosmic rays is converted to that of γ-rays and neutrinos. These "calorimetric" conditions can be achieved in starburst galaxies[158] or galaxy clusters.[187] We will discuss these multimessenger relations in more detail next.

6.1. *IceCube Neutrinos and Fermi Photons*

Photons are produced in association with neutrinos when accelerated cosmic rays produce neutral and charged pions in interactions with photons or nuclei. Targets include strong radiation fields that may be associated with the accelerator as well as concentrations of matter or molecular clouds in their vicinity. Additionally, pions can be produced in the interaction of cosmic rays with the EBL when propagating through the interstellar or intergalactic background. A high-energy flux of neutrinos is produced in the subsequent decay of charged pions via $\pi^+ \to \mu^+ + \nu_\mu$ followed by $\mu^+ \to e^+ + \nu_e + \bar{\nu}_\mu$ and the charge–conjugate processes. High-energy gamma rays result from the decay of neutral pions, $\pi^0 \to \gamma + \gamma$. Pionic gamma

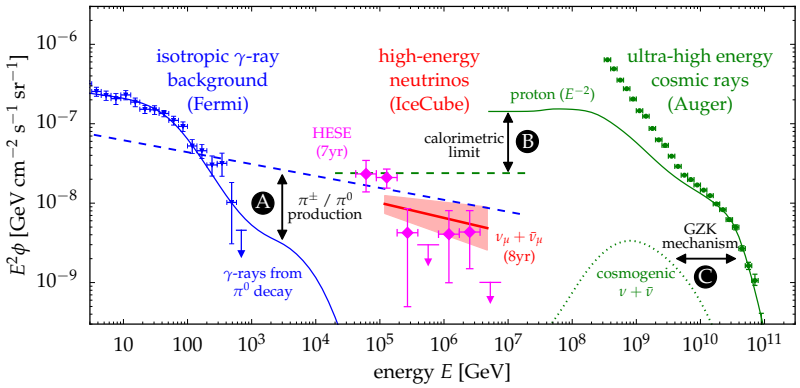

Fig. 20. The spectral flux (ϕ) of neutrinos inferred from the eight-year upgoing track analysis (red fit) and the six-year HESE analysis (magenta fit) compared to the flux of unresolved extragalactic γ-ray sources[105] (blue data) and ultra-high-energy cosmic rays[197] (green data). The neutrino spectra are indicated by the best-fit power-law (solid line) and 1σ uncertainty range (shaded range). We highlight the various multimessenger interfaces: **A:** The joined production of charged pions ($\pi^{\pm}$) and neutral pions (π^0) in cosmic-ray interactions leads to the emission of neutrinos (dashed blue) and γ-rays (solid blue), respectively. **B:** Cosmic ray emission models (solid green) of the most energetic cosmic rays imply a maximal flux (calorimetric limit) of neutrinos from the same sources (green dashed). **C:** The same cosmic ray model predicts the emission of cosmogenic neutrinos from the collision with cosmic background photons (GZK mechanism).

rays and neutrinos carry, on average, 1/2 and 1/4 of the energy of the parent pion, respectively. With these approximations, the neutrino production rate Q_{ν_α} (units of GeV^{-1}s^{-1}) can be related to the one for charged pions as

$$\sum_\alpha E_\nu Q_{\nu_\alpha}(E_\nu) \simeq 3\,[E_\pi Q_{\pi^\pm}(E_\pi)]_{E_\pi \simeq 4E_\nu}\ . \tag{76}$$

Similarly, the production rate of pionic gamma-rays is related to the one for neutral pions as

$$E_\gamma Q_\gamma(E_\gamma) \simeq 2\,[E_\pi Q_{\pi^0}(E_\pi)]_{E_\pi \simeq 2E_\gamma}\ . \tag{77}$$

Note, that the relative production rates of pionic gamma rays and neutrinos only depend on the ratio of charged-to-neutral pions produced in cosmic-ray interactions, denoted by $K_\pi = N_{\pi^\pm}/N_{\pi^0}$. Pion production of cosmic rays in interactions with photons can proceed resonantly in the processes $p + \gamma \to \Delta^+ \to \pi^0 + p$ and $p + \gamma \to \Delta^+ \to \pi^+ + n$. These channels produce charged and neutral pions with probabilities 2/3 and 1/3, respectively. However, the additional contribution of nonresonant pion production

changes this ratio to approximately 1/2 and 1/2. In contrast, cosmic rays interacting with matter, e.g., hydrogen in the Galactic disk, produce equal numbers of pions of all three charges: $p + p \to N_\pi [\pi^0 + \pi^+ + \pi^-] + X$, where N_π is the pion multiplicity. From above arguments we have $K_\pi \simeq 2$ for cosmic ray interactions with gas (pp) and $K_\pi \simeq 1$ for interactions with photons ($p\gamma$).

With this approximation we can combine Eqs. (76) and (77) to derive a simple relation between the pionic gamma-ray and neutrino production rates:

$$\frac{1}{3}\sum_\alpha E_\nu^2 Q_{\nu_\alpha}(E_\nu) \simeq \frac{K_\pi}{4}\left[E_\gamma^2 Q_\gamma(E_\gamma)\right]_{E_\gamma = 2E_\nu} . \tag{78}$$

The prefactor 1/4 accounts for the energy ratio $\langle E_\nu\rangle/\langle E_\gamma\rangle \simeq 1/2$ and the two gamma rays produced in the neutral pion decay. This powerful relation relates pionic neutrinos and gamma rays without any reference to the cosmic ray beam; it simply reflects the fact that a π^0 produces two γ rays for every charged pion producing a $\nu_\mu + \bar{\nu}_\mu$ pair, which cannot be separated by current experiments.

Before applying this relation to a cosmic accelerator, we have to be aware of the fact that, unlike neutrinos, gamma rays interact with photons of the cosmic microwave background before reaching Earth. The resulting electromagnetic shower subdivides the initial photon energy, resulting in multiple photons in the GeV-TeV energy range by the time the photons reach Earth. Calculating the cascaded gamma-ray flux accompanying IceCube neutrinos is straightforward.[107,199]

As an illustration, we show a model of γ-ray and neutrino emission as blue lines in Fig. 20. We assume that the underlying π^0 / $\pi^\pm$ production follows from cosmic-ray interactions with gas in the universe. In this way, the initial emission spectrum of γ-rays and neutrinos from pion decay is almost identical to the spectrum of cosmic rays (assumed to be a power law, $E^{-\Gamma}$), after accounting for the different normalizations and energy scales. The flux of neutrinos arriving at Earth (blue dashed line) follows this initial CR emission spectrum. However, the observable flux of γ-rays (blue solid lines) is strongly attenuated above 100 GeV by interactions with extragalactic background photons.

The overall normalisation of the emission is chosen in a way that the model does not exceed the isotropic γ-ray background observed by the Fermi satellite (blue data). This implies an upper limit on the neutrino flux shown as the blue dashed line. Interestingly, the neutrino data shown

in Fig. 20 saturates this limit above 100 TeV. Moreover, the HESE data that extends to lower energies is only marginally consistent with the upper bound implied by the model (blue dashed line). This example shows that multi-messenger studies of γ-ray and neutrino data are powerful tools to study the neutrino production mechanism and to constrain neutrino source models.[159]

The matching energy densities of the extragalactic gamma-ray flux detected by Fermi and the high-energy neutrino flux measured by IceCube suggest that, rather than detecting some exotic sources, it is more likely that IceCube to a large extent observes the same universe astronomers do. Clearly, an extreme universe modeled exclusively on the basis of electromagnetic processes is no longer realistic. The finding implies that a large fraction, possibly most, of the energy in the nonthermal universe originates in hadronic processes, indicating a larger role than previously thought. The high intensity of the neutrino flux below 100 TeV in comparison to the Fermi data might indicate that these sources are even more efficient neutrino than gamma-ray sources.[164,200]

IceCube is developing methods, most promisingly real-time multiwavelength observations in cooperation with astronomical telescopes, to identify the sources and build on the discovery of cosmic neutrinos to launch a new era in astronomy.[201,202] We will return to a coincident observation of a flaring blazar on September 22, 2017, further on.

6.2. *IceCube Neutrinos and Ultra-High-Energy Cosmic Rays*

The charged pion production rate $Q_{\pi^\pm}$ is proportional to the density of the cosmic-ray nucleons in the beam that produces the pions, Q_N, by a "bolometric" proportionality factor $f_\pi \leq 1$. For a target with nucleon density n and extension ℓ, the efficiency factor for producing pions is $f_\pi \simeq 1 - \exp(-\kappa\ell\sigma n)$, where the cross section σ and inelasticity, i.e., average relative energy loss of the leading nucleon, refer to either $p\gamma$ or pp interactions. The pion production efficiency f_π normalizes the conversion of cosmic-ray energy into pion energy on the target as:

$$E_\pi^2 Q_{\pi^\pm}(E_\pi) \simeq f_\pi \frac{K_\pi}{1+K_\pi} \left[E_N^2 Q_N(E_N)\right]_{E_N = E_\pi/\kappa_\pi} . \tag{79}$$

We already introduced the pion ratio K_π in the previous section, with $K_\pi \simeq 2$ for pp and $K_\pi \simeq 1$ for $p\gamma$ interactions. The factor κ_π denotes the average inelasticity *per pion* that depends on the average pion multiplicity N_π. For,

both, pp and $p\gamma$ interactions this can be approximated as $\kappa_\pi = \kappa/N_\pi \simeq 0.2$. The average energy per pion is then $\langle E_\pi \rangle = \kappa_\pi E_N$ and the average energy of the pionic leptons relative to the nucleon is $\langle E_\nu \rangle \simeq \langle E_\pi \rangle/4 = (\kappa_\pi/4)E_N \simeq 0.05 E_N$.

In general, the CR nucleon emission rate, Q_N, depends on the composition of UHE CRs and can be related to the spectra[c] of nuclei with mass number A as $Q_N(E_N) = \sum_A A^2 Q_A(AE_N)$. In the following we will derive a upper limit on diffuse neutrino fluxes under the assumption that UHE CRs are dominated by protons.[69,70] The local emission rate *density*, $\mathcal{Q} = \rho_0 Q$, at these energies is insensitive to the luminosity evolution of sources at high redshift and can be estimated to be at the level of $\left[E_p^2 \mathcal{Q}_p(E_p)\right]_{10^{19.5}\mathrm{eV}} \sim (0.5 - 2.0) \times 10^{44} \mathrm{erg/Mpc^3/yr}$.[71–73] Note, that CR composition measurements indicate that the mass composition above the ankle also requires a contribution of heavier nuclei. However, the estimated local UHE CR power density based on proton models is a good proxy for that of UHE CR models including heavy nuclei, as long as the spectral index is close to $\Gamma \simeq 2$. For instance, a recent analysis of Auger[74] provides a solution with spectral index $\Gamma \simeq 2.04$ and a combined nucleon density of $[E_N^2 \mathcal{Q}_N(E_N)]_{10^{19.5}\mathrm{eV}} \sim 2.2 \times 10^{43}\,\mathrm{erg/Mpc^3/yr}$.

For the calculation of the (quasi-)diffuse neutrino spectra we start from the contribution of individual sources. A neutrino point-source (PS) at redshift z with spectral emission rate Q_{ν_α} contributes a flux (in units $\mathrm{GeV^{-1} cm^{-2} s^{-1}}$ and summed over flavors)

$$\phi_\nu^{\mathrm{PS}}(E_\nu) = \frac{(1+z)^2}{4\pi d_L^2(z)} \sum_\alpha Q_{\nu_\alpha}((1+z)E_\nu)\,, \tag{80}$$

where d_L is the luminosity distance. For the standard ΛCDM cosmological model,[68] this is simply given by the redshift integral

$$d_L(z) = (1+z) \int_0^z \frac{\mathrm{d}z'}{H(z')}\,. \tag{81}$$

Here, the Hubble parameter H has a local value of $c/H_0 \simeq 4.4$ Gpc and scales with redshift as $H^2(z) = H_0^2[(1+z)^3\Omega_\mathrm{m} + \Omega_\Lambda]$, with $\Omega_\mathrm{m} \simeq 0.3$ and $\Omega_\Lambda \simeq 0.7$. Note that the extra factor $(1+z)^2$ appearing in Eq. (80) follows from the definition of the luminosity distance and accounts for the relation of the energy flux to the differential neutrino flux ϕ. The diffuse

[c]Note that the integrated number of nucleons is linear to mass number, $\int \mathrm{d}E Q_N(E) = \sum_A A \int \mathrm{d}E Q_A(E)$.

neutrino flux from extragalactic sources is given by the integral over co-moving volume $\mathrm{d}V_c = 4\pi(d_L/(1+z))^2\mathrm{d}z/H(z)$. Weighting each neutrino source by its density per co-moving volume $\rho(z)$ gives (see, e.g., Ref.[203]):

$$\phi_\nu(E_\nu) = \frac{c}{4\pi}\int_0^\infty \frac{\mathrm{d}z}{H(z)}\rho(z)\sum_\alpha Q_{\nu_\alpha}((1+z)E_\nu)\,. \tag{82}$$

In the following, we will assume that the neutrino emission rate Q_{ν_α} follows a power law $E^{-\Gamma}$. The flavor-averaged neutrino flux can then be written as

$$\frac{1}{3}\sum_\alpha E_\nu^2\phi_{\nu_\alpha}(E_\nu) = \frac{c}{4\pi}\frac{\xi_z}{H_0}\frac{1}{3}\sum_\alpha E_\nu^2\mathcal{Q}_{\nu_\alpha}(E_\nu)\,, \tag{83}$$

where $\mathcal{Q}_{\nu_\alpha} = \rho_0 Q_{\nu_\alpha}$ is the neutrino emission rate *density* and we introduced the redshift factor

$$\xi_z = \int_0^\infty \mathrm{d}z \frac{(1+z)^{-\Gamma}}{\sqrt{\Omega_\Lambda + (1+z)^3\Omega_\mathrm{m}}}\frac{\rho(z)}{\rho_0}\,. \tag{84}$$

A spectral index of $\Gamma \simeq 2.0$ and no source evolution in the local ($z < 2$) universe, $\rho(z) = \rho_0$, yields $\xi_z \simeq 0.5$. For sources following the star-formation rate, $\rho(z) = (1+z)^3$ for $z < 1.5$ and $\rho(z) = (1+1.5)^3$ for $1.5 < z < 4$, with the same spectral index yields $\xi_z \simeq 2.6$. We already introduced this simplified treatment of the integration of the sources in an evolving universe in section 4.1.

We can now derive the observed diffuse neutrino flux related to the sources of UHE CRs. Combining Eqs. (76) and (79) to relate the local neutrino emission rate density to the CR nucleon rate density, we arrive at the diffuse (per flavor) neutrino flux via Eq. (83):

$$\frac{1}{3}\sum_\alpha E_\nu^2\phi_{\nu_\alpha}(E_\nu) \simeq 3\times 10^{-8} f_\pi \left(\frac{\xi_z}{2.6}\right)\left(\frac{[E_p^2\mathcal{Q}_p(E_p)]_{E_p=10^{19.5}\mathrm{eV}}}{10^{44}\,\mathrm{erg/Mpc^3/yr}}\right)\frac{\mathrm{GeV}}{\mathrm{cm\,s\,sr}}\,. \tag{85}$$

Here, we have assumed *pp* interactions with $K_\pi = 2$. The calorimetric limit, $f_\pi \to 1$, of Eq. (90) corresponds to the *Waxman–Bahcall* (WB) upper limit on neutrino production in UHE CR sources.[69,70] As mentioned in the introduction of this section, these calorimetric conditions can be achieved by a rigidity-dependent cosmic ray "trapping" considered, e.g., in starburst galaxies[158] or galaxy clusters.[187]

It is intriguing that the observed intensity of diffuse neutrinos is close to the level of the WB bound. A more precise correspondence is illustrated by the green lines in Fig. 20 showing a model of UHECR protons that

could account for the most energetic cosmic rays (green data). Note, that the cosmic ray data below 10^{10} GeV is not accounted for by this model and must be supplied by additional sources, not discussed here. If we now consider the case that the UHECR sources are embedded in calorimeters, we can derive the maximal neutrino emission (green dashed line) from the low-energy tail of the proton model. Interestingly, the observed neutrino flux saturates this calorimetric limit. It is therefore feasible that UHECRs and neutrinos observed with IceCube have a common origin. If this is the case, the neutrino spectrum beyond 200 TeV should reflect the energy-dependent release of cosmic rays from the calorimeters. Future studies of the neutrino spectrum beyond 1 PeV can provide supporting evidence for CR calorimeter. In particular, the transition to a thin environment ($f_\pi \ll 1$), that is a necessary condition of UHE CR emission, implies a break or cutoff in the neutrino spectrum.

Note that the proton model in Fig. 20 also contributes to the flux of EeV neutrinos shown as a dotted green line. Ultra-high energy CRs are strongly attenuated by resonant interactions with background photons, as first pointed out by Greisen, Zatsepin and Kuzmin[96,97] (GZK). This GZK mechanism is responsible for the suppression of the UHECR proton flux beyond 5×10^{10} GeV ("GZK cutoff") in Fig. 20 (green solid line) and predicts a detectable flux of cosmogenic neutrinos[24] (green dotted line). The proton fraction of UHE CRs at $E \geq 10^{19.5}$ eV can be probed by EHE neutrino observatories at the level of 10% if the (all flavor) EeV sensitivity reaches $E^2\phi \simeq 10^{-9}\,\mathrm{GeV/cm^2/s/sr}$ and if the sources follow the evolution of star formation rate. The low energy tail of the same population of UHE CR protons can be responsible for the observed neutrino emission below 10 PeV assuming a calorimetric environment.

6.3. *Pinpointing the Astrophysical Sources of Cosmic Neutrinos*

The flux of neutrinos measured by IceCube provides a constraint on the flux from the individual sources that it is composed of. We can investigate under what circumstances IceCube can detect the neutrino emission from individual, presumably nearby, point sources that contribute to the quasi-diffuse emission. Eq. (83) relates the average luminosity of individual neutrino sources to the diffuse flux that is measured by the experiment to be at the level of $E^2\phi_\nu \simeq 10^{-8}\ \mathrm{GeV cm^{-2} s^{-1} sr^{-1}}$ for energies in excess of $\simeq 100\,\mathrm{TeV}$; see Fig. 18. From the measurement, we can infer the average

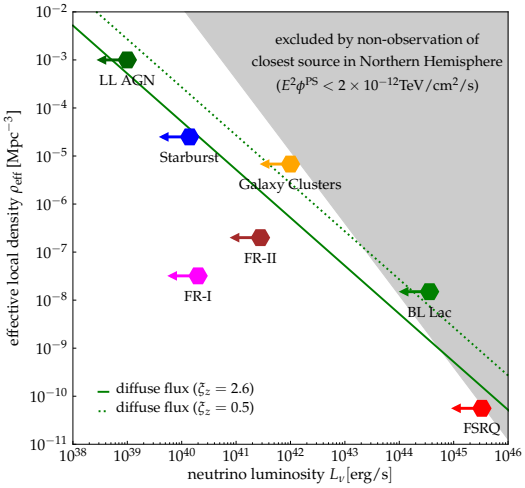

Fig. 21. The effective local density and (maximal) neutrino luminosity of various neutrino source candidates from Ref.[204] The green solid (green dotted) line shows the local density and luminosity of the population of sources responsible for the diffuse neutrino flux of $E^2\phi \simeq 10^{-8}$ GeV cm^{-2} s^{-1} sr^{-1} observed with IceCube, assuming source evolution following the star-formation rate ($\xi_z \simeq 2.6$) or no source evolution ($\xi_z \simeq 0.5$), respectively. The grey-shaded area indicates source populations that are excluded by the nonobservation of point sources in the Northern Hemisphere ($f_{\rm sky} \simeq 0.5$) with discovery potential $E^2\phi^{\rm PS} \simeq 2 \times 10^{-12}$ TeV cm^{-2} s^{-1}.[205]

emission from a single source[203] depending on the local density of sources,

$$\frac{1}{3}\sum_\alpha E_\nu^2 Q_{\nu_\alpha}(E_\nu) \simeq 1.7 \times 10^{43} \left(\frac{\xi_z}{2.6}\right)^{-1} \left(\frac{\rho_0}{10^{-8}\mathrm{Mpc}^{-3}}\right)^{-1} \mathrm{erg\,s}^{-1}\,. \quad (86)$$

For a homogenous distribution of sources, we expect, within the partial field of view $f_{\rm sky}$ of the full sky, one source within a distance d_1 determined by $f_{\rm sky} 4\pi d_1^3/3\,\rho_0 = 1$. In other words, d_1 defines the volume containing one nearby source for a homogeneous source density ρ_0. Defining ϕ_1 as the flux of a source at distance d_1, given by Eq. (80) with $z \simeq 0$ and $d_L \simeq d_1$, we can write the probability distribution $p(\phi)$ of finding the *closest* source of the population with a flux ϕ as (for details see App. of Ref.[203])

$$p(\phi) = \frac{3}{2}\frac{1}{\phi}\left(\frac{\phi_1}{\phi}\right)^{\frac{3}{2}} e^{-\left(\frac{\phi_1}{\phi}\right)^{\frac{3}{2}}}\,. \quad (87)$$

The average flux from the closest source is then $\langle\phi\rangle \simeq 2.7\phi_1$, with median $\phi_{\rm med} \simeq 1.3\phi_1$. Applying this to the closest source introduced above, we

obtain its per-flavor flux:

$$\frac{1}{3}\sum_{\alpha} E_\nu^2 \phi_{\nu_\alpha} \simeq 8{\times}10^{-13} \left(\frac{f_{\rm sky}}{0.5}\right)^{\frac{2}{3}} \left(\frac{\xi_z}{2.6}\right)^{-1} \left(\frac{\rho_0}{10^{-8}{\rm Mpc}^{-3}}\right)^{-\frac{1}{3}} {\rm TeV\,cm^{-2}\,s^{-1}}\,. \tag{88}$$

Interestingly, this value is not far from IceCube's point-source discovery potential at the level of $2 \times 10^{-12}\,{\rm TeV\,cm^{-2}\,s^{-1}}$ in the Northern Hemisphere.[205]

In Figure 21, we show the local density and luminosity of theorized neutrino sources.[204] The grey-shaded region is excluded by the failure to observe these sources as individual point sources, assuming the discovery potential of IceCube in the Northern Hemisphere given in the caption. The green lines show the combination of density and luminosity for sources at the level of the observed IceCube flux, assuming a source density evolution following the star formation rate (solid line) or no evolution (dotted line). We conclude that IceCube is presently sensitive to source populations with local source densities smaller than, conservatively, $10^{-8}\,{\rm Mpc}^{-3}$. Much lower local densities, like BL Lacs FSRQs, are challenged by the nonobservation of individual sources. Some source classes, like Fanaroff-Riley (FR) radio galaxies, have an estimated neutrino luminosity that is likely too low for the observed flux. Note that these estimates depend on the evolution parameter ξ_z, and therefore the exact sensitivity estimate depends on the redshift evolution of the source luminosity density. In addition, this simple estimate can be refined by considering not only the closest source of the population but the combined emission of *known* local sources; see, e.g., Ref.[203]

Is it possible that the sources of the extragalactic cosmic rays are themselves neutrino sources? From the measured cosmic-ray spectrum, one can derive that the emission rate density of nucleons is at the level of [71,72]

$$\mathcal{L}_p = \rho_0 E_p^2 Q_p(E_p) \simeq (1-2) \times 10^{44}\,{\rm erg\,Mpc^{-3}\,yr^{-1}}\,. \tag{89}$$

Combining this with Eq.25 we can derive the diffuse neutrino flux:

$$\frac{1}{3}\sum_{\alpha} E_\nu^2 \phi_{\nu_\alpha}(E_\nu) \simeq f_\pi \frac{\xi_z K_\pi}{1+K_\pi} (2-4) \times 10^{-8}\,{\rm GeV\,cm^{-2}\,s^{-1}\,sr}\,. \tag{90}$$

Here, ξ_z is the evolution factor previously introduced. The equation has been rewritten and some notation adjusted in order to accommodate both pp and γp interactions. Counting particles we derive that

$$\frac{1}{3}\sum_{\alpha} E_\nu Q_{\nu_\alpha}(E_\nu) = E_\pi Q_\pi\,, \tag{91}$$

from which the relation for energy follows by multiplying both sides with E_ν; an additional factor of 1/4 multiplies the right-hand side by the ratio of neutrino to pion energy within the approximations routinely used throughout.

The requirement $f_\pi \leq 1$ limits the neutrino production by the actual sources of the cosmic rays as pointed out by the seminal work by Waxman and Bahcall.[69] For optically thin sources, $f_\pi \ll 1$, neutrino production is only a small by-product of the acceleration process. The energy loss associated with pion production must not limit the sources' ability to accelerate the cosmic rays. On the other hand, optically thick sources, $f_\pi \simeq 1$, may be efficient neutrino emitters. Realistic sources of this type need different zones, one zone for the acceleration process ($f_\pi \ll 1$) and a second zone for the efficient conversion of cosmic rays to neutrinos ($f_\pi \simeq 1$). An example for this scenario are sources embedded in starburst galaxies, where cosmic rays can be stored over sufficiently long timescales to yield significant neutrino production.

For $\xi_z \simeq 2.4$ and $K_\pi \simeq 1-2$, the upper bound resulting from Eq. (90) and $f_\pi = 1$ is at the level of the neutrino flux observed by IceCube. Therefore, it is possible that the observed extragalactic cosmic rays and neutrinos have the same origin. A plausible scenario is a "calorimeter" in which only cosmic rays with energy below a few 10 PeV interact efficiently. An energy dependence of the calorimetric environment can be introduced by energy–dependent diffusion. If $D(E)$ is the diffusion coefficient, then the timescale of escape from the calorimeter is given by the solution to $6D(E)t = d^2$, where d is the effective size of the region. Typically, we have $D(E) \propto E^\delta$ with $\delta \simeq 0.3 - 0.6$. In the following, we again consider the case of protons. Taking $\sigma_{pp} \simeq 8 \times 10^{-26}\,\mathrm{cm}^2$ at $E_p = 100$ PeV and the diffusion coefficient of $D(E_p) \simeq D_{\rm GeV}(E_p/1\mathrm{GeV})^{1/3}$, the pp thickness can be expressed as $\tau_{pp} \simeq ctn_{\rm gas}\sigma_{pp}$ or

$$\tau_{pp} \simeq 0.18 \left(\frac{d}{100\,\mathrm{pc}}\right)^2 \left(\frac{D_{\rm GeV}}{10^{26}\mathrm{cm}^2/\mathrm{s}}\right)^{-1} \left(\frac{E_p}{10\ \mathrm{PeV}}\right)^{-1/3} \left(\frac{n}{100\mathrm{cm}^{-3}}\right) . \tag{92}$$

Here, we have used feasible parameters of starburst galaxies.[158,159] Therefore, depending on the calorimetric environment, it is possible that the flux below a few PeV is efficiently converted to neutrinos and contributes to the TeV–PeV diffuse emission observed by IceCube.

6.4. *Are Blazars the Sources of the Cosmic Neutrinos (and the Extragalactic Cosmic rays)?*

The qualitative matching of the energy densities of photons and neutrinos, discussed in the previous section, suggests that the unidentified neutrino sources contributing to the diffuse flux might have already been observed as strong gamma-ray emitters. Theoretical models[206,207] and recent data analyses[208–210] show that Fermi's extragalactic gamma-ray flux is dominated by blazars. A dedicated IceCube study[211] of Fermi-observed blazars showed no evidence of neutrino emission from these source candidates. However, the inferred limit on the their quasi-diffuse flux leaves room for a significant contribution to IceCube's diffuse neutrino flux at the 10% level and increasing towards PeV. This hypothesis is corroborated by the recent observation of the flaring blazar TXS0506+056 in the direction of a very high energy IceCube neutrino.

IceCube detects one well-localized muon neutrino every few minutes as an up-going track event. These events are dominated by low-energy atmospheric neutrinos. IceCube recently installed an automatic filter that selects in real time rare very high energy events that are potentially cosmic in origin and sends the astronomical coordinates to the Gamma-ray Coordinate Network for possible follow-up by astronomical telescopes. The tenth such alert, IceCube-170922A,[212] on September 22, 2017, reported a well-reconstructed muon neutrino with energy exceeding 180 TeV (most likely energy 290 TeV) and, therefore, with a significant probability of originating in outer space rather than in the Earth's atmosphere.

What makes this alert special is that telescopes detected enhanced gamma-ray activity from a flaring blazar aligned with the cosmic neutrino to within $0.06\circ$. The source is a known blazar, TXS0506+056, and its redshift has been subsequently measured to be $z \simeq 0.34$.[213] Originally detected by NASA's Fermi[214] and Swift[215] satellite telescopes, the alert was followed up by the MAGIC air Cherenkov telescope.[216] MAGIC detected gamma rays with energies exceeding 100 GeV. Several other telescopes subsequently observed the flaring blazar. Given where to look, IceCube searched in archival neutrino data, up to and including October 2017, for evidence of neutrino emission at the location of TXS0506+056. With a redshift of 0.34, we can conclude that the source is a TeV blazar. Several other telescopes subsequently observed the flaring blazar.

It is important to realize that nearby blazars like the Markarian sources are at a redshift that is ten times smaller, and therefore TXS0506+056,

with a similar flux despite the greater distance, is one of the most luminous sources in the Universe. It must belong to a special class of sources that accelerate proton beams revealed by the neutrino. That the source belongs to a subclass is also consistent with the fact that multiple attempts have not found a correlation between the arrival directions of cosmic neutrinos previously observed by IceCube and the various Fermi blazar catalogues that are dominated by 'vanilla' nearby sources.

Given where to look, IceCube searched its archival neutrino data up to and including October 2017, for evidence of neutrino emission at the location of TXS0506+056. When searching the sky for point sources of neutrinos, two analyses have been routinely performed: one looking for a steady emission and one that searches for flares over a variety of timescales. Evidence was found for a spectacular burst of 14 high-energy neutrinos in 110 days. It dominates the flux of the source over the last 9.5 years for which we have data. It is interesting to note that a subset of blazars, around $1 \sim 10\,\%$ of all blazars, bursting once in 10 years at the levels of TXS, can accommodate the diffuse cosmic neutrino flux observed by IceCube. The energy of the neutrino flux generated by the flaring blazars is at the same level as the flux in extragalactic cosmic rays, the Waxman-Bahcall bound.

It is important to note the striking fact that all high-energy spectra, for both photons and neutrinos and for both the 2014 and 2017 bursts, are consistent with a hard E^{-2} spectrum, which is expected for a cosmic accelerator. In fact, the gamma-ray spectrum flattens beyond that during the 110-day period of the 2014 burst. This, combined with the low probability for the coincident observation of Fermi and IceCube, the significance of the 2014 neutrino flare, and the detection of the TeV emission by MAGIC, puts the discovery of the first comic ray accelerator beyond question.

Here, we discuss how identification of TXS 0506+056 help us understand the total diffuse neutrino flux measured by IceCube and how it is tied to the production rate of the very high-energy cosmic rays. In order to calculate the flux of the high-energy neutrinos from a population of sources, we adopt the calculation of the flux introduced in[6] to relate diffuse neutrino flux to the energy injection rate of the cosmic rays and their efficiency to transfer energy from protons (Cosmic rays).

Considering a population of sources, with neutrino luminosity L_ν, the diffuse neutrino flux could be obtained by

$$E^2 \frac{dN}{dE} = \frac{1}{4\pi} \int d^3r \frac{L_\nu}{4\pi r^2} \rho \tag{93}$$

which can be simplified into

$$E^2\frac{dN}{dE} = \frac{c}{4\pi}t_H\xi L_\nu\rho \tag{94}$$

As we plan to work out the diffuse neutrino flux from time dependent (flaring) source, similar to TXS, and within the assumption that a fraction of sources contribute to the neutrino flux, we revise the equation to account for the duration of the flare, total time of observation, and the fraction of sources. Therefore,

$$E^2\frac{dN}{dE} = \frac{c}{4\pi}t_H\xi L_\nu\rho\frac{\Delta t}{T}\mathcal{F} \tag{95}$$

corresponding to

$$3\times10^{-11}\,\mathrm{TeVcm^{-2}s^{-1}sr^{-1}} = \frac{\mathcal{F}}{4\pi}\left(\frac{R_H}{3\,\mathrm{Gpc}}\right)\left(\frac{\xi}{1}\right)\left(\frac{L_\nu}{1.2\times10^{47}\,\mathrm{erg/s}}\right) \times\left(\frac{\rho}{10^{-8}\,\mathrm{Mpc^{-3}}}\right)\left(\frac{\Delta t}{110\,\mathrm{d}}\frac{10\,\mathrm{yr}}{T_{\rm obs}}\right) \tag{96}$$

which results in $\mathcal{F} = 0.05$. In summary, a special class of BL Lac blazars like TXS, that undergo 110 day duration flares would be describing the observed diffuse flux of high-energy cosmic neutrinos. The high-energy neutrino flaring sources constitute 5% of the sources.

The energetics in neutrino production from these sources has to be consistent with the flux of very(ultra) high-energy cosmic rays. Equivalently,

$$E^2\frac{dN}{dE} \simeq \frac{c}{4\pi}\left(\frac{1}{2}(1-e^{-f_\pi})\,\xi t_H\frac{dE}{dt}\right), \tag{97}$$

The cosmic rays injection rate at energies above 10^{16} eV is $(1-2)\times10^{44}\,\mathrm{erg\,Mpc^{-3}yr^{-1}}$. Comparing the results of the Equation 96, we can find the pion efficiency of the neutrino source

$$\left(\frac{L_\nu}{1.2\times10^{47}\,\mathrm{erg/s}}\right)\left(\frac{\rho}{10^{-8}\,\mathrm{Mpc^{-3}}}\right)\left(\frac{\Delta t}{110\,\mathrm{d}}\frac{10\,\mathrm{yr}}{T_{\rm obs}}\right)\left(\frac{\mathcal{F}}{0.05}\right) \simeq \frac{1}{2}(1-e^{-f_\pi})\,\frac{dE/dt}{(1-2)\times10^{44}\,\mathrm{erg\,Mpc^{-3}yr^{-1}}} \tag{98}$$

This corresponds to $f_\pi > 0.8$. In the section on blazar jets we discussed how this can be achieved with a proton beam with low boost factor interacting with the blue photons in the active galaxy. The jet producing the neutrinos is not transparent to TeV photons, only to photons with tens of GeV which is indeed what is observed in the 2014 flare in the Fermi data.

It is also worth noting that on July 31, 2016, IceCube sent out a similar neutrino alert. The AGILE collaboration, which operates an orbiting X-ray

and gamma-ray telescope, reported a day-long blazar flare in the direction of the neutrino, one day before the neutrino detection.[218] Before automatic alerts, in April 2016, the TANAMI collaboration argued for the association of the highest energy IceCube event at the time, dubbed "Big Bird," with the flaring blazar PKS B1424-418.[177] Finally, AMANDA, IceCube's predecessor, observed three neutrinos in coincidence with a rare flare of the blazar 1ES1959+650, detected by the Whipple telescope in 2002.[219] However, these detections did not reach the significance of the observations triggered by IceCube-170922A.

As discussed in the previous sections, the absence of a strong anisotropy of neutrino arrival directions raises the possibility that the cosmic neutrinos originate from a number of relatively weak extragalactic sources. It is indeed important to keep in mind that the interaction rate of a neutrino is so low that it travels unattenuated over cosmic distances through the tenuous matter and radiation backgrounds of the Universe. This makes the identification of individual point sources contributing to the IceCube flux challenging.[203,220–222] Even so, it is also important to realize that IceCube is capable of localizing the sources by observing multiple neutrinos originating in the same location. Not having observed neutrino clusters in the present data raises the question of how many events are required to make such a model-independent identification possible. The answer to this question suggests the construction of a next-generation detector that instruments a ten times larger volume of ice.[223]

7. Beyond Astronomy

IceCube was designed as a discovery instrument that covers a range of areas in multidisciplinary science. Examples include the search for Galactic supernova explosions and the study of neutrinos themselves. With higher energies and high-statistics data samples, opportunities for neutrino physics are varied.

7.1. *Searching for Dark Matter*

Neutrino telescopes are powerful tools in the search for the particle nature of dark matter. By using the deepest ice and a higher density of optical sensors, IceCube's DeepCore subarray lowers the threshold of the detector to $\sim 10\,\mathrm{GeV}$ over a significant fraction of the detector volume; see Fig. 3.

It was initially proposed as a way to enhance IceCube's capabilities for detecting lower mass dark matter particles. It is worth noting that the AMANDA detector, the forerunner and proof of concept for IceCube, received a significant fraction of its initial funding to search for dark matter. Also, in this context, some have considered the isotropic arrival directions of cosmic neutrinos to be a clue that they originate in the Galactic halo as a result of the decay of PeV-energy dark matter particles, a speculation that at this point is perfectly consistent with observations.[150–153,224–227]

More traditionally, IceCube and ANTARES search for dark matter by looking for the annihilation of weakly interacting massive particles (WIMPs) wherever they have accumulated to a high density: in the Sun,[228,229] in the Milky Way,[230–232] and in nearby galaxies.[233] For instance, WIMPs are swept up by the Sun as the solar system moves about the Galactic halo. Though interacting weakly, they will occasionally scatter elastically with nuclei in the Sun and lose sufficient momentum to become gravitationally bound. Over the lifetime of the Sun, WIMPs may accumulate to a density where equilibrium is established between their capture and annihilation. The annihilation of these WIMPs to final states that can decay to neutrinos represents an indirect signature of halo dark matter. This WIMP annihilation signal is revealed by the neutrinos that escape the Sun with minimal absorption. The neutrinos are, for instance, the decay products of heavy quarks and weak bosons resulting from the annihilation of WIMPs into $\chi\chi \to \tau\bar{\tau}$, $b\bar{b}$, or W^+W^-. Neutrino telescopes are sensitive to such neutrinos because of their relatively high energy, above 20 GeV at this point, reflecting the mass of the decaying WIMP.

The beauty of the indirect detection technique using neutrinos originating from the Sun is that the astrophysics of the problem is understood. The source in the Sun has built up over solar time, sampling the dark matter throughout the galaxy. Therefore, any possible structure in the halo has been averaged out. Given a WIMP mass and properties, one can unambiguously predict the signal in a neutrino telescope; if not observed, the model is ruled out. This is in contrast to other indirect searches whose sensitivity depends critically on the structure of halo dark matter; observation requires cuspy structure near the Galactic center or clustering on appropriate scales elsewhere. Observation necessitates not only appropriate WIMP properties but also favorable astrophysical circumstances.

IceCube has established world-leading limits on WIMPs with significant spin-dependent interactions with protons because they result in strong concentrations inside the Sun, a nearby and readily identifiable source.[234,235]

An excess of neutrinos, of GeV or higher energy, over the atmospheric neutrino background in the direction of the Sun is the signature of dark matter. There is no alternative astrophysical explanation of such a signal, which represents a smoking gun for dark matter particles. In most WIMP scenarios, the cross sections for WIMP capture and for WIMP annihilation are large enough so that an equilibrium between capture and annihilation would have been achieved within the age of the solar system.[236] In this case, limits on neutrinos from the Sun can be expressed in terms of the capture cross section. If equilibrium is not reached, weaker limits can still be derived.

The current IceCube limits[228,234,235] are shown in Fig. 22. These are derived from three years of muon neutrino observations; no excess of neutrinos over the atmospheric flux has been found in the direction of the Sun. By including events that start inside DeepCore, the mass range for the WIMP search could be extended down to 20 GeV, which overlaps some of the allowed region from the DAMA experiment.[237] Since the exact branching ratios of WIMP annihilation into different channels is model-dependent, experiments usually choose two annihilation channels that give extreme neutrino spectra to show their results. Annihilation into $b\bar{b}$ is chosen as a representative case producing a soft neutrino spectrum, and annihilation into W^+W^- or $\tau\bar{\tau}$ as a hard spectrum. Assuming a 100% branching ratio to each of these channels brackets the expected neutrino spectrum for any model with branching to more channels. IceCube and Super-K reach bounds at the $10^{-40} - 10^{-41}\mathrm{cm}^2$ level, covering the WIMP mass range, between the two experiments, from a few GeV to 100 TeV. Because of the A^2 coherence factor for scattering on heavy nuclei with atomic number A, the direct detection experiments have an advantage over IceCube for the case of spin-independent interactions. They thus achieve superior limits to IceCube.

7.2. *Neutrino Oscillations*

The first IceCube neutrino oscillation analysis[245] used data from the 79-string detector from May 2010 to May 2011. The analysis was based entirely on ν_μ-induced muons from below the horizon. By taking advantage of the DeepCore subarray of IceCube, neutrino oscillations were observed over an energy range that includes the oscillation minimum of around 25 GeV for propagation through the diameter of the Earth. Data were divided into two samples, muon tracks reconstructed using the entire IceCube detector

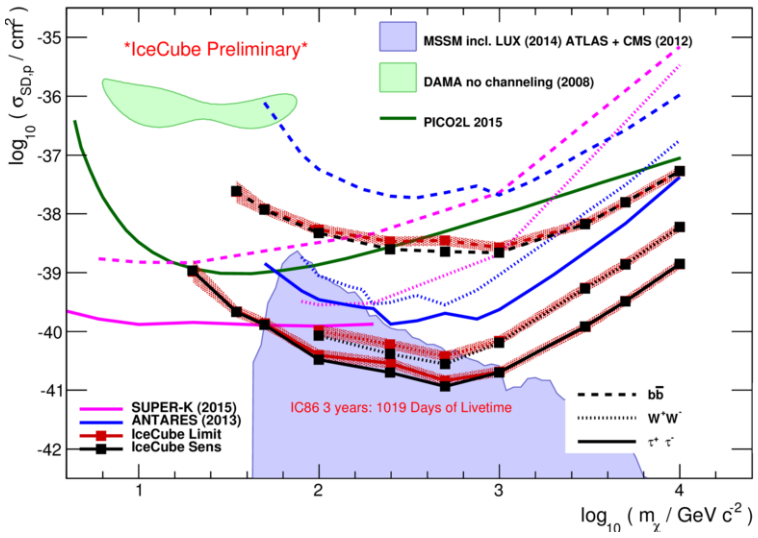

Fig. 22. Upper limits at 90% confidence level on the spin-dependent neutralino-proton cross section assuming that the neutrinos are produced by $b\bar{b}, \tau\bar{\tau}$, and W^+W^- annihilation. Limits from IceCube,[228,234,235] Super-K,[238] and ANTARES[239,240] are shown. Full lines refer to limits on the annihilation channel and dashed lines to the $b\bar{b}$ channel. Direct search results from PICO[241] and tentative signal regions[242–244] (green-shaded area) are included for comparison. The purple-shaded region indicates the allowed parameter space in MSSM supersymmetric dark matter models that are not ruled out by other experiments.

($E_\nu > 100$ GeV) and events starting in DeepCore ($20 < E_\nu < 100$ GeV). The low-energy sample consisted of 719 events, while the high-energy sample included 39,638 events. The high-energy sample, in which standard oscillations do not affect the rates, was used for calibration. A deficit was observed in the low-energy sample, where approximately 25% more events would have been detected in the absence of oscillations. Taking systematic uncertainties into account, including ± 0.05 in the spectral index of the atmospheric neutrino flux at production, the no-oscillation hypothesis was rejected at more than 5σ. The fitted values of the oscillation parameters in a two-flavor fit are $|\Delta m^2_{32}| = 2.3^{+0.5}_{-0.6} \times 10^{-3}$ eV^2 and $\sin^2 2\theta_{23} > 0.93$. For comparison, a recent global three-flavor analysis[246] gives 2.4 eV^2 and 0.95 respectively, with a range of $\pm 5\%$ at 1σ and a slight dependence on the mass hierarchy. While the measured oscillation parameters agree with previous experiments, it is important to realize that they have been measured at a characteristic energy that is higher. The measurement is therefore also

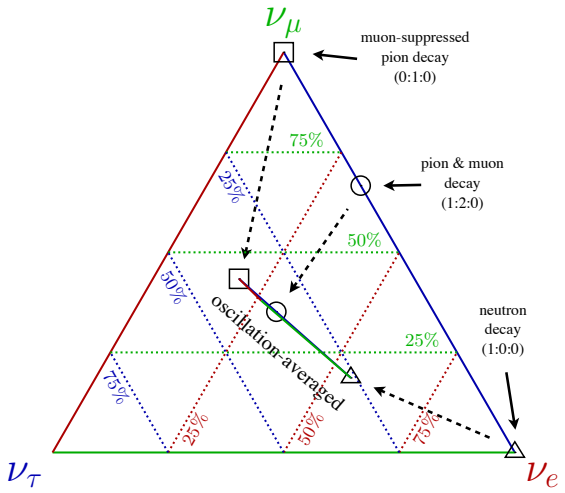

Fig. 23. Neutrino flavor phase space after oscillation. We use the best-fit oscillation parameters $\sin^2\theta_{12} = 0.304$, $\sin^2\theta_{23} = 0.577$, $\sin^2\theta_{13} = 0.0219$, and $\delta = 251^\circ$ following Ref.[247] updated after *Neutrino 2014*. Each position in the triangle parametrizes a general initial flavor ratio ($\nu_e : \nu_\mu : \nu_\tau$). We also indicate specific ratios for neutron decay and pion production. The inner triangle is the corresponding observable phase space after decoherence of the neutrino flavor state over large times or distances.

sensitive to any new neutrino physics, an important consideration when the precision of the IceCube measurements will be significantly improved. The above results will significantly improve with the development of analysis techniques that are optimized to the selection and analysis of low-energy events. Recently, IceCube has also contributed world-best limits on the existence of eV-mass sterile neutrinos.

7.3. *New Neutrino Physics*

Various authors have studied the implications of IceCube's HESE (high-energy starting event) topologies with astrophysical and/or exotic production mechanisms.[248–255] Figure 23 shows the general neutrino flavor phase space ν_e:ν_μ:ν_τ and the expected intrinsic flavor ratio in astrophysical sources from neutron decay (triangle), pion+muon decay (circle), and muon-damped pion decay (square). The observable neutrino flavor ratio is expected to be averaged over many oscillations. This leaves only a very narrow range for the possible flavor composition, which is shown as the line

in the center of Fig. 23. The corresponding observable flavor ratios of the three astrophysical production mechanisms are also indicated. The final parameter space is very close to the "tri-bi-maximal" approximation of mixing angles, which predicts that the final flavor ratio depends only on the initial electron neutrino ratio $x = N_{\nu_e}/N_{\nu_{\rm tot}}$ and $(2/3+x)$:$(7/6-x/2)$:$(7/6-x/2)$.

The precise relation between HESE topologies and flavor composition is nontrivial, since atmospheric backgrounds and detector effects have to be taken into account properly. In a recent IceCube analysis,[135] it was shown that the observation of tracks and cascades is consistent with most astrophysical scenarios within uncertainties. At sub-PeV energies (before ν_τ events can be distinguished from single cascades), the observation is mostly degenerate in terms of the total $\nu_e + \nu_\tau$ ratio, except for the contribution of prompt tau decays into muons. The expected fraction for tracks out of the total number events is about $7/24-x/8$, where we take into account that CC interactions are about three times larger than neutral current interactions at these energies. The uncertainty of the inferred intrinsic electron-neutrino fraction x is hence about eight times higher than the uncertainty of the track fraction. The situation becomes even more challenging if we include backgrounds and systematic uncertainties.

The situation of flavor identification improves at super-PeV neutrino energies. On one hand, the decay length of the τ produced in CC ν_τ interactions becomes resolvable by the detector and can in principle be distinguished from tracks and cascade events as argued before. On the other hand, electron antineutrinos, $\bar{\nu}_e$, can resonantly interact with in-ice electrons via the Glashow resonance, $\bar{\nu}_e e^- \to W^-$, at neutrino energies of about 6.3 PeV. This could be observable as a peak in the cascade spectrum, depending on the relative contribution of $\bar{\nu}_e$ after oscillation. In principle, this will allow us to answer the basic question of whether the cosmic neutrinos are photo- or hadro-produced in the source with different neutrino-to-antineutrino ratios.[256,257]

7.4. *Supernovae and Solar Flares*

In addition to the normal acquisition of events that reconstruct as tracks or cascades in the deep array of IceCube and as air showers in IceTop, the rates at which the PMT voltages cross the thresholds of discriminators in the DOMs are continuously monitored. Typical rates for DOMs in the deep ice are 500 Hz (including correlated afterpulses), most of which is noise. Typical rates in the high-gain DOMs of IceTop are 2-5 kHz, most of

which is induced by low-energy photons, electrons and muons entering the tanks.

A sudden increase in the total summed counting rate of the deep DOMs would signify a potential supernova explosion in the Galaxy. Supernova neutrinos of ~ 10 MeV interacting within a few meters of a DOM would generate enough hits to cause a sharp increase in the summed counting rate followed by a characteristic decline.[258] IceCube records a DC current that tracks the time evolution of the supernova in microsecond time bins. However, the detector records the time of every photoelectron with nanosecond precision and the binning can therefore be improved offline. This will improve the capability to identify the deleptonization burst. The additional measurement of the rate of neutrino events producing two photons is sensitive to the energy of the supernova neutrinos.

In IceTop, sudden changes in rates occur in response to solar events. Forbush decreases, in which the plasma from a solar flare abruptly reduces the rate of cosmic rays entering the atmosphere, are frequently detected and can be analyzed. More rare are sudden increases caused by solar energetic particles that enter the atmosphere with sufficient energy to generate secondary cosmic rays that reach the IceTop tanks. The event of December 13, 2006, was measured with the sixteen tanks (eight stations) then in operation.[259] The flare of May 17, 2012, is currently being analyzed.

7.5. *IceCube, the Facility*

During its construction phase, IceCube demonstrated a significant potential for facilitating a range of other research. For example, a dust logger provided measurements with millimeter precision that are valuable for event reconstruction in IceCube but that also provide a record of surface winds over more than 100,000 years.[260]

Already during construction of AMANDA, antennas forming the RICE detector were deployed in some holes to expand the target volume in the search for cosmogenic neutrinos.[261] An acoustic test setup of receivers in the upper portion of four IceCube holes was deployed in 2007 to explore the acoustic technique for detecting ultra-high-energy neutrinos. A retrievable transmitter (pinger) was submerged briefly in several newly prepared holes at various depths and distances from the receivers to measure the attenuation of sound in ice. The attenuation length of 300 m is significantly less than had been expected.[262] The Askaryan Radio Array (ARA)[263] plans to take advantage of the kilometer-scale attenuation for radio signals in

ice to construct a detector with a 200 km^2 effective area, which should be sufficient to determine the level of production of cosmogenic neutrinos, which at present is highly uncertain. The initially deployed ARA detectors send data to computers housed in the IceCube Lab (ICL) for staging and transmission to the north.

The DM-Ice experiment[264] proposes to repeat the DAMA experiment in the quiet environment of the Antarctic ice. An interesting feature of the observation is the fact that the seasonal modulation of the muon rate has the opposite phase relative to the motion of the Earth through the gas of dark matter as compared to a detector in the Northern Hemisphere. A test detector to explore the noise environment for DM-Ice was deployed at the bottom of an IceCube string in December 2010. Its computers and data transmission are also hosted in the ICL.

The enhancement of the low-energy capabilities of IceCube provided by the DeepCore subarray has led to the PINGU proposal[265] to deploy an additional 40 strings within the existing DeepCore detector. This would lower the threshold to below 5 GeV ($<$ 25 m muon track length in ice). In this energy range, matter effects in the Earth lead to resonant oscillations of $\nu_\mu \leftrightarrow \nu_e$ ($\bar{\nu}_\mu \leftrightarrow \bar{\nu}_e$) for normal (inverted) hierarchy[266] that depend on zenith angle. By taking advantage of the fact that the neutrino cross section is larger than that for antineutrinos, coupled with the excess of ν_μ compared to $\bar{\nu}_\mu$, a measurement sensitive to the neutrino mass hierarchy is possible on a relatively short timescale. PINGU would also have sensitivity to ν_μ disappearance, ν_τ appearance, and maximal mixing. The lower energy threshold would also enhance the indirect searches for dark matter with IceCube as well as the sensitivity to neutrinos from supernova explosions. In addition, there is the potential for neutrino tomography of the Earth with PINGU.

7.6. *From Discovery to Astronomy, and more...*

Accelerators of CRs produce neutrino fluxes limited in energy to roughly 5% of the maximal energy of the protons or nuclei. For Galactic neutrino sources, we expect neutrino spectra with a cutoff of a few hundred TeV. Detection of these neutrinos requires optimized sensitivities in the TeV range. At these energies, the atmospheric muon background limits the field of view of neutrino telescopes to the downward hemisphere. With IceCube focusing on high energies, a second kilometer-scale neutrino telescope in the Northern Hemisphere would ideally be optimized to observe the Galactic

center and the largest part of the Galactic plane.

Following the pioneering work of DUMAND,[8] several neutrino telescope projects were initiated in the Mediterranean in the 1990s.[10–12] In 2008, the construction of the ANTARES detector off the coast of France was completed. With an instrumented volume at about one percent of a cubic kilometer, ANTARES reaches roughly the same sensitivity as AMANDA and is currently the most sensitive observatory for high-energy neutrinos in the Northern Hemisphere. It has demonstrated the feasibility of neutrino detection in the deep sea and has provided a wealth of technical experience and design solutions for deep-sea components.

While less sensitive than IceCube to a diffuse extragalactic neutrino flux, ANTARES has demonstrated its competitive sensitivity to neutrino emission from the Galactic center[232,267] and extragalactic neutrino sources in the Southern Hemisphere.[268] The important synergy between Mediterranean and Antarctic neutrino telescopes has been demonstrated recently by the first joint study of continuous neutrino sources[269] as well as neutrino follow-up campaigns of gravitational waves.[270]

An international collaboration has started construction of a multi-cubic-kilometer neutrino telescope in the Mediterranean Sea, KM3NeT.[271] Major progress has been made in establishing the reliability and the cost-effectiveness of the design. This includes the development of a digital optical module that incorporates 31 3-inch photomultipliers instead of one large photomultiplier tube. The advantages are a tripling of the photocathode area per optical module, a segmentation of the photocathode allowing for a clean identification of coincident Cherenkov photons, some directional sensitivity, and a reduction of the overall number of penetrators and connectors, which are expensive and failure-prone. For all photomultiplier signals exceeding the noise level, time-over-threshold information is digitized and time-stamped by electronic modules housed inside the optical modules. This information is sent via optical fibers to shore, where the data stream will be filtered online for event candidates.

KM3NeT in its second phase[271] will consist of two ARCA units for astrophysical neutrino observations, each consisting of 115 strings (detection units) carrying more than 2,000 optical modules, and one ORCA detector studying fundamental neutrino physics with atmospheric neutrinos. The detection units are anchored to the seabed with deadweights and kept vertical by submerged buoys. The vertical distances between optical modules will be 36 meters, with horizontal distances between detection units at about 90 meters. Construction is now ongoing near Capo Passero (east of

Fig. 24. The KM3NeT optical module (from Ref.[271]). The optical module consists of a glass sphere with a diameter of 42 cm, housing 31 photosensors (yellowish disks). The glass sphere can withstand the pressure of the water and is transparent to the faint light that must be detected to see neutrinos.

Sicily).

A parallel effort is underway in Lake Baikal with the construction of the deep underwater neutrino telescope Baikal-GVD (Gigaton Volume Detector).[272] The first GVD cluster, named DUBNA, was upgraded in spring 2016 to its final size (288 optical modules, 120 meters in diameter, 525 meters high, and instrumented volume of 6 Mton). Each of the eight strings consists of three sections with 12 optical modules. Deployment of a second cluster was completed in spring 2017.

Further progress requires larger instruments. IceCube therefore proposes as a next step capitalizing on the opportunity of instrumenting $10\,\mathrm{km}^3$ of glacial ice at the South Pole and thereby improving on IceCube's sensitive volume by an order of magnitude.[273] This large gain is made possible by the unique optical properties of the Antarctic glacier revealed by the construction of IceCube. As a consequence of the extremely long photon absorption lengths in the deep Antarctic ice, the spacing between strings of light sensors can be increased from 125 to over 250 meters without significant loss of performance of the instrument. The instrumented volume can therefore grow by one order of magnitude while keeping the construction budget of a next-generation instrument at the level of the cost of the current IceCube detector. The new facility will increase the event rates of cosmic events from hundreds to thousands over several years.

IceCube has discovered a flux of extragalactic cosmic neutrinos with an energy density that matches that of extragalactic high-energy photons and UHE CRs. This may suggest that neutrinos and high-energy CRs share

a common origin. Identification of the sources by observation of multiple neutrino events from these sources with IceCube will undoubtedly be challenging and require even larger detectors. In the meantime, the possibility exists for revealing the sources by the comprehensive IceCube multimessenger program as illustrated by the observation of IceCube-170922A.

Construction of a next-generation instrument with at least five times higher sensitivity would likely result in the observation of cosmogenic neutrinos.[223] The rate expected with IceCube currently is only one event per year, assuming that all cosmic rays are protons (and it is difficult to imagine that a significant component of the highest energy neutrinos would not be protons). Obviously, higher sensitivity would also benefit the wide range of measurements performed with the present detector, from the search for dark matter to the precision limits on any violation of Lorentz invariance.

8. Acknowledgements

I thank my IceCube collaborators for discussions. This research was supported in part by the U.S. National Science Foundation under Grants No. OPP-0236449 and PHY-0354776; by the U.S. Department of Energy under Grant No. DE-FG02-95ER40896; by the University of Wisconsin Research Committee with funds granted by the Wisconsin Alumni Research Foundation.

References

1. F. Reines and C. L. Cowan, The neutrino, *Nature.* **178**, 446–449 (1956). doi: 10.1038/178446a0.
2. F. Halzen and S. R. Klein, Astronomy and astrophysics with neutrinos, *Phys. Today.* **61N5**, 29–35 (2008). doi: 10.1063/1.2930733.
3. A. Roberts, The Birth of high-energy neutrino astronomy: A Personal history of the DUMAND project, *Rev.Mod.Phys.* **64**, 259–312 (1992). doi: 10.1103/RevModPhys.64.259.
4. T. K. Gaisser, F. Halzen, and T. Stanev, Particle astrophysics with high-energy neutrinos, *Phys.Rept.* **258**, 173–236 (1995). doi: 10.1016/0370-1573(95)00003-Y.
5. J. Learned and K. Mannheim, High-energy neutrino astrophysics, *Ann.Rev.Nucl.Part.Sci.* **50**, 679–749 (2000). doi: 10.1146/annurev.nucl.50.1.679.
6. F. Halzen and D. Hooper, High-energy neutrino astronomy: The Cosmic ray connection, *Rept.Prog.Phys.* **65**, 1025–1078 (2002). doi: 10.1088/0034-4885/65/7/201.

7. M. Markov, On high energy neutrino physics. pp. 578–581 (1960).
8. J. Babson et al., Cosmic Ray Muons in the Deep Ocean, *Phys.Rev.* **D42**, 3613–3620 (1990). doi: 10.1103/PhysRevD.42.3613.
9. V. Balkanov et al., The BAIKAL neutrino project: Status report, *Nucl.Phys.Proc.Suppl.* **118**, 363–370 (2003). doi: 10.1016/S0920-5632(03)01334-3.
10. G. Aggouras et al., A measurement of the cosmic-ray muon flux with a module of the NESTOR neutrino telescope, *Astropart.Phys.* **23**, 377–392 (2005). doi: 10.1016/j.astropartphys.2005.02.001.
11. J. Aguilar et al., First results of the Instrumentation Line for the deep-sea ANTARES neutrino telescope, *Astropart.Phys.* **26**, 314–324 (2006). doi: 10.1016/j.astropartphys.2006.07.004.
12. E. Migneco, Progress and latest results from Baikal, Nestor, NEMO and KM3NeT, *J.Phys.Conf.Ser.* **136**, 022048 (2008). doi: 10.1088/1742-6596/136/2/022048.
13. IceCube Collaboration. Icecube preliminary design document (2001). `http://www.icecube.wisc.edu/science/publications/pdd/pdd.pdf`.
14. J. Ahrens et al., Sensitivity of the IceCube detector to astrophysical sources of high energy muon neutrinos, *Astropart.Phys.* **20**, 507–532 (2004). doi: 10.1016/j.astropartphys.2003.09.003.
15. J. K. Becker, High-energy neutrinos in the context of multimessenger physics, *Phys.Rept.* **458**, 173–246 (2008). doi: 10.1016/j.physrep.2007.10.006.
16. A. Achterberg et al., Multi-year search for a diffuse flux of muon neutrinos with AMANDA-II, *Phys. Rev.* **D76**, 042008 (2007). doi: 10.1103/PhysRevD.76.042008,10.1103/PhysRevD.77.089904. [Erratum: Phys. Rev.D77,089904(2008)].
17. W. Rhode et al., Limits on the flux of very high-energetic neutrinos with the Frejus detector, *Astropart. Phys.* **4**, 217–225 (1996). doi: 10.1016/0927-6505(95)00038-0.
18. R. Engel, D. Seckel, and T. Stanev, Neutrinos from propagation of ultrahigh-energy protons, *Phys.Rev.* **D64**, 093010 (2001). doi: 10.1103/PhysRevD.64.093010.
19. K. Kotera and A. V. Olinto, The Astrophysics of Ultrahigh Energy Cosmic Rays, *Ann. Rev. Astron. Astrophys.* **49**, 119–153 (2011). doi: 10.1146/annurev-astro-081710-102620.
20. M. Ahlers and F. Halzen, High-energy cosmic neutrino puzzle: a review, *Rept. Prog. Phys.* **78**(12), 126901 (2015). doi: 10.1088/0034-4885/78/12/126901.
21. Y. Farzan and A. Yu. Smirnov, Coherence and oscillations of cosmic neutrinos, *Nucl. Phys.* **B805**, 356–376 (2008). doi: 10.1016/j.nuclphysb.2008.07.028.
22. R. Gandhi, C. Quigg, M. H. Reno, and I. Sarcevic, Ultrahigh-energy neutrino interactions, *Astropart. Phys.* **5**, 81–110 (1996). doi: 10.1016/0927-6505(96)00008-4.
23. A. Cooper-Sarkar, P. Mertsch, and S. Sarkar, The high energy neutrino

cross-section in the Standard Model and its uncertainty, *JHEP.* **08**, 042 (2011). doi: 10.1007/JHEP08(2011)042.
24. V. Berezinsky and G. Zatsepin, Cosmic rays at ultrahigh-energies (neutrino?), *Phys.Lett.* **B28**, 423–424 (1969). doi: 10.1016/0370-2693(69)90341-4.
25. F. Halzen, Astroparticle physics with high energy neutrinos: from amanda to icecube, *Eur. Phys. J.* **C46**, 669–687 (2006). doi: 10.1140/epjc/s2006-02536-4.
26. F. Halzen and D. Saltzberg, Tau-neutrino appearance with a 1000 megaparsec baseline, *Phys. Rev. Lett.* **81**, 4305–4308 (1998). doi: 10.1103/PhysRevLett.81.4305.
27. E. Middell. Search for atmospheric neutrino induced particle showers with IceCube 40. In *Proceedings, 32nd International Cosmic Ray Conference (ICRC 2011): Beijing, China, August 11-18, 2011*, vol. 4, pp. 246–249 (2011). doi: 10.7529/ICRC2011/V04/1097. URL `http://www.ihep.ac.cn/english/conference/icrc2011/paper/proc/v4/v4_1097.pdf`.
28. S. R. Klein. Cascades from nu(E) above 10**20 eV. In *INFN Eloisatron Project 44th Workshop on QCD at Cosmic Energies: The Highest Energy Cosmic Rays and QCD Erice, Italy, August 29-September 5, 2004* (2004).
29. Particle Data Group. URL `pdg.lbl.gov` .
30. J. G. Learned and S. Pakvasa, Detecting tau-neutrino oscillations at PeV energies, *Astropart.Phys.* **3**, 267–274 (1995). doi: 10.1016/0927-6505(94)00043-3.
31. R. Abbasi et al., Measurement of the atmospheric neutrino energy spectrum from 100 GeV to 400 TeV with IceCube, *Phys.Rev.* **D83**, 012001 (2011). doi: 10.1103/PhysRevD.83.012001.
32. M. Aartsen et al., Measurement of the Atmospheric ν_e flux in IceCube, *Phys.Rev.Lett.* **110**(15), 151105 (2013). doi: 10.1103/PhysRevLett.110.151105.
33. S. Schönert, T. K. Gaisser, E. Resconi, and O. Schulz, Vetoing atmospheric neutrinos in a high energy neutrino telescope, *Phys.Rev.* **D79**, 043009 (2009). doi: 10.1103/PhysRevD.79.043009.
34. T. K. Gaisser, T. Stanev, and S. Tilav, Cosmic Ray Energy Spectrum from Measurements of Air Showers, *Front. Phys.(Beijing).* **8**, 748–758 (2013). doi: 10.1007/s11467-013-0319-7.
35. M. Aglietta et al., Upper limit on the prompt muon flux derived from the LVD underground experiment, *Phys.Rev.* **D60**, 112001 (1999). doi: 10.1103/PhysRevD.60.112001.
36. A. Schukraft, A view of prompt atmospheric neutrinos with IceCube, *Nucl.Phys.Proc.Suppl.* **237-238**, 266–268 (2013). doi: 10.1016/j.nuclphysbps.2013.04.105.
37. R. Enberg, M. H. Reno, and I. Sarcevic, Prompt neutrino fluxes from atmospheric charm, *Phys.Rev.* **D78**, 043005 (2008). doi: 10.1103/PhysRevD.78.043005.
38. T. K. Gaisser, Atmospheric leptons, *EPJ Web Conf.* **52**, 09004 (2013). doi: 10.1051/epjconf/20125209004.

39. P. Desiati and T. K. Gaisser, Seasonal variation of atmospheric leptons as a probe of charm, *Phys. Rev. Lett.* **105**, 121102 (2010). doi: 10.1103/PhysRevLett.105.121102.
40. P. Sommers, Ultra-high energy cosmic rays: Observational results, *Astropart. Phys.* **39-40**, 88–94 (2012). doi: 10.1016/j.astropartphys.2012.04.011.
41. W. Baade and F. Zwicky, Cosmic Rays from Super-novae, *Proceedings of the National Academy of Science.* **20**, 259–263 (May, 1934). doi: 10.1073/pnas.20.5.259.
42. H.E.S.S Collaboration, *Nature.* **531**, 476–479 (2016).
43. V. L. Ginzburg and S. I. Syrovatskii, *The origin of cosmic rays* (1969).
44. Y. Butt, Beyond the myth of the supernova-remnant origin of cosmic rays, *Nature.* **460**, 659–772 (2009). doi: 10.1038/nature08127.
45. T. K. Gaisser, Origin of cosmic radiation, *AIP Conf.Proc.* **558**, 27–42 (2001). doi: 10.1063/1.1370778.
46. E. Waxman, *Phys. Rev. Letters.* **75**, 386 (1995).
47. M. Gonzalez-Garcia, M. Maltoni, and J. Rojo, Determination of the atmospheric neutrino fluxes from atmospheric neutrino data, *JHEP.* **0610**, 075 (2006). doi: 10.1088/1126-6708/2006/10/075.
48. K. Daum et al., Determination of the atmospheric neutrino spectra with the Frejus detector, *Z.Phys.* **C66**, 417–428 (1995). doi: 10.1007/BF01556368.
49. R. Abbasi et al., Determination of the Atmospheric Neutrino Flux and Searches for New Physics with AMANDA-II, *Phys.Rev.* **D79**, 102005 (2009). doi: 10.1103/PhysRevD.79.102005.
50. R. Abbasi et al., The Energy Spectrum of Atmospheric Neutrinos between 2 and 200 TeV with the AMANDA-II Detector, *Astropart.Phys.* **34**, 48–58 (2010). doi: 10.1016/j.astropartphys.2010.05.001.
51. R. Abbasi et al., A Search for a Diffuse Flux of Astrophysical Muon Neutrinos with the IceCube 40-String Detector, *Phys.Rev.* **D84**, 082001 (2011). doi: 10.1103/PhysRevD.84.082001.
52. M. Honda, T. Kajita, K. Kasahara, S. Midorikawa, and T. Sanuki, Calculation of atmospheric neutrino flux using the interaction model calibrated with atmospheric muon data, *Phys.Rev.* **D75**, 043006 (2007). doi: 10.1103/PhysRevD.75.043006.
53. G. Barr, T. Gaisser, P. Lipari, S. Robbins, and T. Stanev, A Three - dimensional calculation of atmospheric neutrinos, *Phys.Rev.* **D70**, 023006 (2004). doi: 10.1103/PhysRevD.70.023006.
54. M. G. Aartsen et al., An All-Sky Search for Three Flavors of Neutrinos from Gamma-Ray Bursts with the IceCube Neutrino Observatory, *Astrophys. J.* **824**(2), 115 (2016). doi: 10.3847/0004-637X/824/2/115.
55. S. Adrian-Martinez et al., First search for neutrinos in correlation with gamma-ray bursts with the ANTARES neutrino telescope, *JCAP.* **1303**, 006 (2013). doi: 10.1088/1475-7516/2013/03/006.
56. E. Berezhko, Cosmic rays from active galactic nuclei, *Astrophys.J.* **684**, L69–L71 (2008). doi: 10.1086/592233.
57. J. Becker Tjus, B. Eichmann, F. Halzen, A. Kheirandish, and S. Saba, High-

energy neutrinos from radio galaxies, *Phys.Rev.* **D89**(12), 123005 (2014). doi: 10.1103/PhysRevD.89.123005.
58. D. Hooper, A Case for Radio Galaxies as the Sources of IceCube's Astrophysical Neutrino Flux, *JCAP.* **1609**(09), 002 (2016). doi: 10.1088/1475-7516/2016/09/002.
59. T. Gaisser, Neutrino astronomy: Physics goals, detector parameters (1997).
60. M. Ahlers, L. A. Anchordoqui, H. Goldberg, F. Halzen, A. Ringwald, et al., Neutrinos as a diagnostic of cosmic ray galactic/extra-galactic transition, *Phys.Rev.* **D72**, 023001 (2005). doi: 10.1103/PhysRevD.72.023001.
61. R. Abbasi et al., Time-Integrated Searches for Point-like Sources of Neutrinos with the 40-String IceCube Detector, *Astrophys.J.* **732**, 18 (2011). doi: 10.1088/0004-637X/732/1/18.
62. TeVCat Catalog, `http://tevcat.uchicago.edu` .
63. J. Alvarez-Muniz and F. Halzen, Possible high-energy neutrinos from the cosmic accelerator RX J1713.7-3946, *Astrophys.J.* **576**, L33–L36 (2002). doi: 10.1086/342978.
64. J. K. Becker, F. Halzen, A. O'Murchadha, and M. Olivo, Neutrino emission from high-energy component gamma-ray bursts (2010).
65. T. K. Gaisser, Very high energy photons and neutrinos: Implications for UHECR, *EPJ Web Conf.* **53**, 01012 (2013). doi: 10.1051/epjconf/20135301012.
66. F. Halzen, Neutrino astronomy: An update, *Riv.Nuovo Cim.* **36**(03), 81–104 (2013). doi: 10.1393/ncr/i2013-10086-y.
67. S. R. Kelner, F. A. Aharonian, and V. V. Bugayov, Energy spectra of gamma-rays, electrons and neutrinos produced at proton-proton interactions in the very high energy regime, *Phys. Rev.* **D74**, 034018 (2006). doi: 10.1103/PhysRevD.74.034018,10.1103/PhysRevD.79.039901. [Erratum: Phys. Rev.D79,039901(2009)].
68. C. Patrignani et al., Review of Particle Physics, *Chin. Phys.* **C40**(10), 100001 (2016). doi: 10.1088/1674-1137/40/10/100001.
69. E. Waxman and J. N. Bahcall, High-energy neutrinos from astrophysical sources: An Upper bound, *Phys.Rev.* **D59**, 023002 (1999). doi: 10.1103/PhysRevD.59.023002.
70. J. N. Bahcall and E. Waxman, High-energy astrophysical neutrinos: The Upper bound is robust, *Phys.Rev.* **D64**, 023002 (2001). doi: 10.1103/PhysRevD.64.023002.
71. M. Ahlers and F. Halzen, Minimal Cosmogenic Neutrinos, *Phys.Rev.* **D86**, 083010 (2012). doi: 10.1103/PhysRevD.86.083010.
72. B. Katz, E. Waxman, T. Thompson, and A. Loeb, The energy production rate density of cosmic rays in the local universe is $\sim 10^{44-45}$erg Mpc^{-3} yr^{-1} at all particle energies (2013).
73. E. Waxman. The Origin of IceCube?s Neutrinos: Cosmic Ray Accelerators Embedded in Star Forming Calorimeters. pp. 33–45 (2017). doi: 10.1142/9789814759410_0003. URL `http://inspirehep.net/record/1402566/files/arXiv:1511.00815.pdf`.
74. A. Aab et al., Combined fit of spectrum and composition data as measured

by the Pierre Auger Observatory, *JCAP.* **1704**(04), 038 (2017). doi: 10.1088/1475-7516/2017/04/038.
75. K. Mannheim and R. Schlickeiser, Interactions of Cosmic Ray Nuclei, *Astron. Astrophys.* **286**, 983–996 (1994).
76. F. Halzen and A. Kheirandish, High Energy Neutrinos from Recent Blazar Flares (2016).
77. F. Krauß et al., TANAMI Blazars in the IceCube PeV Neutrino Fields, *Astron. Astrophys.* **566**, L7 (2014). doi: 10.1051/0004-6361/201424219.
78. E. Waxman and J. N. Bahcall, High-energy neutrinos from cosmological gamma-ray burst fireballs, *Phys.Rev.Lett.* **78**, 2292–2295 (1997). doi: 10.1103/PhysRevLett.78.2292.
79. D. Guetta, D. Hooper, J. Alvarez-Muniz, F. Halzen, and E. Reuveni, Neutrinos from individual gamma-ray bursts in the BATSE catalog, *Astropart. Phys.* **20**, 429–455 (2004). doi: 10.1016/S0927-6505(03)00211-1.
80. S. Hummer, P. Baerwald, and W. Winter, Neutrino Emission from Gamma-Ray Burst Fireballs, Revised, *Phys. Rev. Lett.* **108**, 231101 (2012). doi: 10.1103/PhysRevLett.108.231101.
81. M. Ahlers, M. C. Gonzalez-Garcia, and F. Halzen, GRBs on probation: testing the UHE CR paradigm with IceCube, *Astropart. Phys.* **35**, 87–94 (2011). doi: 10.1016/j.astropartphys.2011.05.008.
82. R. Abbasi et al., Constraints on the Extremely-high Energy Cosmic Neutrino Flux with the IceCube 2008-2009 Data, *Phys.Rev.* **D83**, 092003 (2011). doi: 10.1103/PhysRevD.84.079902,10.1103/PhysRevD.83.092003.
83. N. Senno, K. Murase, and P. Mészáros, Choked Jets and Low-Luminosity Gamma-Ray Bursts as Hidden Neutrino Sources, *Phys. Rev.* **D93**(8), 083003 (2016). doi: 10.1103/PhysRevD.93.083003.
84. M. Bottcher and C. D. Dermer, High-energy gamma-rays from ultrahigh-energy cosmic ray protons in gamma-ray bursts, *Astrophys. J.* **499**, L131–L134 (1998). doi: 10.1086/311366.
85. M. Gonzalez-Garcia, F. Halzen, and S. Mohapatra, Identifying Galactic PeVatrons with Neutrinos, *Astropart.Phys.* **31**, 437–444 (2009). doi: 10.1016/j.astropartphys.2009.05.002.
86. M. Ahlers, P. Mertsch, and S. Sarkar, On cosmic ray acceleration in supernova remnants and the FERMI/PAMELA data, *Phys. Rev.* **D80**, 123017 (2009). doi: 10.1103/PhysRevD.80.123017.
87. A. A. Abdo et al., Discovery of TeV Gamma-Ray Emission from the Cygnus Region of the Galaxy, *Astrophys. J.* **658**, L33–L36 (2007). doi: 10.1086/513696.
88. F. Halzen, A. Kheirandish, and V. Niro, Prospects for Detecting Galactic Sources of Cosmic Neutrinos with IceCube: An Update (2016).
89. S. Gabici and F. A. Aharonian, Searching for galactic cosmic ray pevatrons with multi-TeV gamma rays and neutrinos, *Astrophys. J.* **665**, L131 (2007). doi: 10.1086/521047.
90. M. Ackermann et al., Detection of the Characteristic Pion-Decay Signature in Supernova Remnants, *Science.* **339**, 807 (2013). doi: 10.1126/science.1231160.

91. A. A. Abdo, Observations of the young supernova remnant RX J1713.7-3946 with the Fermi Large Area Telescope, *Astrophys. J.* **734**, 28 (2011). doi: 10.1088/0004-637X/734/1/28.
92. F. Halzen, A. Kappes, and A. O'Murchadha, Prospects for identifying the sources of the Galactic cosmic rays with IceCube, *Phys.Rev.* **D78**, 063004 (2008). doi: 10.1103/PhysRevD.78.063004.
93. A. Kappes, F. Halzen, and A. O. Murchadha, Prospects of identifying the sources of the galactic cosmic rays with IceCube, *Nucl. Instrum. Meth.* **A602**, 117–119 (2009). doi: 10.1016/j.nima.2008.12.049.
94. M. G. Aartsen et al., All-sky search for time-integrated neutrino emission from astrophysical sources with 7 years of IceCube data (2016).
95. S. Adrian-Martinez et al., Constraints on the neutrino emission from the Galactic Ridge with the ANTARES telescope, *Phys. Lett.* **B760**, 143–148 (2016). doi: 10.1016/j.physletb.2016.06.051.
96. K. Greisen, End to the cosmic ray spectrum?, *Phys.Rev.Lett.* **16**, 748–750 (1966). doi: 10.1103/PhysRevLett.16.748.
97. G. Zatsepin and V. Kuzmin, Upper limit of the spectrum of cosmic rays, *JETP Lett.* **4**, 78–80 (1966).
98. S. Yoshida and M. Teshima, Energy spectrum of ultrahigh-energy cosmic rays with extragalactic origin, *Prog.Theor.Phys.* **89**, 833–845 (1993). doi: 10.1143/PTP.89.833.
99. R. Protheroe and P. Johnson, Propagation of ultrahigh-energy protons over cosmological distances and implications for topological defect models, *Astropart.Phys.* **4**, 253 (1996). doi: 10.1016/0927-6505(95)00039-9.
100. V. Berezinsky, A. Z. Gazizov, and S. I. Grigorieva, On astrophysical solution to ultrahigh-energy cosmic rays, *Phys. Rev.* **D74**, 043005 (2006). doi: 10.1103/PhysRevD.74.043005.
101. Z. Fodor, S. D. Katz, A. Ringwald, and H. Tu, Bounds on the cosmogenic neutrino flux, *JCAP.* **0311**, 015 (2003). doi: 10.1088/1475-7516/2003/11/015.
102. H. Yuksel and M. D. Kistler, Enhanced cosmological GRB rates and implications for cosmogenic neutrinos, *Phys. Rev.* **D75**, 083004 (2007). doi: 10.1103/PhysRevD.75.083004.
103. H. Takami, K. Murase, S. Nagataki, and K. Sato, Cosmogenic neutrinos as a probe of the transition from Galactic to extragalactic cosmic rays, *Astropart. Phys.* **31**, 201–211 (2009). doi: 10.1016/j.astropartphys.2009.01.006.
104. A. A. Abdo et al., The Spectrum of the Isotropic Diffuse Gamma-Ray Emission Derived From First-Year Fermi Large Area Telescope Data, *Phys. Rev. Lett.* **104**, 101101 (2010). doi: 10.1103/PhysRevLett.104.101101.
105. M. Ackermann et al., The spectrum of isotropic diffuse gamma-ray emission between 100 MeV and 820 GeV, *Astrophys. J.* **799**, 86 (2015). doi: 10.1088/0004-637X/799/1/86.
106. V. Berezinsky, A. Gazizov, M. Kachelriess, and S. Ostapchenko, Restricting UHECRs and cosmogenic neutrinos with Fermi-LAT, *Phys.Lett.* **B695**, 13–18 (2011). doi: 10.1016/j.physletb.2010.11.019.
107. M. Ahlers, L. Anchordoqui, M. Gonzalez-Garcia, F. Halzen, and S. Sarkar,

GZK Neutrinos after the Fermi-LAT Diffuse Photon Flux Measurement, *Astropart.Phys.* **34**, 106–115 (2010). doi: 10.1016/j.astropartphys.2010.06.003.

108. G. B. Gelmini, O. Kalashev, and D. V. Semikoz, Gamma-Ray Constraints on Maximum Cosmogenic Neutrino Fluxes and UHECR Source Evolution Models, *JCAP.* **1201**, 044 (2012). doi: 10.1088/1475-7516/2012/01/044.
109. G. Decerprit and D. Allard, Constraints on the origin of ultrahigh energy cosmic rays from cosmogenic neutrinos and photons, *Astron.Astrophys.* **535**, A66 (2011). doi: 10.1051/0004-6361/201117673.
110. J. Heinze, D. Boncioli, M. Bustamante, and W. Winter, Cosmogenic Neutrinos Challenge the Cosmic Ray Proton Dip Model, *Astrophys. J.* **825**(2), 122 (2016). doi: 10.3847/0004-637X/825/2/122,10.3204/PUBDB-2016-01612.
111. A. D. Supanitsky, Implications of gamma-ray observations on proton models of ultrahigh energy cosmic rays, *Phys. Rev.* **D94**(6), 063002 (2016). doi: 10.1103/PhysRevD.94.063002.
112. M. G. Aartsen et al., Constraints on ultra-high-energy cosmic ray sources from a search for neutrinos above 10 PeV with IceCube (2016).
113. D. Hooper, A. Taylor, and S. Sarkar, The Impact of heavy nuclei on the cosmogenic neutrino flux, *Astropart.Phys.* **23**, 11–17 (2005). doi: 10.1016/j.astropartphys.2004.11.002.
114. M. Ave, N. Busca, A. V. Olinto, A. A. Watson, and T. Yamamoto, Cosmogenic neutrinos from ultra-high energy nuclei, *Astropart.Phys.* **23**, 19–29 (2005). doi: 10.1016/j.astropartphys.2004.11.001.
115. D. Hooper, S. Sarkar, and A. M. Taylor, The intergalactic propagation of ultrahigh energy cosmic ray nuclei, *Astropart.Phys.* **27**, 199–212 (2007). doi: 10.1016/j.astropartphys.2006.10.008.
116. D. Allard, M. Ave, N. Busca, M. Malkan, A. Olinto, et al., Cosmogenic Neutrinos from the propagation of Ultrahigh Energy Nuclei, *JCAP.* **0609**, 005 (2006). doi: 10.1088/1475-7516/2006/09/005.
117. L. A. Anchordoqui, H. Goldberg, D. Hooper, S. Sarkar, and A. M. Taylor, Predictions for the Cosmogenic Neutrino Flux in Light of New Data from the Pierre Auger Observatory, *Phys.Rev.* **D76**, 123008 (2007). doi: 10.1103/PhysRevD.76.123008.
118. R. Aloisio, V. Berezinsky, and A. Gazizov, Ultra High Energy Cosmic Rays: The disappointing model, *Astropart.Phys.* **34**, 620–626 (2011). doi: 10.1016/j.astropartphys.2010.12.008.
119. K. Kotera, D. Allard, and A. Olinto, Cosmogenic Neutrinos: parameter space and detectabilty from PeV to ZeV, *JCAP.* **1010**, 013 (2010). doi: 10.1088/1475-7516/2010/10/013.
120. M. Ahlers and J. Salvado, Cosmogenic gamma-rays and the composition of cosmic rays, *Phys.Rev.* **D84**, 085019 (2011). doi: 10.1103/PhysRevD.84.085019.
121. E. Roulet, G. Sigl, A. van Vliet, and S. Mollerach, PeV neutrinos from the propagation of ultra-high energy cosmic rays, *JCAP.* **1301**, 028 (2013). doi: 10.1088/1475-7516/2013/01/028.
122. L. Yacobi, D. Guetta, and E. Behar, Implication of the Non-detection of

gzk Neutrinos, *Astrophys. J.* **823**(2), 89 (2016). doi: 10.3847/0004-637X/823/2/89.
123. J. Ahrens et al., Muon track reconstruction and data selection techniques in AMANDA, *Nucl.Instrum.Meth.* **A524**, 169–194 (2004). doi: 10.1016/j.nima.2004.01.065.
124. M. Aartsen et al., Energy Reconstruction Methods in the IceCube Neutrino Telescope, *JINST.* **9**, P03009 (2014). doi: 10.1088/1748-0221/9/03/P03009.
125. C. Kopper, W. Giang, and N. Kurahashi. Observation of Astrophysical Neutrinos in Four Years of IceCube Data. In Proceedings of ICRC2015 **1081** (2015).
126. S. Schoenen and L. Rädel, *Proceedings of ICRC2015.* **1079**, 642 (2015).
127. M. G. Aartsen et al., Evidence for Astrophysical Muon Neutrinos from the Northern Sky with IceCube, *Phys. Rev. Lett.* **115**(8), 081102 (2015). doi: 10.1103/PhysRevLett.115.081102.
128. M. G. Aartsen et al., Observation and Characterization of a Cosmic Muon Neutrino Flux from the Northern Hemisphere using six years of IceCube data, *Astrophys. J.* **833**(1), 3 (2016). doi: 10.3847/0004-637X/833/1/3.
129. M. G. Aartsen et al., The IceCube Neutrino Observatory - Contributions to ICRC 2017 Part II: Properties of the Atmospheric and Astrophysical Neutrino Flux (2017).
130. M. G. Aartsen et al., Measurement of the Atmospheric ν_e Spectrum with IceCube, *Phys. Rev.* **D91**, 122004 (2015). doi: 10.1103/PhysRevD.91.122004.
131. M. Aartsen et al., Search for neutrino-induced particle showers with IceCube-40, *Phys.Rev.* **D89**, 102001 (2014). doi: 10.1103/PhysRevD.89.102001.
132. M. Aartsen et al., First observation of PeV-energy neutrinos with IceCube, *Phys.Rev.Lett.* **111**, 021103 (2013). doi: 10.1103/PhysRevLett.111.021103.
133. M. G. Aartsen et al., Evidence for High-Energy Extraterrestrial Neutrinos at the IceCube Detector, *Science.* **342**, 1242856 (2013). doi: 10.1126/science.1242856.
134. T. K. Gaisser, K. Jero, A. Karle, and J. van Santen, A generalized self-veto probability for atmospheric neutrinos, *Phys.Rev.* **D90**, 023009 (2014). doi: 10.1103/PhysRevD.90.023009.
135. M. G. Aartsen et al., Flavor Ratio of Astrophysical Neutrinos above 35 TeV in IceCube, *Phys. Rev. Lett.* **114**(17), 171102 (2015). doi: 10.1103/PhysRevLett.114.171102.
136. M. G. Aartsen et al., Lowering IceCube's Energy Threshold for Point Source Searches in the Southern Sky, *Astrophys. J.* **824**(2), L28 (2016). doi: 10.3847/2041-8205/824/2/L28.
137. M. Ahlers and K. Murase, Probing the Galactic Origin of the IceCube Excess with Gamma-Rays, *Phys.Rev.* **D90**, 023010 (2014). doi: 10.1103/PhysRevD.90.023010.
138. J. C. Joshi, W. Winter, and N. Gupta, How Many of the Observed Neutrino Events Can Be Described by Cosmic Ray Interactions in the Milky Way? **3414**, 3419 (2013). doi: 10.1093/mnras/stu189,10.1093/mnras/stu2132.

139. A. Neronov, D. Semikoz, and C. Tchernin, PeV neutrinos from interactions of cosmic rays with the interstellar medium in the Galaxy, *Phys.Rev.* **D89**, 103002 (2014). doi: 10.1103/PhysRevD.89.103002.
140. M. Kachelriess and S. Ostapchenko, Neutrino yield from Galactic cosmic rays, *Phys.Rev.* **D90**, 083002 (2014). doi: 10.1103/PhysRevD.90.083002.
141. D. Gaggero, D. Grasso, A. Marinelli, A. Urbano, and M. Valli, The gamma-ray and neutrino sky: A consistent picture of Fermi-LAT, Milagro, and IceCube results, *Astrophys. J.* **815**(2), L25 (2015). doi: 10.1088/2041-8205/815/2/L25.
142. A. Neronov and D. V. Semikoz, Evidence the Galactic contribution to the IceCube astrophysical neutrino flux, *Astropart. Phys.* **75**, 60–63 (2016). doi: 10.1016/j.astropartphys.2015.11.002.
143. D. Fox, K. Kashiyama, and P. Mészáros, Sub-PeV Neutrinos from TeV Unidentified Sources in the Galaxy, *Astrophys.J.* **774**, 74 (2013). doi: 10.1088/0004-637X/774/1/74.
144. M. Gonzalez-Garcia, F. Halzen, and V. Niro, Reevaluation of the Prospect of Observing Neutrinos from Galactic Sources in the Light of Recent Results in Gamma Ray and Neutrino Astronomy, *Astropart.Phys.* **57-58**, 39–48 (2014). doi: 10.1016/j.astropartphys.2014.04.001.
145. L. A. Anchordoqui, H. Goldberg, T. C. Paul, L. H. M. da Silva, and B. J. Vlcek, Estimating the contribution of Galactic sources to the diffuse neutrino flux, *Phys. Rev.* **D90**(12), 123010 (2014). doi: 10.1103/PhysRevD.90.123010.
146. S. Razzaque, The Galactic Center Origin of a Subset of IceCube Neutrino Events, *Phys.Rev.* **D88**, 081302 (2013). doi: 10.1103/PhysRevD.88.081302.
147. C. Lunardini, S. Razzaque, K. T. Theodoseau, and L. Yang, Neutrino Events at IceCube and the Fermi Bubbles, *Phys.Rev.* **D90**, 023016 (2014). doi: 10.1103/PhysRevD.90.023016.
148. A. M. Taylor, S. Gabici, and F. Aharonian, A Galactic Halo Origin of the Neutrinos Detected by IceCube, *Phys.Rev.* **D89**, 103003 (2014). doi: 10.1103/PhysRevD.89.103003.
149. O. Kalashev and S. Troitsky, Fluxes of diffuse gamma rays and neutrinos from cosmic-ray interactions with the circumgalactic gas, *Phys. Rev.* **D94** (6), 063013 (2016). doi: 10.1103/PhysRevD.94.063013.
150. B. Feldstein, A. Kusenko, S. Matsumoto, and T. T. Yanagida, Neutrinos at IceCube from Heavy Decaying Dark Matter, *Phys.Rev.* **D88**(1), 015004 (2013). doi: 10.1103/PhysRevD.88.015004.
151. A. Esmaili and P. D. Serpico, Are IceCube neutrinos unveiling PeV-scale decaying dark matter?, *JCAP.* **1311**, 054 (2013). doi: 10.1088/1475-7516/2013/11/054.
152. Y. Bai, R. Lu, and J. Salvado, Geometric Compatibility of IceCube TeV-PeV Neutrino Excess and its Galactic Dark Matter Origin, *JHEP.* **01**, 161 (2016). doi: 10.1007/JHEP01(2016)161.
153. K. Murase, R. Laha, S. Ando, and M. Ahlers, Testing the Dark Matter Scenario for PeV Neutrinos Observed in IceCube, *Phys. Rev. Lett.* **115**(7), 071301 (2015). doi: 10.1103/PhysRevLett.115.071301.

154. S. M. Boucenna, M. Chianese, G. Mangano, G. Miele, S. Morisi, O. Pisanti, and E. Vitagliano, Decaying Leptophilic Dark Matter at IceCube, *JCAP.* **1512**(12), 055 (2015). doi: 10.1088/1475-7516/2015/12/055.
155. M. Chianese, G. Miele, and S. Morisi, Dark Matter interpretation of low energy IceCube MESE excess, *JCAP.* **1701**(01), 007 (2017). doi: 10.1088/1475-7516/2017/01/007.
156. T. Cohen, K. Murase, N. L. Rodd, B. R. Safdi, and Y. Soreq, γ-ray Constraints on Decaying Dark Matter and Implications for IceCube, *Phys. Rev. Lett.* **119**(2), 021102 (2017). doi: 10.1103/PhysRevLett.119.021102.
157. N. Gupta, Galactic PeV Neutrinos, *Astropart.Phys.* **48**, 75–77 (2013). doi: 10.1016/j.astropartphys.2013.07.003.
158. A. Loeb and E. Waxman, The Cumulative background of high energy neutrinos from starburst galaxies, *JCAP.* **0605**, 003 (2006). doi: 10.1088/1475-7516/2006/05/003.
159. K. Murase, M. Ahlers, and B. C. Lacki, Testing the Hadronuclear Origin of PeV Neutrinos Observed with IceCube, *Phys.Rev.* **D88**(12), 121301 (2013). doi: 10.1103/PhysRevD.88.121301.
160. H.-N. He, T. Wang, Y.-Z. Fan, S.-M. Liu, and D.-M. Wei, Diffuse PeV neutrino emission from ultraluminous infrared galaxies, *Phys.Rev.* **D87**(6), 063011 (2013). doi: 10.1103/PhysRevD.87.063011.
161. L. A. Anchordoqui, T. C. Paul, L. H. M. da Silva, D. F. Torres, and B. J. Vlcek, What IceCube data tell us about neutrino emission from star-forming galaxies (so far), *Phys.Rev.* **D89**, 127304 (2014). doi: 10.1103/PhysRevD.89.127304.
162. X.-C. Chang and X.-Y. Wang, The diffuse gamma-ray flux associated with sub-PeV/PeV neutrinos from starburst galaxies, *Astrophys.J.* **793**(2), 131 (2014). doi: 10.1088/0004-637X/793/2/131.
163. I. Tamborra, S. Ando, and K. Murase, Star-forming galaxies as the origin of diffuse high-energy backgrounds: Gamma-ray and neutrino connections, and implications for starburst history, *JCAP.* **1409**(09), 043 (2014). doi: 10.1088/1475-7516/2014/09/043.
164. K. Bechtol, M. Ahlers, M. Di Mauro, M. Ajello, and J. Vandenbroucke, Evidence against star-forming galaxies as the dominant source of IceCube neutrinos, *Astrophys. J.* **836**(1), 47 (2017). doi: 10.3847/1538-4357/836/1/47.
165. Extragalactic star-forming galaxies with hypernovae and supernovae as high-energy neutrino and gamma-ray sources: the case of the 10 TeV neutrino data, *Astrophys. J.* **806**(1), 24 (2015). doi: 10.1088/0004-637X/806/1/24.
166. F. Stecker, C. Done, M. Salamon, and P. Sommers, High-energy neutrinos from active galactic nuclei, *Phys.Rev.Lett.* **66**, 2697–2700 (1991). doi: 10.1103/PhysRevLett.66.2697.
167. F. W. Stecker, PeV neutrinos observed by IceCube from cores of active galactic nuclei, *Phys.Rev.* **D88**(4), 047301 (2013). doi: 10.1103/PhysRevD.88.047301.
168. O. Kalashev, D. Semikoz, and I. Tkachev, Neutrinos in IceCube from AGN's

(2014).
169. Y. Bai, A. Barger, V. Barger, R. Lu, A. Peterson, et al., Neutrino Lighthouse at Sagittarius A*, *Phys.Rev.* **D90**, 063012 (2014). doi: 10.1103/PhysRevD.90.063012.
170. S. S. Kimura, K. Murase, and K. Toma, Neutrino and Cosmic-Ray Emission and Cumulative Background from Radiatively Inefficient Accretion Flows in Low-Luminosity Active Galactic Nuclei, *Astrophys. J.* **806**, 159 (2015). doi: 10.1088/0004-637X/806/2/159.
171. X. Wang and A. Loeb, Cumulative neutrino background from quasar-driven outflows (2016).
172. F. Tavecchio and G. Ghisellini, High-energy cosmic neutrinos from spine-sheath BL Lac jets, *Mon. Not. Roy. Astron. Soc.* **451**(2), 1502–1510 (2015). doi: 10.1093/mnras/stv1023.
173. P. Padovani and E. Resconi, Are both BL Lacs and pulsar wind nebulae the astrophysical counterparts of IceCube neutrino events?, *Mon.Not.Roy.Astron.Soc.* **443**, 474–484 (2014). doi: 10.1093/mnras/stu1166.
174. C. D. Dermer, K. Murase, and Y. Inoue, Photopion Production in Black-Hole Jets and Flat-Spectrum Radio Quasars as PeV Neutrino Sources, *JHEAp.* **3-4**, 29–40 (2014). doi: 10.1016/j.jheap.2014.09.001.
175. M. Petropoulou, S. Dimitrakoudis, P. Padovani, A. Mastichiadis, and E. Resconi, Photohadronic origin of γ-ray BL Lac emission: implications for IceCube neutrinos, *Mon. Not. Roy. Astron. Soc.* **448**(3), 2412–2429 (2015). doi: 10.1093/mnras/stv179.
176. P. Padovani, M. Petropoulou, P. Giommi, and E. Resconi, A simplified view of blazars: the neutrino background, *Mon. Not. Roy. Astron. Soc.* **452**(2), 1877–1887 (2015). doi: 10.1093/mnras/stv1467.
177. M. Kadler et al., Coincidence of a high-fluence blazar outburst with a PeV-energy neutrino event (2016).
178. P. Padovani, E. Resconi, P. Giommi, B. Arsioli, and Y. L. Chang, Extreme blazars as counterparts of IceCube astrophysical neutrinos, *Mon. Not. Roy. Astron. Soc.* **457**(4), 3582–3592 (2016). doi: 10.1093/mnras/stw228.
179. A. Neronov, D. V. Semikoz, and K. Ptitsyna, Strong constraints on hadronic models of blazar activity from Fermi and IceCube stacking analysis, *Astron. Astrophys.* **603**, A135 (2017). doi: 10.1051/0004-6361/201630098.
180. S. Ando and J. F. Beacom, Revealing the supernova-gamma-ray burst connection with TeV neutrinos, *Phys.Rev.Lett.* **95**, 061103 (2005). doi: 10.1103/PhysRevLett.95.061103.
181. K. Murase and K. Ioka, TeV-PeV Neutrinos from Low-Power Gamma-Ray Burst Jets inside Stars, *Phys.Rev.Lett.* **111**(12), 121102 (2013). doi: 10.1103/PhysRevLett.111.121102.
182. I. Tamborra and S. Ando, Inspecting the supernova–gamma-ray-burst connection with high-energy neutrinos, *Phys. Rev.* **D93**(5), 053010 (2016). doi: 10.1103/PhysRevD.93.053010.
183. P. Mészáros and E. Waxman, TeV neutrinos from successful and choked gamma-ray bursts, *Phys. Rev. Lett.* **87**, 171102 (2001). doi: 10.1103/

PhysRevLett.87.171102.
184. P. B. Denton and I. Tamborra, Exploring the Properties of Choked Gamma-Ray Bursts with IceCube's High Energy Neutrinos (2017).
185. S. Dado and A. Dar, Origin of the High Energy Cosmic Neutrino Background, *Phys.Rev.Lett.* **113**(19), 191102 (2014). doi: 10.1103/PhysRevLett.113.191102.
186. K. Kashiyama and P. Mészáros, Galaxy Mergers as a Source of Cosmic Rays, Neutrinos, and Gamma Rays, *Astrophys.J.* **790**, L14 (2014). doi: 10.1088/2041-8205/790/1/L14.
187. V. Berezinsky, P. Blasi, and V. Ptuskin, Clusters of galaxies as a storage room for cosmic rays, *Astrophys J.* **487**, 529–535 (1997). doi: 10.1086/304622.
188. K. Murase, S. Inoue, and S. Nagataki, Cosmic Rays Above the Second Knee from Clusters of Galaxies and Associated High-Energy Neutrino Emission, *Astrophys.J.* **689**, L105 (2008). doi: 10.1086/595882.
189. F. Zandanel, I. Tamborra, S. Gabici, and S. Ando, High-energy gamma-ray and neutrino backgrounds from clusters of galaxies and radio constraints, *Astron. Astrophys.* **578**, A32 (2015). doi: 10.1051/0004-6361/201425249.
190. X.-Y. Wang and R.-Y. Liu, Tidal disruption jets of supermassive black holes as hidden sources of cosmic rays: explaining the IceCube TeV-PeV neutrinos, *Phys. Rev.* **D93**(8), 083005 (2016). doi: 10.1103/PhysRevD.93.083005.
191. N. Senno, K. Murase, and P. Mészáros, High-energy Neutrino Flares from X-Ray Bright and Dark Tidal Disruption Events, *Astrophys. J.* **838**(1), 3 (2017). doi: 10.3847/1538-4357/aa6344.
192. L. Dai and K. Fang, Can tidal disruption events produce the IceCube neutrinos?, *Mon. Not. Roy. Astron. Soc.* **469**(2), 1354–1359 (2017). doi: 10.1093/mnras/stx863.
193. C. Lunardini and W. Winter, High Energy Neutrinos from the Tidal Disruption of Stars, *Phys. Rev.* **D95**(12), 123001 (2017). doi: 10.1103/PhysRevD.95.123001.
194. D. Biehl, D. Boncioli, C. Lunardini, and W. Winter, Tidally disrupted stars as a possible origin of both cosmic rays and neutrinos at the highest energies (2017).
195. M. Aartsen et al., Observation of High-Energy Astrophysical Neutrinos in Three Years of IceCube Data, *Phys.Rev.Lett.* **113**, 101101 (2014). doi: 10.1103/PhysRevLett.113.101101.
196. M. G. Aartsen et al. The IceCube Neutrino Observatory - Contributions to ICRC 2015 Part II: Atmospheric and Astrophysical Diffuse Neutrino Searches of All Flavors. In *Proceedings, 34th International Cosmic Ray Conference (ICRC 2015): The Hague, The Netherlands, July 30-August 6, 2015* (2015). URL `http://inspirehep.net/record/1398539/files/arXiv:1510.05223.pdf`.
197. A. Aab et al. The Pierre Auger Observatory: Contributions to the 34th International Cosmic Ray Conference (ICRC 2015). In *Proceedings, 34th International Cosmic Ray Conference (ICRC 2015): The Hague, The*

Netherlands, July 30-August 6, 2015 (2015). URL `http://inspirehep.net/record/1393211/files/arXiv:1509.03732.pdf`.

198. M. Di Mauro and F. Donato, Composition of the Fermi-LAT isotropic gamma-ray background intensity: Emission from extragalactic point sources and dark matter annihilations, *Phys. Rev.* **D91**(12), 123001 (2015). doi: 10.1103/PhysRevD.91.123001.
199. R. J. Protheroe and T. Stanev, Electronphoton cascading of very high-energy gamma-rays in the infrared background, *Monthly Notices of the Royal Astronomical Society.* **264**(1), 191–200 (1993). doi: 10.1093/mnras/264.1.191. URL `http://dx.doi.org/10.1093/mnras/264.1.191`.
200. K. Murase, D. Guetta, and M. Ahlers, Hidden Cosmic-Ray Accelerators as an Origin of TeV-PeV Cosmic Neutrinos, *Phys. Rev. Lett.* **116**(7), 071101 (2016). doi: 10.1103/PhysRevLett.116.071101.
201. M. G. Aartsen et al., Very High-Energy Gamma-Ray Follow-Up Program Using Neutrino Triggers from IceCube, *JINST.* **11**(11), P11009 (2016). doi: 10.1088/1748-0221/11/11/P11009.
202. M. G. Aartsen et al., The IceCube Realtime Alert System, *Astropart. Phys.* **92**, 30–41 (2017). doi: 10.1016/j.astropartphys.2017.05.002.
203. M. Ahlers and F. Halzen, Pinpointing Extragalactic Neutrino Sources in Light of Recent IceCube Observations, *Phys. Rev.* **D90**(4), 043005 (2014). doi: 10.1103/PhysRevD.90.043005.
204. P. Mertsch, M. Rameez, and I. Tamborra, Detection prospects for high energy neutrino sources from the anisotropic matter distribution in the local universe (2016).
205. M. G. Aartsen et al., The IceCube Neutrino Observatory - Contributions to ICRC 2017 Part I: Searches for the Sources of Astrophysical Neutrinos (2017).
206. M. Ajello et al., The Luminosity Function of Fermi-detected Flat-Spectrum Radio Quasars, *Astrophys. J.* **751**, 108 (2012). doi: 10.1088/0004-637X/751/2/108.
207. M. Di Mauro, F. Donato, G. Lamanna, D. A. Sanchez, and P. D. Serpico, Diffuse γ-ray emission from unresolved BL Lac objects, *Astrophys. J.* **786**, 129 (2014). doi: 10.1088/0004-637X/786/2/129.
208. M. Ackermann et al., Resolving the Extragalactic γ-Ray Background above 50 GeV with the Fermi Large Area Telescope, *Phys. Rev. Lett.* **116**(15), 151105 (2016). doi: 10.1103/PhysRevLett.116.151105.
209. H.-S. Zechlin, A. Cuoco, F. Donato, N. Fornengo, and A. Vittino, Unveiling the Gamma-ray Source Count Distribution Below the Fermi Detection Limit with Photon Statistics, *Astrophys. J. Suppl.* **225**(2), 18 (2016). doi: 10.3847/0067-0049/225/2/18.
210. M. Lisanti, S. Mishra-Sharma, L. Necib, and B. R. Safdi, Deciphering Contributions to the Extragalactic Gamma-Ray Background from 2 GeV to 2 TeV, *Astrophys. J.* **832**(2), 117 (2016). doi: 10.3847/0004-637X/832/2/117.
211. M. G. Aartsen et al., The contribution of Fermi-2LAC blazars to the diffuse TeV-PeV neutrino flux, *Astrophys. J.* **835**(1), 45 (2017). doi: 10.3847/1538-4357/835/1/45.

212. C. Kopper and E. Blaufuss, IceCube-170922A - IceCube observation of a high-energy neutrino candidate event., *GRB Coordinates Network, Circular Service, No. 21916, #1 (2017).* **21916** (2017).
213. S. Paiano, R. Falomo, A. Treves, and R. Scarpa, The redshift of the BL Lac object TXS 0506+056, *Astrophys. J.* **854**(2), L32 (2018). doi: 10.3847/2041-8213/aaad5e.
214. Y. T. Tanaka, S. Buson, and D. Kocevski, Fermi-LAT detection of increased gamma-ray activity of TXS 0506+056, located inside the IceCube-170922A error region., *The Astronomer's Telegram.* **10791** (Sept., 2017).
215. P. A. E. A. Keivani, J. A. Kennea, D. B. Fox, D. F. Cowen, J. P. Osborne, F. E. Marshall, and Swift-IceCube Collaboration, Further Swift-XRT observations of IceCube 170922A, *The Astronomer's Telegram.* **10792** (Sept., 2017).
216. R. Mirzoyan, First-time detection of VHE gamma rays by MAGIC from a direction consistent with the recent EHE neutrino event IceCube-170922A, *The Astronomer's Telegram.* **10817** (Oct., 2017).
217. `http://gcn.gsfc.nasa.gov` .
218. F. Lucarelli et al., AGILE detection of a candidate gamma-ray precursor to the ICECUBE-160731 neutrino event, *Astrophys. J.* **846**(2), 121 (2017). doi: 10.3847/1538-4357/aa81c8.
219. M. K. Daniel et al., Spectrum of very high energy gamma-rays from the blazar 1ES1959+650 during flaring activity in 2002, *Astrophys. J.* **621**, 181 (2005). doi: 10.1086/427406.
220. P. Lipari, Perspectives of High Energy Neutrino Astronomy, *Nucl.Instrum.Meth.* **A567**, 405–417 (2006). doi: 10.1016/j.nima.2006.05.249.
221. J. K. Becker, A. Groß, K. Münich, J. Dreyer, W. Rhode, and P. L. Biermann, Astrophysical implications of high energy neutrino limits, *Astropart.Phys.* **28**, 98–118 (2007). doi: 10.1016/j.astropartphys.2007.04.007.
222. A. Silvestri and S. W. Barwick, Constraints on Extragalactic Point Source Flux from Diffuse Neutrino Limits, *Phys.Rev.* **D81**, 023001 (2010). doi: 10.1103/PhysRevD.81.023001.
223. M. Aartsen et al., IceCube-Gen2: A Vision for the Future of Neutrino Astronomy in Antarctica (2014).
224. A. Bhattacharya, M. H. Reno, and I. Sarcevic, Reconciling neutrino flux from heavy dark matter decay and recent events at IceCube, *JHEP.* **1406**, 110 (2014). doi: 10.1007/JHEP06(2014)110.
225. A. Esmaili, S. K. Kang, and P. D. Serpico, IceCube events and decaying dark matter: hints and constraints, *JCAP.* **1412**(12), 054 (2014). doi: 10.1088/1475-7516/2014/12/054.
226. J. F. Cherry, A. Friedland, and I. M. Shoemaker, Neutrino Portal Dark Matter: From Dwarf Galaxies to IceCube, *JCAP* (2014).
227. A. Esmaili and P. D. Serpico, Gamma-ray bounds from EAS detectors and heavy decaying dark matter constraints, *JCAP.* **1510**(10), 014 (2015). doi: 10.1088/1475-7516/2015/10/014.
228. M. Aartsen et al., Search for dark matter annihilations in the Sun with

the 79-string IceCube detector, *Phys.Rev.Lett.* **110**(13), 131302 (2013). doi: 10.1103/PhysRevLett.110.131302.

229. S. Adrian-Martinez et al., Limits on Dark Matter Annihilation in the Sun using the ANTARES Neutrino Telescope, *Phys. Lett.* **B759**, 69–74 (2016). doi: 10.1016/j.physletb.2016.05.019.
230. R. Abbasi et al., Search for Dark Matter from the Galactic Halo with the IceCube Neutrino Observatory, *Phys.Rev.* **D84**, 022004 (2011). doi: 10.1103/PhysRevD.84.022004.
231. R. Abbasi et al., Search for Neutrinos from Annihilating Dark Matter in the Direction of the Galactic Center with the 40-String IceCube Neutrino Observatory (2012).
232. S. Adrian-Martinez et al., Search of Dark Matter Annihilation in the Galactic Centre using the ANTARES Neutrino Telescope, *JCAP.* **1510**(10), 068 (2015). doi: 10.1088/1475-7516/2015/10/068.
233. M. Aartsen et al., IceCube Search for Dark Matter Annihilation in nearby Galaxies and Galaxy Clusters, *Phys.Rev.* **D88**(12), 122001 (2013). doi: 10.1103/PhysRevD.88.122001.
234. M. Rameez and T. M. (for the IceCube Collaboration), Search for Dark Matter annihilations in the Sun using the completed IceCube neutrino telescope, *PoS.* **ICRC2015**(1209) (2015).
235. M. Z. (for the IceCube Collaboration), Improved methods for solar Dark Matter searches with the Ice- Cube neutrino telescope, *PoS.* **ICRC2015** (1099) (2015).
236. P. Gondolo, J. Edsjo, P. Ullio, L. Bergstrom, M. Schelke, and E. A. Baltz, DarkSUSY: Computing supersymmetric dark matter properties numerically, *JCAP.* **0407**, 008 (2004). doi: 10.1088/1475-7516/2004/07/008.
237. P. Ullio, M. Kamionkowski, and P. Vogel, Spin dependent WIMPs in DAMA?, *JHEP.* **07**, 044 (2001). doi: 10.1088/1126-6708/2001/07/044.
238. K. Choi et al., Search for neutrinos from annihilation of captured low-mass dark matter particles in the Sun by Super-Kamiokande, *Phys. Rev. Lett.* **114**(14), 141301 (2015). doi: 10.1103/PhysRevLett.114.141301.
239. M. Ageron et al., ANTARES: the first undersea neutrino telescope, *Nucl. Instrum. Meth.* **A656**, 11–38 (2011). doi: 10.1016/j.nima.2011.06.103.
240. C. Tönnis et al., Overview of dark matter searches with ANTARES, *PoS.* **ICRC2015**(1207) (2015).
241. C. Amole et al., Dark Matter Search Results from the PICO-2L C_3F_8 Bubble Chamber, *Phys. Rev. Lett.* **114**(23), 231302 (2015). doi: 10.1103/PhysRevLett.114.231302.
242. C. Savage, G. Gelmini, P. Gondolo, and K. Freese, Compatibility of DAMA/LIBRA dark matter detection with other searches, *JCAP.* **0904**, 010 (2009). doi: 10.1088/1475-7516/2009/04/010.
243. C. E. Aalseth et al., Search for an Annual Modulation in a P-type Point Contact Germanium Dark Matter Detector, *Phys. Rev. Lett.* **107**, 141301 (2011). doi: 10.1103/PhysRevLett.107.141301.
244. R. Agnese et al., Silicon Detector Dark Matter Results from the Final Exposure of CDMS II, *Phys. Rev. Lett.* **111**(25), 251301 (2013). doi:

10.1103/PhysRevLett.111.251301.
245. M. G. Aartsen et al., Measurement of Atmospheric Neutrino Oscillations with IceCube, *Phys. Rev. Lett.* **111**(8), 081801 (2013). doi: 10.1103/PhysRevLett.111.081801.
246. G. L. Fogli, E. Lisi, A. Marrone, D. Montanino, A. Palazzo, and A. M. Rotunno, Global analysis of neutrino masses, mixings and phases: entering the era of leptonic CP violation searches, *Phys. Rev.* **D86**, 013012 (2012). doi: 10.1103/PhysRevD.86.013012.
247. M. Gonzalez-Garcia, M. Maltoni, J. Salvado, and T. Schwetz, Global fit to three neutrino mixing: critical look at present precision, *JHEP*. **1212**, 123 (2012). doi: 10.1007/JHEP12(2012)123.
248. O. Mena, S. Palomares-Ruiz, and A. C. Vincent, Flavor Composition of the High-Energy Neutrino Events in IceCube, *Phys.Rev.Lett.* **113**(9), 091103 (2014). doi: 10.1103/PhysRevLett.113.091103.
249. L. Fu and C. M. Ho, Flavor Ratios and Mass Hierarchy at Neutrino Telescopes (2014).
250. E. Aeikens, H. Ps, S. Pakvasa, and P. Sicking, Flavor ratios of extragalactic neutrinos and neutrino shortcuts in extra dimensions, *JCAP*. **1510**(10), 005 (2015). doi: 10.1088/1475-7516/2015/10/005.
251. L. Fu, C. M. Ho, and T. J. Weiler, The Propagation Matrix and Flavor Triangle for Cosmic Neutrinos (2014).
252. X.-J. Xu, H.-J. He, and W. Rodejohann, Constraining Astrophysical Neutrino Flavor Composition from Leptonic Unitarity, *JCAP*. **1412**, 039 (2014). doi: 10.1088/1475-7516/2014/12/039.
253. S. Palomares-Ruiz, O. Mena, and A. C. Vincent, On the flavor composition of the high-energy neutrinos in IceCube (2014).
254. A. Palladino, G. Pagliaroli, F. Villante, and F. Vissani, What is the Flavor of the Cosmic Neutrinos Seen by IceCube?, *Phys.Rev.Lett.* **114**(17), 171101 (2015). doi: 10.1103/PhysRevLett.114.171101.
255. A. Palladino and F. Vissani, New parametrization of cosmic neutrino oscillations (2015).
256. L. A. Anchordoqui, H. Goldberg, F. Halzen, and T. J. Weiler, Neutrinos as a diagnostic of high energy astrophysical processes, *Phys.Lett.* **B621**, 18–21 (2005). doi: 10.1016/j.physletb.2005.06.056.
257. W. Winter, Photohadronic Origin of the TeV-PeV Neutrinos Observed in IceCube, *Phys.Rev.* **D88**, 083007 (2013). doi: 10.1103/PhysRevD.88.083007.
258. R. Abbasi et al., IceCube Sensitivity for Low-Energy Neutrinos from Nearby Supernovae, *Astron.Astrophys.* **535**, A109 (2011). doi: 10.1051/0004-6361/201117810.
259. R. Abbasi et al., Solar Energetic Particle Spectrum on 13 December 2006 Determined by IceTop, *Astrophys. J.* **689**, L65–L68 (2008). doi: 10.1086/595679.
260. R. C. Bay, R. A. Rohde, P. B. Price, and N. E. Bramall, South pole paleowind from automated synthesis of ice core records, *Journal of Geophysical Research: Atmospheres*. **115**(D14), n/a–n/a (2010). ISSN 2156-2202. doi:

10.1029/2009JD013741. URL http://dx.doi.org/10.1029/2009JD013741. D14126.

261. I. Kravchenko, S. Hussain, D. Seckel, D. Besson, E. Fensholt, J. Ralston, J. Taylor, K. Ratzlaff, and R. Young, Updated Results from the RICE Experiment and Future Prospects for Ultra-High Energy Neutrino Detection at the South Pole, *Phys. Rev.* **D85**, 062004 (2012). doi: 10.1103/PhysRevD.85.062004.
262. R. Abbasi et al., Measurement of Acoustic Attenuation in South Pole Ice, *Astropart. Phys.* **34**, 382–393 (2011). doi: 10.1016/j.astropartphys.2010.10.003.
263. P. Allison, J. Auffenberg, R. Bard, J. Beatty, D. Besson, et al., Design and Initial Performance of the Askaryan Radio Array Prototype EeV Neutrino Detector at the South Pole, *Astropart.Phys.* **35**, 457–477 (2012). doi: 10.1016/j.astropartphys.2011.11.010.
264. J. Cherwinka et al., A Search for the Dark Matter Annual Modulation in South Pole Ice, *Astropart. Phys.* **35**, 749–754 (2012). doi: 10.1016/j.astropartphys.2012.03.003.
265. The IceCube-Gen2 Collaboration. PINGU LOI .
266. E. K. Akhmedov, S. Razzaque, and A. Yu. Smirnov, Mass hierarchy, 2-3 mixing and CP-phase with Huge Atmospheric Neutrino Detectors, *JHEP.* **02**, 082 (2013). doi: 10.1007/JHEP02(2013)082,10.1007/JHEP07(2013)026. [Erratum: JHEP07,026(2013)].
267. S. Adrian-Martinez et al., Searches for Point-like and extended neutrino sources close to the Galactic Centre using the ANTARES neutrino Telescope, *Astrophys. J.* **786**, L5 (2014). doi: 10.1088/2041-8205/786/1/L5.
268. S. Adrian-Martinez et al., Search for Cosmic Neutrino Point Sources with Four Year Data of the ANTARES Telescope, *Astrophys. J.* **760**, 53 (2012). doi: 10.1088/0004-637X/760/1/53.
269. S. Adrian-Martinez et al., The First Combined Search for Neutrino Point-sources in the Southern Hemisphere With the Antares and Icecube Neutrino Telescopes, *Astrophys. J.* **823**(1), 65 (2016). doi: 10.3847/0004-637X/823/1/65.
270. A. Albert et al., Search for High-energy Neutrinos from Binary Neutron Star Merger GW170817 with ANTARES, IceCube, and the Pierre Auger Observatory, *Astrophys. J.* **850**(2), L35 (2017). doi: 10.3847/2041-8213/aa9aed.
271. S. Adrian-Martinez et al., Letter of intent for KM3NeT 2.0, *J. Phys.* **G43** (8), 084001 (2016). doi: 10.1088/0954-3899/43/8/084001.
272. A. D. Avrorin et al., Status and recent results of the BAIKAL-GVD project, *Phys. Part. Nucl.* **46**(2), 211–221 (2015). doi: 10.1134/S1063779615020033.
273. M. G. Aartsen et al., IceCube-Gen2 - The Next Generation Neutrino Observatory at the South Pole: Contributions to ICRC 2015 (2015).